UNDERSTANDING PRECISION POLYOLEFINS BY SOLID STATE NUCLEAR MAGNETIC RESONANCE SPECTROSCOPY AND X-RAY SCATTERING

By

YUYING WEI

A DISSERTATION PRESENTED TO THE GRADUATE SCHOOL
OF THE UNIVERSITY OF FLORIDA IN PARTIAL FULFILLMENT
OF THE REQUIREMENTS FOR THE DEGREE OF
DOCTOR OF PHILOSOPHY

UNIVERSITY OF FLORIDA

2010

To my family

ACKNOWLEDGMENTS

During my four-year study in the Graduate School at the University of Florida, I have received wonderful help, support, encouragement, advice, guidance, and friendship from a great number of people. I would not have been able to finish my PhD study smoothly, or not at all, without help from these people.

First and foremost, I would like to acknowledge my advisor, Professor Ken Wagener, for his guidance, advice, encouragement, patience, and understanding during the course of my graduate life. I thank him for opening the door to let me join the research group, for always being around whenever he is needed, for his advice and suggestions extracted from his wisdom and experience, for his understanding of culture differences, for his constant support and positive influence on not only my research but also my view of the world, for all the time he spent with me talking about both science and life, and for his confidence in my abilities as a chemist… Just as he said, he is not my boss, he is my advisor. I received advice from Professor Wagener regarding all aspects of my life in Gainesville. I will be thankful forever for his presence in my life.

I also thank Professor Russ Bowers. It has been a great privilege for me to work with him in solid state NMR. Professor Bowers not only introduced me solid state NMR techniques but more importantly, all the fun of being a physical chemist. His encouragement, kindness, friendship, and guidance have been one of the sources directing me to my goals.

I want to thank the members of my committee (Dr. David Powell, Professors Charles Martin, and Elliot Douglas) for their helpful discussions and help during my time at Florida. In addition, I want to thank Professor Valentin Cracium for the help on X-ray scattering technique. Furthermore, I want to thank Dr. Kathryn Williams for her helpful

discussions of the DSC results and for editing my manuscripts. Special thanks go to Dr. Ben Smith and Mrs. Lori Clark in the graduate office for all their help and advice.

I thank Mrs. Sara Klossner, and Mrs. Gena Borrero on the Butler floor for their help and friendship. It is Sara who treats trivial and ordinary daily business with beautiful smiles. I appreciated all the fun that I had at Gena's house.

Further, I would like to thank Dr. Tammy Davidson and Dr. James Horvath for their kindness and help when I taught labs under their supervision. I thank all of the excellent employees in the IT shop, stock room, business office, and main office for all their help and support.

During my four-year stay in Gainesville, I particularly acknowledge all the previous and present members in Wagener group. When I just joined the group, I received both a warm welcome and detailed help from Dr. Giovanni Rojas, Dr. Erik Berda, Dr. James Leonard, and Dr. Emine Boz. Each of them shared their synthetic knowledge as well as friendship with me. I want to thank Professor Fabio Zuluaga, Bora Inci, and Brian Aitken for their great help on synthesis. Being a member in the Wagener research group has been my pleasure. I thank Dr. Kate Opper, Paula Delgado, Sam Popwell, Pascale Atallah, Diane Turek, Chet Simocko, Ashlyn Dennis, Luke Fisher, and Chip Few for their company and friendship.

I also want to thank all the members on the Butler floor, especially Dr. Jianguo Mei and people in the lab of 309 Sisler Hall: Frank Arroyave, Erik Shen, David Liu, and Dr. Chad Amb. I would like to express my appreciation to members in Bowers research group. Special acknowledgement goes to Dr. Chi-Yuan Cheng for his help on solid state

NMR operations and friendship. I thank Dr. Caroline Pointer-Keenan, Ryan Wood, Chris Reeg, Chris Akel, and Dr. Amrish Menjoge for their friendship and help.

Since I spent six months in total at Mainz, Germany, I want to offer my special acknowledgement to the people at Max Planck Institute for Polymer Research. First of all, I want to thank Prof. Dr. Hans Spiess and Prof. Dr. Klaus Müllen for offering me the chance to do research at Mainz. Also, I want to thank Professor Spiess for his great guidance, advice, and vision in solid state NMR field. Moreover, I thank Dr. Robert Graf for his detailed education and help on the operations of NMR spectrometers at AK-Spiess group, for his solid knowledge on NMR, for his strict attitude towards science, and for his warm friendship. I also want to thank all the members of AK-Spiess group for their help and friendship, special acknowledgement goes to Dr. Matthias Junk, Dr. Shu Jie, Dr. Michael Hansen, Dr. Anne Bohle, and Dr. Mujeeb Khan. I also want to thank Dr. Werner Steffen, Dr. Guenter Auernhammer, Miao Wang, and Dr. Ingo Lieberwirth for their friendship and collaborations. I want to thank my friends outside of AK-Spiess group: Katja Nillis, Robert Haschick, Jiawei Shen, and Bin Miao, for their friendship.

I would like to thank my parents for their endless love, belief, devotion, support and sacrifices they have made that allowed me to become a person that I am today. I want to thank my husband Kevin and my daughter Abbie. They have been everything for me. Without their love, care, support, and belief in me, I would be incomplete. I want to thank my two brothers for their love and care of the families I have in China. I thank all my friends in and out of Gainesville for their friendship and all the help!

TABLE OF CONTENTS

page

LIST OF TABLES

LIST OF FIGURES

LIST OF ABBREVIATIONS

PE	Polyethylene
ADMET	Acyclic diene metathesis
NMR	Nuclear magnetic resonance
SS-NMR	Solid state nuclear magnetic resonance
WAXS	Wide angle X-ray scattering
HDPE	High-density polyethylene
LDPE	Low-density polyethylene
UHMWPE	Ultra high molecular Weight
LLDPE	Linear low-density polyethylene
VLDPE	Very low-density polyethylene
XRD	X-ray diffraction
DSC	Differential scanning calorimeter
TGA	Thermal gravimetric analysis
MS	Mass spectrometry
MALDI	Matrix-assisted laser desorption/ionization
TOF	Time of fly
IR	Infrared spectroscopy
GPC	Gel permeation chromatography
TEM	Transmission electron microscopy
CP	Cross polarization
MAS	Magic angle spinning
SPE	Single pulse excitation
AFM	Atomic force microscopy
T_m	Melting temperature

T_g	Glass transition temperature
X_c	Degree of crystallinity
T_1	Spin lattice relaxation time
T_2	Spin spin relaxation time
SUPER	Separation of undistorted powder patterns by effortless recoupling
REDOR	Rotational-echo double-resonance
REREDOR	Rotor encoding rotational-echo double-resonance
CSA	Chemical shift anisotropy
1D	One dimensional
2D	Two dimensional
3D	Three dimensional
FID	Free induced decay
CR	Crystalline region
NCR	Non-crystalline region
AR	Amorphous region

Abstract of Dissertation Presented to the Graduate School
of the University of Florida in Partial Fulfillment of the
Requirements for the Degree of Doctor of Philosophy

UNDERSTANDING PRECISION POLYOLEFINS BY SOLID STATE NUCLEAR MAGNETIC RESONANCE SPECTROSCOPY AND X-RAY SCATTERING

By

Yuying Wei

August, 2010

Chair: Kenneth B. Wagener
Major: Chemistry

In commercial polyethylene (PE), the microstructure, i.e. the branching, determines the macroscopic properties of the polymers as well as its wide applications. To better understand the structure-property-performance relationship, precision polyolefins prepared via acyclic diene metathesis (ADMET) polycondensation chemistry are used as model structures. Due to the intrinsic nature of ADMET polymerization, precision polyolefins can be prepared having, without equivocation, known branch identity and exact location of the branches along the polyolefin backbone.

Precision polyethylenes with alkyl branches are selected as structural models to investigate the influence of branch identity and frequency on polymer morphology and chain dynamics. Several analytical methods are employed, mainly solid state nuclear magnetic resonance (SS-NMR) spectroscopy and wide angle X-ray scattering (WAXS) techniques.

Deuterium SS-NMR is mostly appropriate for investigating chain dynamics because of the quandrupolar interaction. Deuterated precision polymer samples synthesized by selectively labeling the site of interest are studied using advanced ^{2}H and ^{13}C SS-NMR. A unique spectrum appears for ADMET precision polymer with a CD_3

branch on each and every 15th carbon along the main chain: a regular Pake pattern exists with a half static line width, indicating the presence of axial rotation sufficiently fast due to the motions of methyl groups embedded in the crystalline regions. The axial rotation is also observed by ^{13}C NMR. For lower branch content, the twist motions are decoupled (pinned defects), while for higher branch contents collective motion (rotator phase) is found. For the first time, the presence of the rotator phase in polyethylene crystalline region has been evidenced by solid state NMR.

Besides SS-NMR, powder X-ray scattering has also been applied to precision polymers. Wide angle X-ray scattering provides important information about crystallinity and the unit cell, as well as the lamellar structure. Combining the results from solid state NMR and X-ray scattering, a clear understanding of morphology has been achieved. When the side chain switches from the methyl group to a bigger substituent, such as the butyl group, the thermal behavior of polymer changes significantly. The influences of the branches on crystallinity and chain packing are investigated by SS-NMR and XRD. It is found that the scattering patterns of methyl-branched and butyl-branched polymers are different from that of the linear ADMET PE. Small branches, such as the methyl group, are incorporated in the unit cell, while the branches as large as or larger than the propyl group are excluded from the unit cell.

CHAPTER 1
INTRODUCTION

Since it was first produced in large scale in 1936, industrial polyethylene (PE) has been the most manufactured polymer worldwide. Depending on the synthetic methodology and polymer processing, PE can be classified into various types, such as high density polyethylene (HDPE), low density polyethylene (LDPE), linear low density polyethylene (LLDPE), ultra high molecular polyethylene (UHMPE), etc. Each type exhibits distinct macroscopic properties, and correspondingly various performances in broad applications. To understand the structure-property-performance relationships of these materials, precision polyolefins are used as model structures for commercial polyethylenes. In precision polyethylene, the branch identity and branch frequency can be precisely controlled, while in commercial PE, there are many variables, including the branch size, branch spacer, and branch distribution. By limiting the freedom of the system, a better understanding of branching in PE can be achieved.

It is believed that the macroscopic properties are inherently dependent on the micro-structural features. For instance, the thermal behavior of PE is determined by the chain-packing in the crystalline region; likewise, the mechanical properties of PE are correlated to the dynamics of both the main chain and the side branches.

Various analytical methods have been employed to investigate the structures and physical properties of precision polyolefins. This research focuses on two of these methods: solid state nuclear magnetic resonance spectroscopy (SS-NMR) and wide angle X-ray scattering (WAXS). SS-NMR is recognized for its capability of understanding structure and dynamics of condensed matter. Coupled with a high magnetic field, the modern pulse sequences have been used to study many nuclei,

such as ^{1}H, ^{2}H, and ^{13}C, by offering NMR signals with good resolution and high sensitivity. WAXS is well-known for investigating ordered structures. Information related to the degree of crystallinity, crystal structure, and unit cell dimension can be obtained directly. Other analytical techniques, such as differential scanning calorimetry (DSC), transmission electron microscopy (TEM), are also used to understand the thermal behaviors and morphologies of the materials, respectively.

This dissertation is organized as follows: in Chapter 2, commercial polyethylene (different structures and their synthesis), and precision polyolefins (synthesis and uniqueness) are briefly reviewed. The comparison of commercial PE to precision PE is presented. Precision polyolefins with various branches are discussed to investigate the influence of branching on the thermal, mechanical, dynamic, and morphological properties of these unique structures.

Chapter 3 describes the two main analytical techniques that are employed in the dissertation: SS-NMR and WAXS, including the fundamental principles, the instrumentation, operation, and data interpretation. Chapter 3 elucidates the analytical tools used to understand the effects of branch identity and frequency on polymer macroscopic properties.

In Chapter 4, the branch frequency effect is discussed using three precision polyolefins as examples: PE21-CD_3, PE15-CD_3, and PE9-CD_3. The ^{2}H NMR spectra under static conditions and ^{13}C NMR spectra with magic angle spinning are explored. By combining the results from these two measurements, a motional model is proposed, and the concept of “rotator phase” presenting in the crystalline region of polyethylene is

evidenced. The results indicate that the branch frequency indeed has significant influence on the structures.

Lineshape analysis of ^{2}H SS-NMR is specifically described in Chapter 5. By applying a deuterium T_1 filter prior to the solid echo pulse sequence, experimental amorphous spectra can be acquired. The crystalline spectra are calculated by subtracting the experimental amorphous signals from the fully relaxed total spectra. With software simulation, the experimental spectra can be fit to various combinations of motional models.

In Chapter 6, the influence of the branch identity on morphology is investigated by sampling the precision polyolefins with alkyl branches on each and every 21^{st} carbon along the ethylene backbone. WAXS and SS-NMR data imply that the smaller branches, such as the methyl and the ethyl groups, are incorporated in the crystalline unit cell, while the bulkier groups, propyl and larger, are excluded from the crystalline unit cell.

In Chapter 7, the ADMET precision polyolefins with reduced branch frequency, PE39-R with the alkyl group R on each and every 39^{th} backbone carbon, are explored. This series of polymers exhibit more complicated crystalline structures. The SS-NMR shows a broad peak representing the methyl branch, and a splitting of chemical shift belonging to α carbon on the backbone. The chain folding and packing in PE39-CH_3 implies the presence of more than one crystalline structure.

Chapter 8 presents a summary of the dissertation and suggestions for future research.

CHAPTER 2
COMMERCIAL POLYETHYLENE AND PRECISION POLYOLEFINS

2.1 Commercial Polyethylenes

2.1.1 Classifications of Commercial Polyethylenes

Polyethylene (PE) has the simplest molecular structure in commercial polymers, characterized by its long backbone of covalently linked CH_2 units with methyl groups as terminated chain ends. In spite of its deceptively simple chemical composition, PE has been widely used in many applications since it was first synthesized accidently by the German chemist Hans von Pechmann in 1898.[1] It exhibits diverse applications as a result of low cost, flexibility, ductlility, clarity, lightness, nontoxicity, good mechanical and thermal stability, and excellent electric resistance, etc. The versatility of this polymeric material arises chiefly from branching, which acts as “defects” in the crystalline regions and modifies the nature of the structure. For instance, the introduction of alkyl branches in PE lowers its crystallinity level. In principle, the degree of crystallinity is inversely proportional to the degree of defects in the structure, i.e., the more the defects, the lower the crystallinity level will be. Since the chain packing in crystalline regions is denser than that in the non-crystalline regions, the overall density of polymers is determined mostly by the portion of crystalline domains. Less branching (fewer “defects”) results in denser materials. In general, the macroscopic properties, such as density, are strongly related to branching and crystallinity of the material. For a pure polyethylene, specifically, PE with no branching at all, its density is 1 g/cm^3; for a totally amorphous PE, which possesses high level of branching, its density is 0.85 g/cm^3.

Based on its density and branching, PE is roughly classified into four different categories, high density polyethylene (HDPE), low density polyethylene (LDPE), linear

low density polyethylene (LLDPE), and very low density polyethylene (VLDPE), with their schematic structures shown in Figure 2-1.

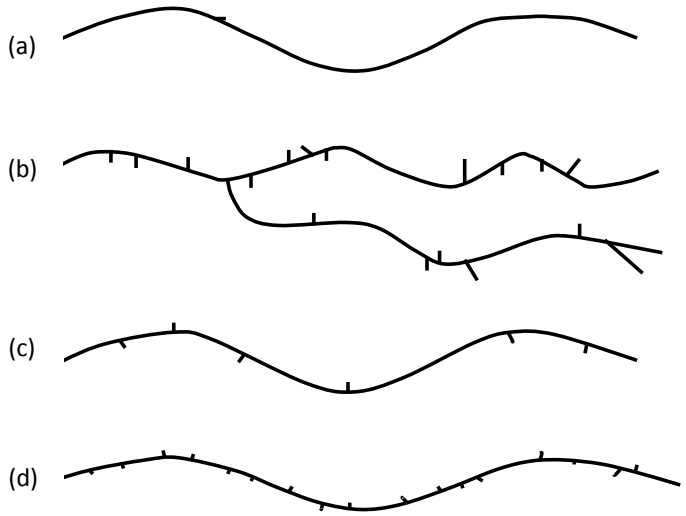

Figure 2-1. Schematic representations of commercial polyethylenes: (a) high density polyethylene; (b) low density polyethylene; (c) linear low density polyethylene; (d) very low density polyethylene.

High density polyethylene (HDPE), or low pressure polyethylene, as shown in of Figure2-1(a), has a typical density falling in the range of 0.94–0.97 g/cm^3. Consisting of negligible branching to perturb the crystalline organization, HDPE has the chemical structure which is the closest to pure polyethylene. It is also termed as linear polyethylene (LPE) due to its low level of branching and highly linear structure. HDPE has rather high crystallinity compared to any other types of polyethylene. Thus it appears opaque, behaves tough and stiff, and withstands rather high temperature[2] (see mechanical and thermal data shown in Table 2-1). HDPE is utilized widely as carrier bags, pipes, bottles, toys, etc.

Low density polyethylene (LDPE), or high pressure polyethylene, is so named because of its relatively low density falling in the range of 0.90–0.94 g/cm^3, which

results from the low crystallization level due to the substantial concentrations of branching. The branches are primarily ethyl and butyl groups together with some rather long chain branches. Determined by the nature of polymerization process at the high pressure at which LDPE is manufactured, the short-chain branches are clustered randomly and separated by the long runs of non-branched ethylene sequence. Long-chain branches, which are displaced randomly along the backbone, can themselves be branched as well, illustrated in Figure 2-1 (b). Compared to HDPE, LDPE contains more and larger defects, which undoubtedly inhibit the chains packing into a crystalline structure. Consequently, LDPE has weaker intermolecular (instantaneous dipole-dipole) interactions, as well as less temperature and chemical resistance. It appears to be softer and more flexible than HDPE. Major applications for LDPE consist of heavy duty sacks, refuse sacks, films, and for general packaging.[3]

Linear low density polyethylene (LLDPE) is a linear version of polyethylene, with a significant concentration of short-chain branches, seen in Figure 2-1 (c). The incorporation of a high number of branches in LLDPE discourages the formation of crystalline structures in terms of crystal size and perfection. The big difference between LLDPE and LDPE is the absence of long-chain branching, arising from different polymerization processes of these two types of materials. LLDPE has relatively narrower distribution of molecular weight, more linear structure, and apparently different mechanical, thermal, and rheological responses (data shown in Table 2-1). LLDPE is used for almost all of the traditional applications for polyethylene, including plastic bags, sheets, food wrap, toys, pipes, buckets, and containers. However, the predominant

usage of LLDPE is in the film industry due to its good mechanical property and relative transparency.[3]

Table 2-1. General properties for various classes of commercial polyethylenes

Property	HDPE	LDPE	LLDPE	VLDPE
Branch Lengths and Content	Few or no branches	SCB & LCB	Numerous SCB, no LCB	Large numbers of SCB
Density, g/cm^3	0.94-0.97	0.91-0.94	0.90-0.94	0.86-0.90
X_c (% from density)	62-82	42-62	34-62	4-34
X_c (% from calorimetry)	55-77	30-54	22-55	0-22
T_m, $^{\circ}$C	125-132	98-115	100-125	60-100
Heat of Fusion, cal/g	38-53	21-37	15-43	0-15
Thermal Expansivity, 10^{-6} in/in/$^{\circ}$C	60-100	100-200	70-150	150-270
Heat Distortion Temperature, $^{\circ}$C at 66 psi	80-90	40-44	55-80	--
Flexural Modulus, kpsi at 73 $^{\circ}$F	145-225	35-48	40-160	<40
Tensile Modulus, kpsi	155-200	25-50	38-130	<38
Tensile Yield Stress, kpsi	2.6-4.5	1.3-2.8	1.1-2.8	<1.1
Tensile Strength at Break, kpsi	3.2-4.5	1.2-4.5	1.9-4.5	2.5-4.5
Tensile Elongation at Break, %	10-1,500	100-650	100-950	100-600
Industrial Production	Low pressure Ziegler process	High pressure, radical reaction	Metallocene process	Metallocene process
Number of Branches per 1000 Carbon Atoms[4]	<4 (Phillips), 5-7 (Ziegler)	20-30 (methyl), 3-5 (*n*-butyl)	--	Numerous

Data adapted from *Handbook of polyethylene: structures, properties, and applications*.[2]
X_c denotes the degree of crystallinity. T_m denotes the melting temperature.
SCB: short-chain branches; LCB: long-chain branches.

Very low density polyethylene (VLDPE), also known as ultra low density polyethylene (ULDPE), is a special class of linear low density polyethylene, defined by

its density falling in the range of 0.86-0.90 g/cm^3. VLDPE has much higher level of short-chain branches, illustrated in Figure 2-1 (d). The extremely high concentration of branches effectively inhibits crystal organization of the polymer chains, resulting in quite low crystallinity level or even no crystals at all, i.e., completely amorphous solids, as shwon in Table 2-1. A typical separation of branches would fall in the range of 7-25 backbone carbon atoms.[2] Like LLDPE, VLDPE is more flexible and less brittle in comparison with HDPE. VLDPE is used mainly for hoses and tubing, food containers and packaging.

There are some other classification criteria. For instance, based on molecular weight, PE can be divided into high molecular weight PE (HMWPE), ultra high molecular weight PE (UHMWPE); based on the primary structure, PE can be classified to be linear PE, branched PE, grafted PE, crosslinked PE. Herein, we focus on the branching in polyethylene and choose the classification by macromolecular density and nature of branches.

2.1.2 Industrial Manufacturing/Processing of Polyethylene

The first laboratory polyethylene was created accidently in 1898 by Hans von Pechmann when heating diazomethane.[1] After 35 years, on March 29th 1933, Eric Fawcett and Reginald Gibbon at the British company Imperial Chemical Industries (ICI) made the first industrial PE by accident (again) when reacting ethylene with benzaldehyde at high pressure.[2] However, it was not until 1935 when Michael Perrrin determined the experimental conditions for consistent producting high pressure polyethylene, known today as low density polyethylene.[5] Before World War II, PE was almost exclusively utilized as an electrical insulator due to its high dielectric strength, low loss factor, and easy processing. In the years following, Union Carbide, du Pont,

and ICI made significant improvements and discoveries that led to revolutions in polyethylene production. One of the most important insights was the determination of high content branching in high pressure PE revealed by infrared spectroscopy.[6] The branches were identified to be ethyl and butyl groups with content of around twenty branches for every 1000 backbone carbons.[2] This insight was greatly appreciated in the PE industry, because subsequent investigations indicated considerable effects of branching on the physical, rheological, and mechanical behaviors. Such an important correlation allows the tailoring of commercial polymers to meet particular application requirements by controlling the polymerization process, thus the content of branches.

With the development of industrial polyethylene, the processes of making this material can be divided into five relatively distinct routes: (a) high-pressure process; (b) Ziegler process; (c) Phillips Petroleum (Indiana) process; (d) Standard Oil process; and (e) metallocene process.

(a) High-Pressure Process

Low density polyethylene resins are made exclusively via free radical polymerization by a high pressure process. The conditions required to make the high level branched polyethylene is quite simple: a suitable amount of appropriate free radical, controlled polymerization conditions of high pressure at 100 to 300 MPa, and temperature at 80 to 300 ºC.[2, 3] Commonly used initiators include benzoyl peroxide, azodiisobutyronitrile or oxygen.[3] This polymerization process involves initiation, chain propagation, chain branching, chain transfer, and termination steps. Chain branching occurs when radical transfer occurs intramolecularly (resulting in short-chain branching) or intermolecularly (giving rise to long-chain branching).

(b) Ziegler Process

Ziegler-Natta catalysis and metal oxide catalysis are the two industrial processes used to produce high density polyethylene. The Ziegler process occurs at relatively low pressure and temperature. The typical operating temperature is around 70 ºC, which varies with the mode of the starting material of a gaseous reaction mixture or a slurry, the production facility is controlled at below the melting point, around 30-100 ºC; for solution reactors, higher operation temperatures can be reached, typically 100-200 ºC.[2] Typical operating pressure ranges from atmospheric to as high as 2.1 MPa, varying with the modes of the reaction mixture as well. For the gas/slurry mode, the operating pressure is higher than that for the solution mode. One advantage of the Ziegler process lies in the flexibility and variety of Ziegler catalysts, which consist chiefly of a transition metal halide and alkyl aluminium compounds. The one commonly used in production of HDPE is the complex of triethyl aluminium with titanium tetrachloride.[2]

(c) Phillips Petroleum Process

The Phillips process involves the use of a metal oxide catalyst at medium pressure (1.4-3.5 MPa) and temperature (130-160 ºC).[3] The typical industrial Phillips catalyst is chromium oxide on silica gel. Commercial polymers produced by this process have a rather low melt flow index of 0.2-5 and exhibits the highest material density among any commercial PE, as high as 0.96 g/cm^3. Due to the nature of polymerization mechanism involving metal oxide catalysts, the resulting polymers are highly stereospecific. Temperature plays a very important role in the conversion rate and molecular weight of the final product. For instance, when the operating temperature in a typical Phillips process increases from 140 ºC to just over 170 ºC, the melt flow index increases 40

times, and correspondingly the molecular weight decreases. Therefore, in industry, polyethylene with high molecular mass can be realized by the low temperature Phillips process.

(d) Standard Oil (Indiana) Process

Besides the Ziegler and Phillips processes, the Indiana process has been demonstrated to be another applicable industrial process in the production of high density polyethylene. This process operates at a pressure of 4-10 MPa and temperature of 200-300 ºC, with supported molybdenum-alumina as catalysts and sodium or calcium as promoters.[3, 7] The Indiana process shares many similarities to the Phillips process: They are capable of producing HDPE with densities as high as 0.96 g/cm^3, both are sensitive to operating temperatures.

(e) Metallocene Process

Characterized by the usage of metallocene compounds as catalysts, this relatively new process brings unique structural and physical properties to the polyethylene industry. In contrast to the Ziegler-Natta catalysts, which are heterogeneous and contain multiple catalytic sites, the metallocene catalysts are homogeneous and have only a single catalytic site. This is the reason why metallocene catalysts are also referred to as single-site catalysts in the industrial environment. A typical metallocene molecule consists of an organometallic coordination compound, in which one or two cyclic ligands are bonded to a central transition metal, usually zirconium or titanium. The uniqueness of metallocene process lies in the catalysts, which have sound productivity and activity, giving rise to narrow molecular weight distributions and simple tailoring of the final products by controlled modification of the catalyst. Interestingly, stereospecific

polymers, such as isotactic and syndiotactic polymers, can be manufactured by using chiral metallocene catalysts. LLDPE from metallocene process is denoted as mLLDPE, produced by copolymerization of ethylene with a small amount of higher alpha olefins like 1-butane, 1-hexene, and 1-octene. Compared to the traditional LLDPEs, mLLDPE materials show superior mechanical response and narrower molecular weight distributions. Metallocene grades of VLDPE, denoted as mVLDPE, first introduced by Exxon Mobile in 2010,[4] exhibit more desirable mechanical and molecular properties in contrast to the conventional VLDPE. However, the metallocene process has not demonstrated much impact on mHDPE, which is the metallocene version of HDPE.[2]

2.1.3 Relationship of Microstructure to Physical Properties

Polyethylene is the simplest member in the family of thermoplastic materials, composed of a long chain of aliphatic hydrocarbons. For all grades of commercial PE, the physical properties differ in one way or another, largely related to the microstructure. Structural variables that significantly influence the macroscopic properties include: (a) degree of short-chain branching, (b) degree of long-chain branching, (c) the distributions of chain lengths and branch concentration, (d) molecular weight and its distribution, (e) residue of comonomer, and (f) impurities including residue of catalysts.[3]

2.1.3.1 Density

As mentioned previously, the density is the chief physical property used in industry to classify the polyethylene grades. Governed by the polymerization process, density is strongly related to the type and concentration of branches. HDPE produced via low pressure process has negligible numbers of branches. Hence, the *all-trans* ethylene sequence has no difficulty packing into large crystalline structures. Moreover, the crystalline region is denser than the non-crystalline region: the former has a density of 1

g/cm^3, while the latter of 0.85 g/cm^3.[4] Density can then be correlated to branch content and degree of crystallinity, as seen in Figure 2-2. Two types of PEs are sampled: LLDPEs with weight-averaged molecular weights in the range of 65,000-130,000 g/mol, and HDPE resin with weight-averaged molecular weight of 61,000 g/mol. From Figure 2-2, two trends can be observed: Density and crystallinity decrease as the branch concentration increases; the slowly-cooled polymers obtain higher density compared to quenched materials, indicating an influence from the thermal process. The molecular weight and its distribution also play an important role in the determination of the density of PE. In general, density drops in some extent with the large increase of molecular weight.

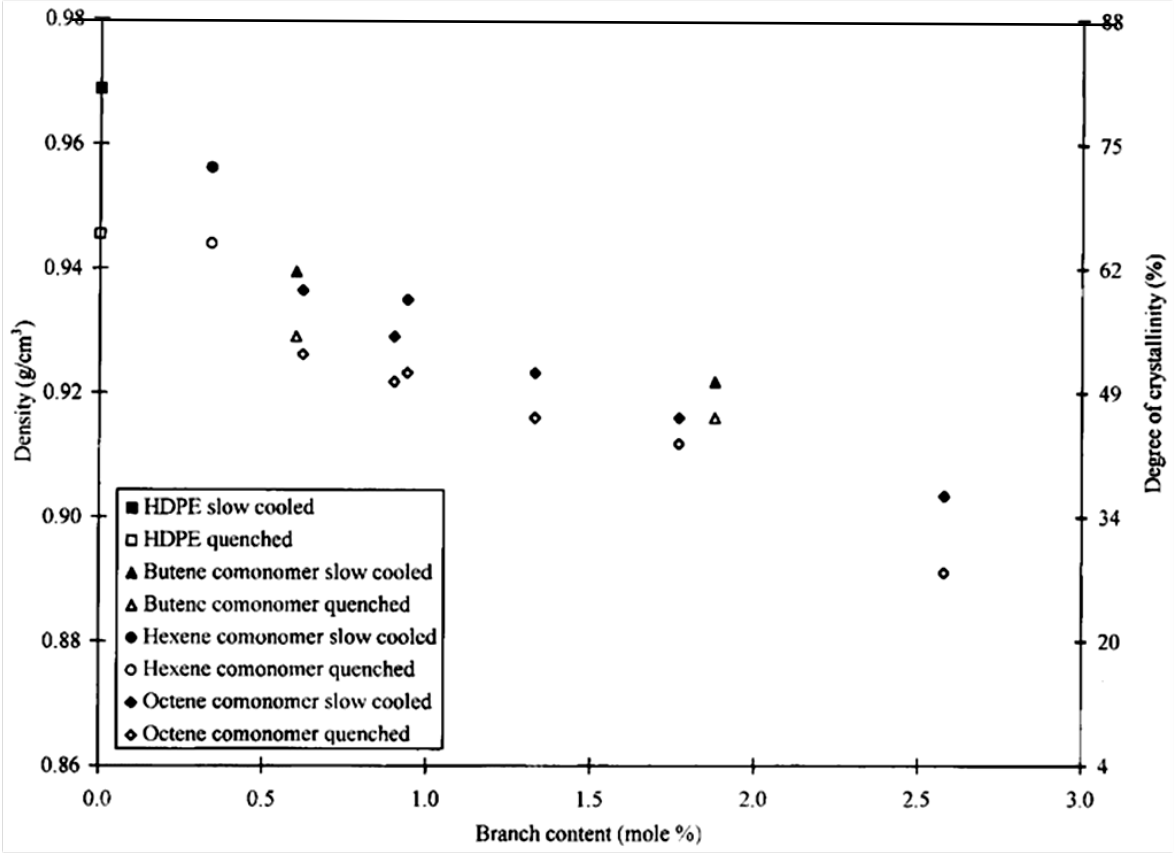

Figure 2-2. Plot of density and degree of crystallinity as functions of branch content for compression-molded HDPE and LLDPE resins (*Figure adopted from ref. 2*)

2.1.3.2 Crystallization and morphology

The physical properties of PE, such as density, are determined by the semi-crystalline nature. The presence of three phases—crystalline, interphase, and amorphous phase—offers unique physical properties to PE and to other semi-crystalline polyolefins. Such simple evidence lies in the fact that PE is both tough and resilient: the former property originates from the ordered packing in the crystalline region, while the latter comes from the highly disordered amorphous region.

Crystallinity is, in turn, determined by the polymerization process, catalyst, temperature, pressure, cooling rate, etc. The crystallinity level, usually termed as "degree of crystallinity (Xc)", is used to characterize the percentage of crystal structure in the whole material. In fact, the degree of crystallinity is intrinsically controlled by the microstructure, i.e., the branching in PE. Figure 2-2 clearly shows the relationship between crystallinity level and branch content. In general, the degree of crystallinity drops as branch content arises, particularly at a low level of branching. This observation is not difficult to understand. The introduction of branches in PE hinders the main chain from packing into an ordered crystalline array, in terms of both size and perfection. It is commonly believed that the branches are preferentially excluded from the crystalline phase, and the ability of commercial PE to crystallize largely depends on the distribution of *all-trans* ethylene segments.[2, 8-10] Therefore, the size of the crystal structure of PE is constrained by the branch spacer, or in other words, the defect-free ethylene sequence between the adjacent branches. The higher the branch content, the shorter the available main chain that can crystallize, consequently, the smaller the crystal structure, the lower the crystallinity level.

The relative arrangement of the crystalline phase and non-crystalline phase, their portions, sizes, shapes, spatial orientations, and connectivity modes, determine the physical properties of PE as a universal material. In crystallography, any crystal structure is built up from many periodic repeating unit cells, which are the smallest structural motifs, much like monomers are the construction units for polymers. A specific unit cell can be determined by six parameters: lengths of three axes a, b, c, and angles between phases α, β, γ, seen in Figure 2-3 (a).

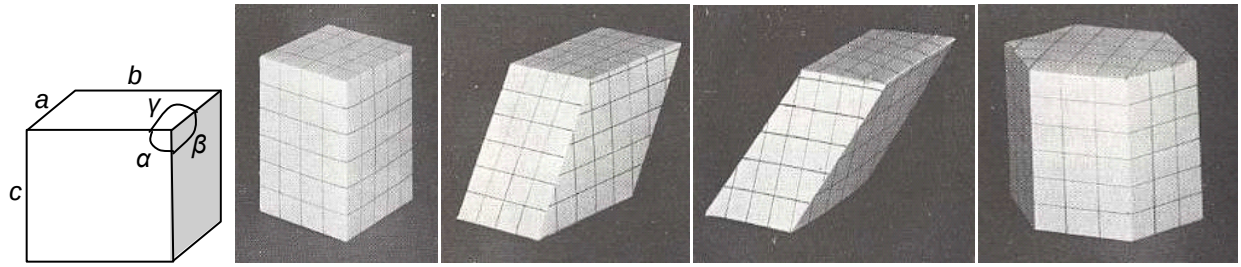

$a \neq b \neq c$
$\alpha = \beta = \gamma = 90°$

$a \neq b \neq c$
$\alpha = \gamma = 90°$
$\gamma \neq 120°$

$a \neq b \neq c$
$\alpha \neq \beta \neq \gamma \neq 90°$

$a = b \neq c$
$\alpha = \beta = 90°$
$\gamma = 120°$

(a) (b) (c) (d) (e)

Figure 2-3. Typical unit cell structures and their characteristic dimensional values: (a) General unit cell; (b) Orthorhombic unit cell; (c) Monoclinic unit cell; (d) Triclinic unit cell; (e) Hexagonal unit cell

There are three types of unit cells present in commercial polyethylene: orthorhombic, monoclinic, and hexagonal crystals, as shown in Figure 2-3 (b), (c) and (e). The polymer chain arrangement and the quantitative dimensional data of the three PE crystals are illustrated in Figure 2-4 (a), (b), and (c), respectively.

The orthorhombic unit cell is a cuboid with three unequal axes and three plane angles being right angle, seen in Figure 2-3 (b). With the pioneered contributions from C. W. Bunn[11] and V. Vand[12], the crystal structure of commercial PE has been accepted

to be orthorhombic. Figure 2-4 (a) gives the chain orientation and crystal dimensions of this structure measured for commercial high density polyethylene at room temperature.[2] It is worth noticing that the structure shown herein is an idealistic case without consideration of ill-defined branching. When structural “defects” are introduced into the polymers, low density polyethylene and linear low density polyethylene display increased a and b axis values. Interestingly, the length with covalent main chain bonds, (i.e., c axis dimension) shows less dependence on branching.[13, 14]

The monoclinic and hexagonal unit cells are metastable crystal forms for PE. Upon stretching,[15] pressing,[16] heating, or inject molding processing,[17] the metastable monoclinic crystal can be obtained by a transition from the more stable orthorhombic crystal. And when the deformation conditions are removed, the equilibrium orthorhombic crystal form will return. Originated from high pressure and high temperature crystallization, the hexagonal crystal form of PE is sometimes referred to as the “rotator” phase, in that some individual chain segments are capable of rotational motion at random phase angles relative to their adjacent stems.[18, 19] The configuration of polyethylene chains and the sizes of metastable crystal forms are displayed in Figure 2-4 (b) and (c).

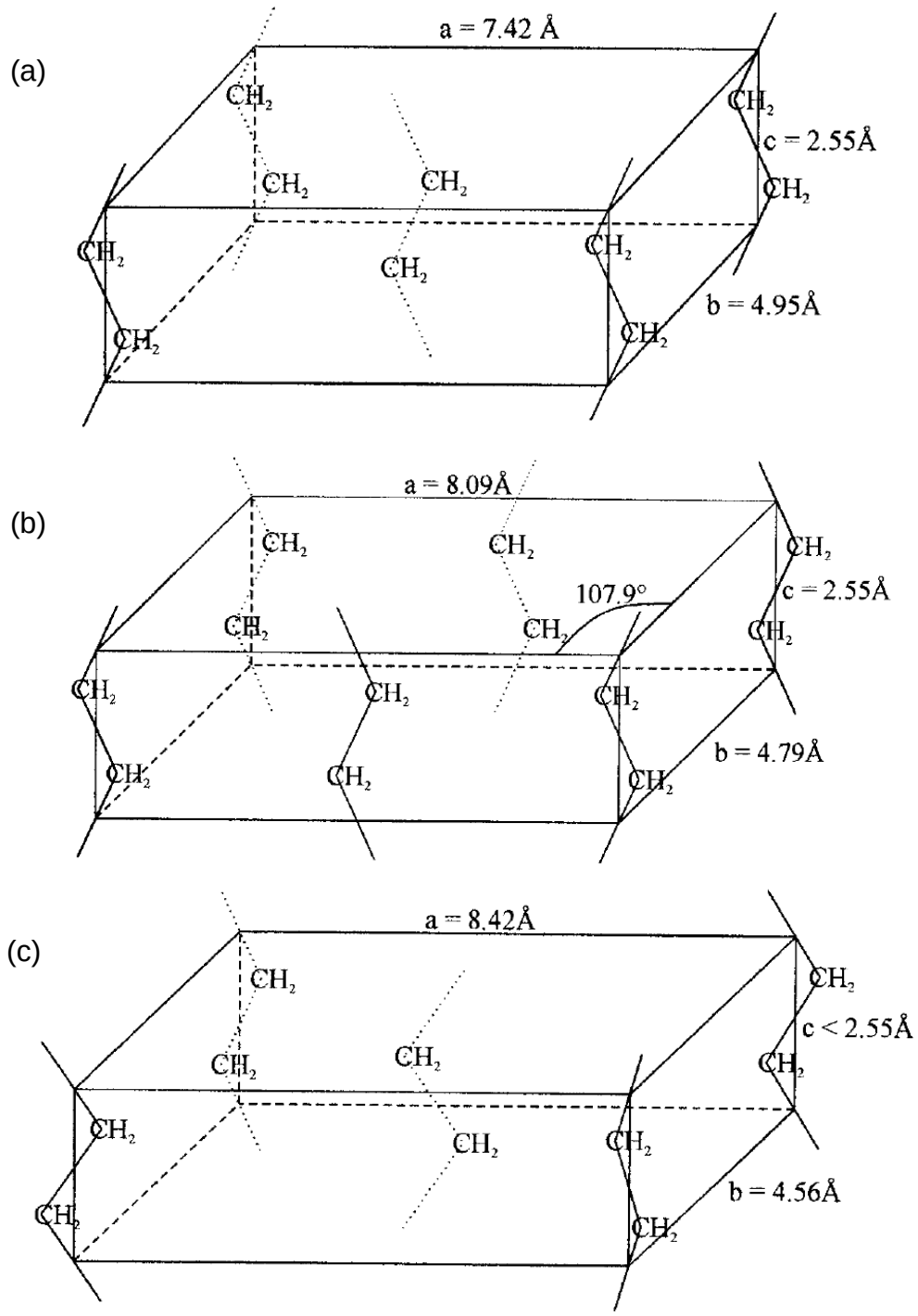

Figure 2-4. Three unit cell structures in commercial PE and their characteristic dimensional values: (a) Orthorhombic unit cell; (b Monoclinic unit cell; and (c) Hexagonal unit cell (figures adapted from reference[2])

2.1.3.3 Thermal properties

As a semi-crystalline polymer, PE displays characteristic thermal properties with melting occurring within a range of temperatures associated with the crystalline structure and glass transition behaviour associated with the amorphous phase.

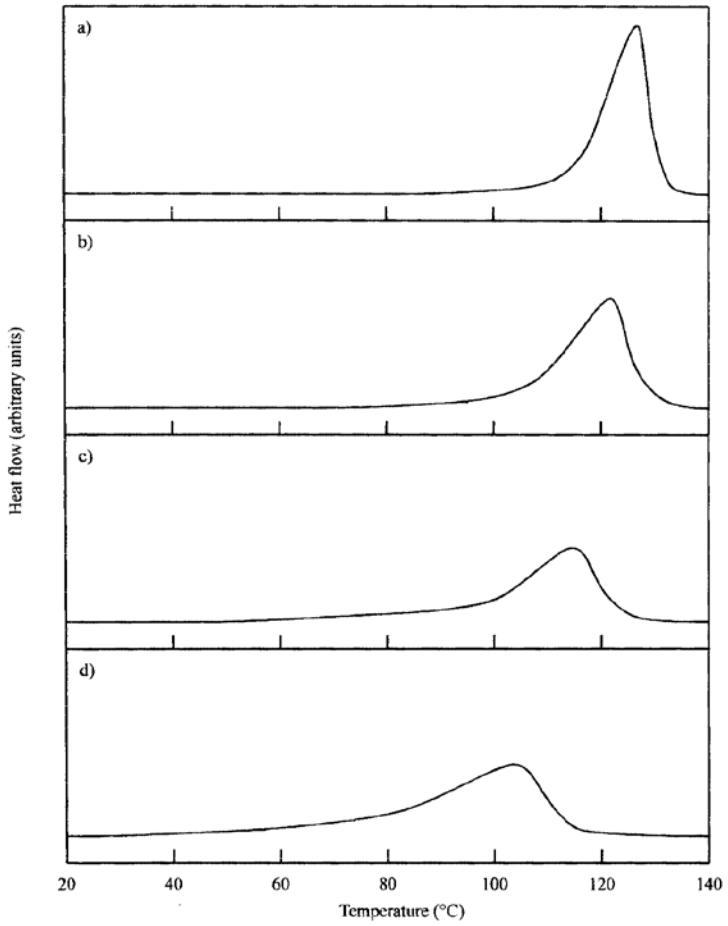

Figure 2-5. Plot of heat flow of three types of PE samples as function of temperature/heating rates. (a) Slow-cooled high density polyethylene of moderate molecular weight; (b) quench-cooled high density polyethylene of moderate molecular weight; (c) quench-cooled linear low density polyethylene of moderate molecular weight; (d) quench-cooled low density polyethylene (*Figure adopted from ref. 2*)

Polymeric materials consist of numerous unequal polymer chains, which have different chain lengths and branching from each other, causing a distribution of

crystalline structure in terms of size and orientation. Melting is a thermal transition in which atoms on segmental chains in the crystalline region vibrate so violently that they leave the equilibrium position within the crystal lattice resulting in collapse of the crystal structure. This melting process is accomplished by absorbing energy, normally by thermal heating. The melting temperature is related to the thickness of lamellae formed in the crystalline phase of PE: the thicker the lamellae, the higher the melting temperature. The dispersed lamellar thickness due to the random displacement of branches along the backbone causes the dispersion in melting temperature, and consequently the breadth of melting range. This melting range for commercial PE can span from less than 10 ºC up to 70 ºC when undergoing the transition from semi-crystalline solid state to molten state.

Since crystallization is thermal process dependent, the melting range of the crystalline structure is also related to the thermal history. Figure 2-5 illustrates the melting behaviours of two type PE samples undergoing various thermal treatments. It is clear that the slowly cooled and quenched HDPEs show significantly different melting ranges. The slowly cooled HDPE exhibits a sharper melting peak and narrower melting range, as a consequence of thicker lamellae and narrower distribution due to more perfect organization of chain packing in crystalline regions. Also, when other parameters, such as molecular weight remain constant, the melting is a function of branching. From (b), (c), and (d) in Figure 2-5, all three PE samples (HDPE, LLDPE, LDPE) possess various branch content: HDPE < LLDPE < LDPE. Their melting peaks when all quenched from the molten state show the reverse order: HDPE > LLDPE > LDPE.

In addition, semi-crystalline polymers including PE undergo several secondary thermal transitions arising from the localized order of structure. The glass transition is such a second-order process. Thermoplastic samples are extremely rigid and brittle below a critical temperature, termed as glass transition temperature T_g. It is commonly accepted that below T_g, the polymer chains in the highly disordered regions have little or no freedom to move and the polymer shows glass-like behavior. Above the T_g, by absorbing more energy, those chains in the amorphous phase have greater freedom to move to certain extent and polymer behaviour is rubber-like. The transition from the glass-like state to the rubber-like state is referred to as “glass transition” or “γ transition”, which is associated with the non-crystalline components in semi-crystalline polymers. Commercial PE samples have T_g ranging from -130 ºC to -100 ºC, a range that is well below room temperature and thus facilitates the universal applications of PE. Similar to the melting process, the glass transition is also dependent on processing history and measuring techniques/routes.

2.1.3.4 Other physical properties

Other physical properties, especially mechanical, rheological, and optical, are essentially correlated to the branching in PE.[2, 9, 11, 20-24] For instance, regarding the mechanical behaviour, the crystalline regions in PE show moduli two orders of magnitude greater than those of the non-crystalline regions,[2] indicating a strong relationship between the mechanical strength and the degree of crystallinity, which, as demonstrated previously, is determined by the type and number of branches.

The rheological properties of molten PE are crucial in processing the final merchandise. In the molten state, PE is rather viscous and considered as a viscoelastic liquid. The viscosity and elasticity of polyethylene materials are strongly correlated to

the chain entanglement in both molten and solid states, in turn a function of molecular weight, its distribution, and the nature of branching of PE resins, with detailed mechanical data shown in Table 2-1.

So far, combining the essence of polyethylene and its manufacture, a logical relationship of structure-property-performance can be established, illustrated in Figure 2-6. The microscopic properties, such as branching, molecular weight and its distribution, chain packing, and chain dynamics originats from the industrial production or lab synthesis. Moreover, the macroscopic behaviors, like morphological, thermal, mechanical, morphological, and rheological properties, of polymeric materials are dependent on the intrinsic microstructure, i.e., the nature of branching. Guided by the macroscopic properties, it is possible to select polymers for various applications.

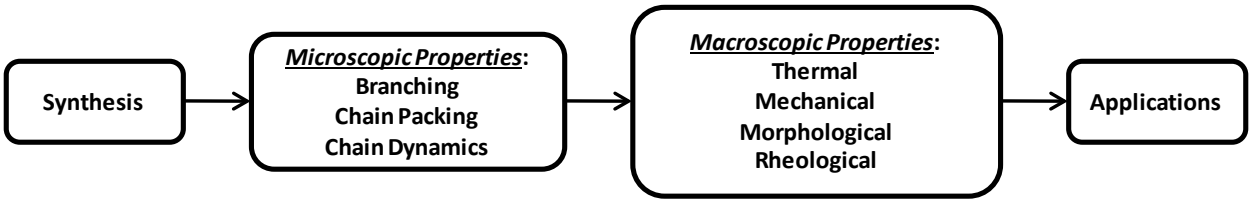

Figure 2-6. Relationship of structure-property-performance of polymeric materials

Studying carefully the “relationship chain” in Figure 2-6, one has no difficulty to find that microscopic properties are key to linking synthesis/manufacturing with polymer behaviors. Any fundamental understanding of branching effects will be of great importance to guide manufacturing and to predict the material’s applications. A great deal of research has been performed on the subject. However, due to the nature of “randomness” for commercial polyethylene, specifically, the random sizes of branches,

the random distribution of branches along the backbone, and the random spacing between two adjacent branches, the fundamental relationship between branching and the macro-properties is not yet clear. Therefore, there is an obvious need for model polyethylenes. The basic requirement of these model polyethylenes is to limit the "randomness", i.e., to study the influence of one parameter by fixing some other variables in commercial PE. This can be realized via a family of precision polyolefins to be discussed in detail in the following section.

2.2 Precision Polyolefins

2.2.1 Structure of Precision Polyolefins

The nature of branching in commercial PE samples is "random", i.e., the type, number, and frequency of the branches are not defined. To better understand the influence of microstructure on macroscopic properties, precision PEs are introduced as structural models, which reduce the number of variables in the PE system.

Precision polyolefins are defined as "polyolefins in which certain featural structures are defined". The primary structures of these polymers can be controlled by one type of metathesis chemistry, specifically, acyclic diene metathesis (ADMET) polycondensation chemistry. The basic structure of these model polymers is illustrated in Figure 2-7. Compared to commercial structures, the pendant side groups R are displaced regularly on the polyethylene backbone. The branch identity ***R*** and the branch spacer ***x*** are defined precisely.

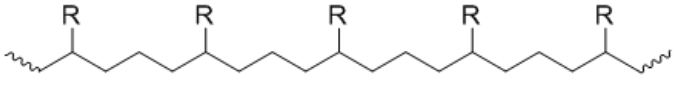

Figure 2-7. General chemical structure of precision polyolefins. Branch identity R is displaced regularly along the polyethylene backbone. Branch spacing, the distance between the adjacent branches is defined.

The branch identity R can be any functional group that is compatible with ADMET chemistry. So far, the advances in this area have shown that branches R can be alkyl groups[25-37], siloxane units[38-42], halide groups[43-48], biological active groups[49-54], acid groups[55-60], conjugated functional groups, and even some ionic groups[61]. The branch spacing, denoting the number of carbon atoms on the main chain between two adjacent branches, can be an integer tuned from 2 to 38, according to the synthetic efforts to date.[36]

2.2.2 Synthesis of Acyclic Diene Metathesis (ADMET) Precision Polymers

The synthesis of precision polyolefins can be realized via acyclic diene metathesis (ADMET), which is a type of step-growth olefin metathesis capable of preventing short chain branching distribution from chain transfer/walking, which occurs in chain propagation chemistry. The soul of making regularly branched precision polyolefins lies in the synthesis of *α,ω*-diene monomers. It is the nature of the monomers that brings the precision to the polymer structures.

2.2.2.1 Monomer synthesis

There are two methodologies present in the synthesis of the symmetric diene monomers, shown in Figure 2-8 and Figure 2-9, respectively.

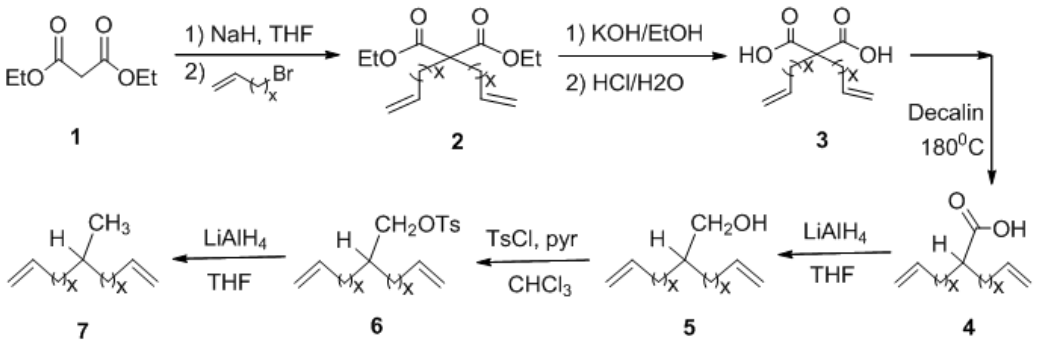

Figure 2-8. Precision monomer synthesis methodology starting with malonate

The monomer synthetic route #1, exampled by a methyl branched monomer, is illustrated in Figure 2-8. Briefly, the starting diethylmalonate ***1*** can be easily disubstituted with an alkenyl halide possessing the appropriate methylene spacing. The resulting diester ***2*** is saponified followed by decarboxylation to produce the pure monoacid ***4***, which is then selectively reduced with lithium aluminum hydride (LAH) to yield the primary alcohol ***5***. The symmetric diene monomer of interest ***7*** can be obtained with mesylation of the primary alcohol and the subsequent reduction via hydride displacement. The same methodology has been successfully applied to synthesize ethyl-branched[31] and hexyl-branched[34] ADMET precision polyolefins.

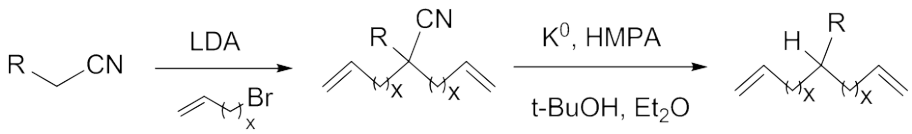

8 9 10

Figure 2-9. Precision monomer synthesis methodology via cyanide chemistry

An optional monomer synthesis route (Figure 2-9) starts with the α,α-dialkylation of primary nitrile ***8*** in the presence of base such as lithium diisopropylamide, followed by decyanation of α,ω-cyanodiolefin ***9*** via radical reaction to yield α,ω-diene monomer ***10***. This newly designed cyanide methodology offers quantitative yield with short synthetic steps,[27] and has been proved to be well-suited for making alkyl-branched symmetric α,ω-diene monomers. To date, the alkyl branches vary from small groups, like the methyl group, to larger ones, like the hexyl group, and even to the adamantyl group.[29, 37]

2.2.2.2 Polymer synthesis

Once the symmetric diene monomer of interest is achieved, the polymerization can be readily realized via acyclic diene metathesis polycondensation chemistry, shown in Figure 2-10.

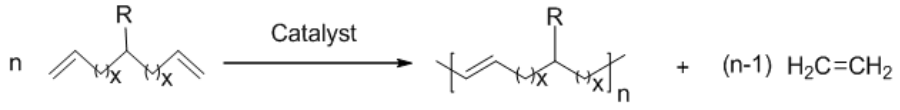

Figure 2-10. Acyclic diene metathesis polymerization scheme in general.

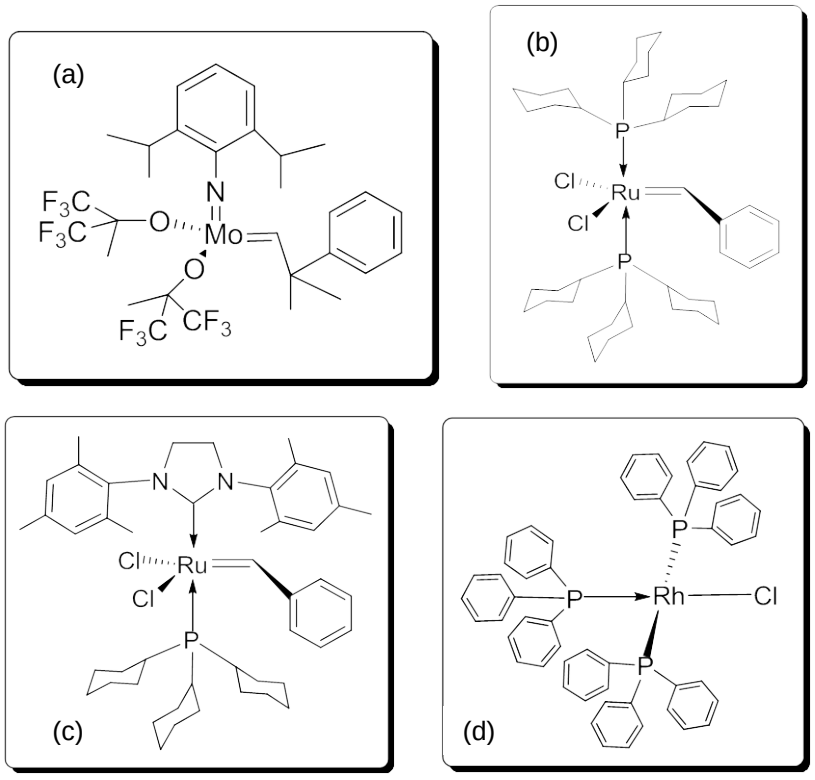

Figure 2-11. Metathesis and hydrogenation Catalysts: (a) Shrock's molybdenum catalyst; (b) 1st generation Grubb's; (c) 2nd generation Grubbs' catalyst; (d) Wilkinson catalyst

Pure, moisture-free monomers are generally polymerized in bulk under mild step polycondensation conditions with the help of organometallic catalysts, such as Shrock's [Mo] catalyst or 1st and 2nd generation Grubb's [Ru] catalysts. Considering that the 2nd generation Grubbs' catalyst can cause isomerization and correspondingly disrupts the precision of ADMET polymers,[62, 63] Shrock's and 1st generation Grubbs' catalyst are much more widely used in ADMET chemistry. The structures of the catalysts are shown in Figure 2-11.

The polymerization is conducted under appropriate vacuum to protect the moisture and air sensitive catalysts. Another prupose of vacuum is to remove gaseous ethylene from the reaction system, and pushing the equilibrium to the right side, i.e., the polymer side, in order to accomplish the polymerization.

The precise alkyl branched ADMET polymers can be readily produced by hydrogenation of the unsaturated products in Figure 2-10 with exhaustive gaseous hydrogen at relatively high pressure and temperature, as illustrated in Figure 2-12.

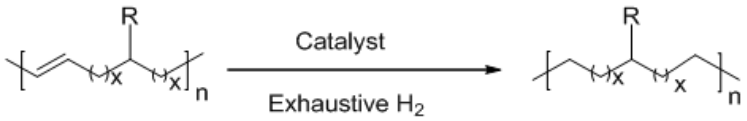

Figure 2-12. Hydrogenation of unsaturated ADMET precision polymers

ADMET is such a useful but simple chemistry. It provides a unique way to transfer the symmetry in the α,ω-diene monomers to the unsaturated and eventually the saturated ADMET precision polymers. However, due to the nature of ADMET polymerization, the precisely branched ADMET polymers possess controlled primary structure, but undetermined stereochemistry; the orientation of branches in principle can

be at any direction with respect to the ethylene backbone. Moreover, constrained by the essence of step condensation, the molecular weights (M_w) of these polymers is normally less than 100,000 g/mol, which are not comparable with that of commercial polyethylenes produced via chain propagation chemistry.

Purely linear polyethylene can be treated as a perfect model for commercial polyethylene, as well as for ADMET precision polyolefins, because of its non-branched structure. The synthesis of linear ADMET PE is quite simple: ADMET polymerization of 1,9-decadiene followed by hydrogenation, shown in Figure 2-13.

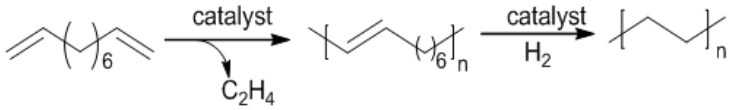

Figure 2-13. Laboratory synthesis of linear ADMET PE. Step 1: ADMET polymerization of 1,9-decadiene; step 2: hydrogenation of unsaturated linear PE

2.2.3 Synthesis of ADMET Random Polymers

To model the mechanized random polyethylene structures, the need to study the effects of "randomness" of branch frequency is fulfilled by the so-called "ADMET random polymers", which have controlled branch identity but random distribution of branches along the main chain. These ADMET random polymers with irregular branch spacing can be easily yielded by copolymerization of two symmetric α,ω-diene monomers possessing various branch spacing,[31, 32, 37] seen in Figure 2-14. By carefully controlling the ratio of the two monomers, one can calculate the average branch concentration. Or with the required branch concentration in mind, one can easily deduce the mixing ratio of the two starting monomers. Based on this, pairs of precision and

random ADMET polyolefins have been successfully synthesized in order to compare their macroscopic behaviors.[32, 37]

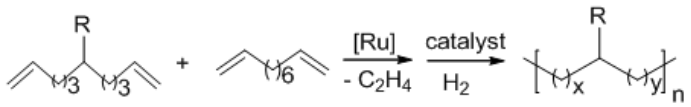

Figure 2-14. Synthesis of ADMET random polyolefins with irregular branch spacing

Of course, to model the effect of "randomness" of branch identity, another type of ADMET random polyolefin can be similarly achieved by copolymerizing two diene monomers with various branch identities followed by hydrogenation. The scheme of synthesis is illustrated in Figure 2-15. So far, this type of ADMET random polymer has generated little attention and is included for completion of "randomness" influence. Recalling that low density polyethylene contains both short-chain and long-chain branches, the 2nd type of ADMET random polymers will be suitable structural models for understanding the effects of unequal branch identity in LDPE.

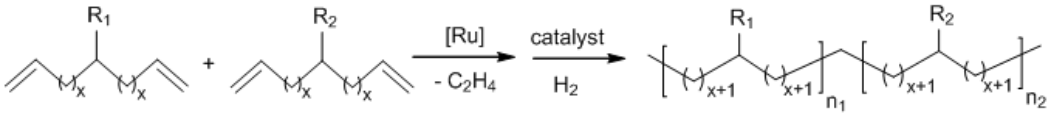

Figure 2-15. Synthesis of ADMET random polyolefins with unequal branch identities

2.3 Comparison of Commercial Polyethylene (PE) to ADMET PE

As mentioned, different types of commercial PE, whether Ziegler-Natta catalyzed or metallocene catalyzed, are produced via conventional chain propagation chemistry. In contrast, ADMET polymers are based on step polycondensation chemistry. Their

totally different polymerization mechanisms result in microstructures with both similarities and variations: the same polyethylene backbone but different branching.

2.3.1 Structure Modeling

It is well established that the type, size, content, and distribution of branches significantly affect the physical properties of PE-based materials. Although numerous researches have been undertaken on the subject, the influence of branching is still unclear due to the complexity of macromolecules. This in turn constrains the manipulation of production processes and understanding of the end products.

Among the unclear fields in PE chemistry, some questions generate particular interest in this dissertation work. One is the location of branches. It is commonly accepted that the sections of polyethylene main chains without defects maintain higher priority to crystallize than the sections with defects.[8, 9, 22, 48, 64-66] Thermodynamically, small branches, like the methyl groups, are capable of being incorporated into the crystalline regions.[2, 8, 21] As for larger branches, polymer scientists tend to believe that larger groups are present only in the non-crystalline regions. The question then arises. *How large can the branches be and still be incorporated into the unit cells?* LLDPE differs from LDPE, in that the former has only short-chain branches while the latter has both short-chain and long-chain branches. These materials exhibit essentially distinguished physical properties. Therefore, unveiling the location of branches in various phases could be very helpful for understanding their effects on the macroscopic properties.

The influence of branch content forms another interesting subject. As illustrated in Figure 2-2, branch content influences the density and degree of crystalline for PE resins. Also, the mechanical properties, such as ductility, are dependent directly on the

branch concentration. Polyethylene sequences with no or small defects/branches tend to pack into ordered structures. Since the polymer chains are “rigid” in terms of folding, *what is the shortest branch spacing needed to maintain the all-trans polyethylene structure in crystalline regions?*

To answer the two questions mentioned above, a typical experimental design will be addressed to vary the parameter of interest while fixing the rest of the variables. For instance, to determine how large the branches can be when incorporated into the crystalline domains, one could fix the branch content and branch distribution and vary only the size of the branches. However, this is not feasible for merchandized polymeric materials.

The advent of ADMET chemistry offers such required structure models through determined primary structures: the branch identity and branch spacing can be controlled, according to the synthetic scheme of ADMET polymers in Figure 2-7. Therefore ADMET polyolefins can serve as excellent models for commercial PE-based structures.

If the variables in PE-based structures can be treated as freedoms of a spot in three-dimensional (3D) space, the relationship of ADMET precision polymers, ADMET random polymers, and commercial PE can be interpreted as cartoons shown in Figure 2-16. Three variables in terms of branching are present in commercial polyethylene structures: the branch identity, branch spacing, and the heterogeneity of branch distribution. The three axes $+x, +y, +z$ indicate the three variables, respectively. Since none of the branching variables is determined for any PE-based commercial material, the merchandized structure therefore has three types of freedom. Such a structure can

be cartooned as mixture of spots with various coordinate (x, y, z) representing (branch distribution, branch spacer, branch identity), illustrated as the red cuboid in Figure 2-16 (c).

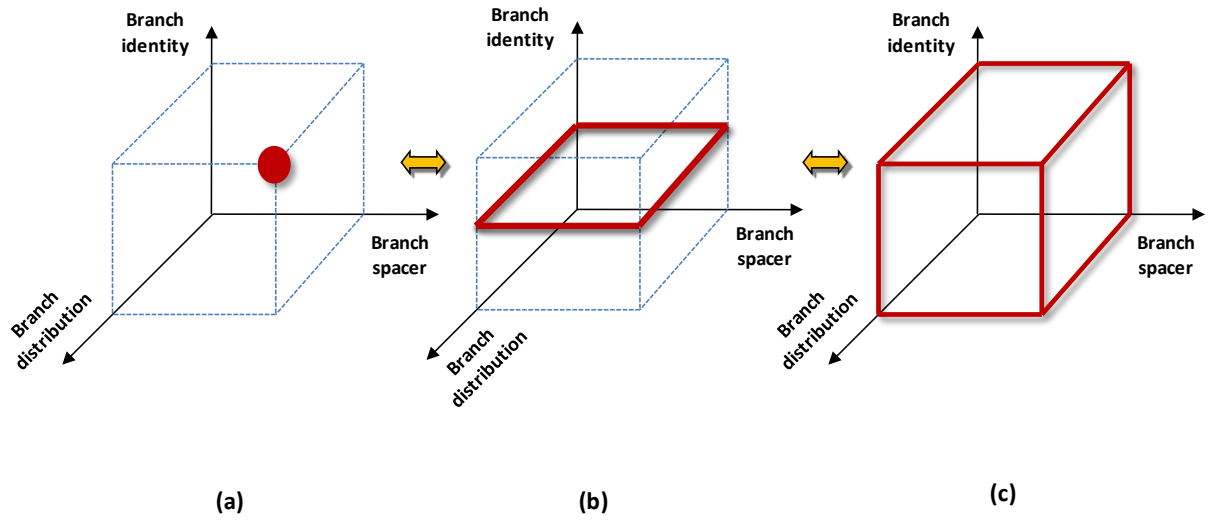

Figure 2-16: Correlation of ADMET PEs to commercial PE: (a) ADMET precision polyolefin, (b) ADMET random polyolefin, and (c) commercial PE

As far as ADMET precision polyolefins are concerned, the branching freedom is actually zero—for a specific ADMET precision polyethylene structure, the branch spacer (z-axis), branch distribution (x-axis), and branch identity (y-axis) are fixed once the polymer is prepared. Therefore, ADMET precision polyethylene can be represented by one defined spot in the coordinate system, illustrated as a red spot in Figure 2-16 (a).

The case for ADMET random polyethylene falls in middle of above two extreme conditions: it encompasses two branching variables (branch spacer and branch regularity) and one fixed branching parameter (branch identity), if the ADMET random polyolefins in Figure 2-15 are sampled. Therefore, the structure of a specific ADMET random polyethylene can be cartooned as mixture of spots on a horizontal surface (x, y)

with fixed z axis (branch identity is fixed), illustrated as a red rectangular surface in Figure 2-16 (b).

The above structure modelling cartoons allow PE structures to be pictured as follows: from point (ADMET precision PE) to surface (ADMET random PE) to 3D structure (commercial PE). Therefore, one can declare confidently that ADMET polymers provide beautiful structural models for the commercial PE-based materials by allowing investigation of the branching variables separately. This understanding of ADMET polymers, both precision and random, will in no doubt decipher the complex structure-property-performance for the PE-based commercial materials.

2.3.2 Comparison of Physical Properties

ADMET polymers exhibit very different physical behaviours from the commercial PEs due to the introduction of precision into the structure. The thermal behaviours of these two families of PE are compared in Figure 2-17. The peak melting temperatures of commercial PEs (HDPE, LDPE, LLDPE, and VLEPE) are shown on the top part. The peak T_ms observed for several series of ADMET precision and random polyolefins sampled with methyl-branched and butyl-branched polymers are shown below the commercial ones. It is clear that by varying branch identity or spacer, the T_ms for ADMET polymers can span around 200 ºC. Such a wide range not only covers the melting range for commercial PEs but also extending the T_m to even lower temperatures.

The **PE-X-Methyl**, a group of ADMET precision polyethylenes with methyl branches regularly displaced on every X^{th} carbon along the backbone, with branch spacer X ranging from 7 to 39 (corresponding to a branch content of 143 to 25 methyl

groups / 1000 backbone carbons), exhibits peak melting points ranging from -60 ºC to 92 ºC, spanning around 150 ºC.[26, 28] In contrast, the group of random versions, **RPE-$\bar{X}$-Methyl**, denotes a series of ADMET random polyethylenes with methyl branches irregularly displaced on the backbone. Calculated from the ratio of the starting α,ω diene monomers (refer to Figure 2-14), the average branch spacer $\bar{X}$, which defines the average position of the branch on each and every $\bar{X}^{th}$ backbone carbon, can range from 17 to 666 (corresponding to an average branch content of 55.6 to 1.5 per 1000 backbone carbons).[32] The **RPE-$\bar{X}$-Methyl** polymers display peak melting points range from 50 ºC to 130 ºC.

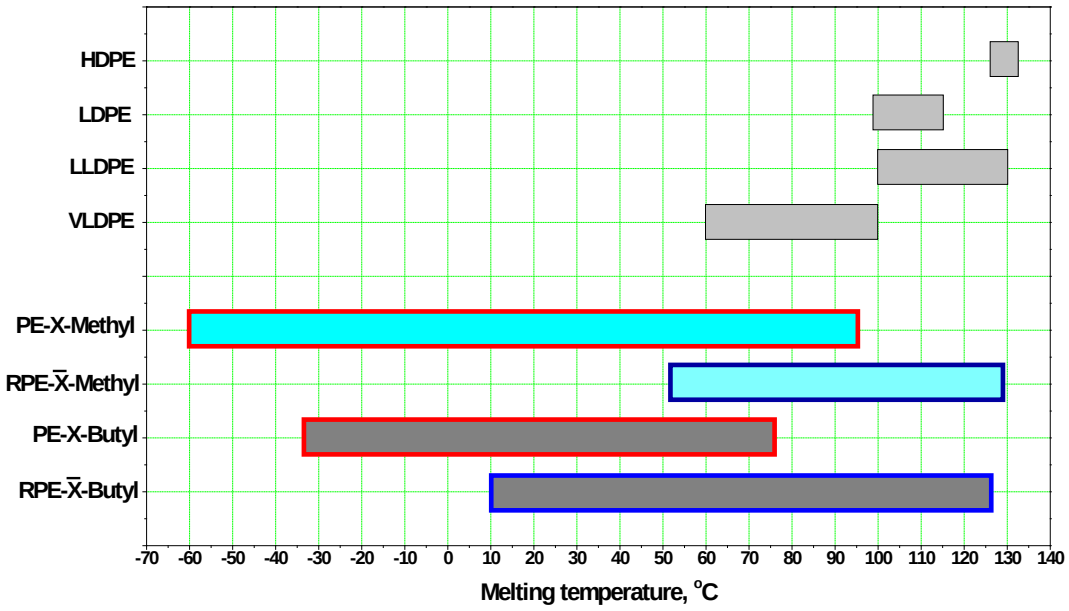

Figure 2-17. Peak melting temperatures of commercial PE, ADMET precision and random PEs. **PE-X-Methyl**: a group of ADMET precision PEs with methyl branches precisely displaced on every X^{th} carbon along the backbone, branch spacer ***X*** ranging from 7 to 39. **RPE-$\bar{X}$-Methyl**: a series of ADMET random PEs with methyl branches irregularly displaced on the backbone, average branch spacer $\bar{X}$ ranging from 17 to 666. **PE-X-Butyl**: a group of ADMET precision PE with butyl groups, branch spacer *X* in the range of 15 to 39. **RPE-$\bar{X}$-Butyl**: a series of ADMET random PEs with butyl groups irregularly pendant on the backbone, average branch spacer $\bar{X}$ ranging from 23 to 400.

As for the butyl-branched ADMET polymers, **PE-X-Butyl** and **RPE-X-Butyl**, represent the precision and random versions, separately. The peak melting temperatures for **PE-X-Butyl** span from -33 ºC to 75 ºC, when branch spacer X ranges from to 15 to 39 (corresponding to branch concentrations ranging from 67 to 25 per 1000 backbone carbons). The random polymers **RPE-$\bar{X}$-Butyl** obtain peak melting temperatures span from 10ºC to 126 ºC, when average branch spacer $\bar{X}$ varies from 23 to 400 (corresponding to branch contents ranges from 43.5 to 2.5 per 1000 backbone carbons).

Noticeably, the melting points of **RPE-$\bar{X}$-Methyl** when $\bar{X}$=666 ($T_m = 129$ ℃), and **RPE-$\bar{X}$-Butyl** when $\bar{X}$=400 ($T_m = 126$ ℃), are rather close to the melting temperature of HDPE ($T_m = 125{\sim}132$ ℃), indicating the extreme level of perturbation caused by the branching. Moreover, unbranched ADMET PE has a peak melting temperature of 133 ºC, identical to that of HDPE. However, the melting curves of ADMET polymers observed via differential scanning calorimetry (DSC) are relatively sharper than those of the commercial PEs, implying a much narrower distribution of lamellar structures.[28, 29, 48]

Wide angle X-ray scattering measurements of unbranched ADMET PE has identified the crystal unit cell to be orthorhombic and provided the quantitative unit cell data,[29, 48] as illustrated in Figure 2-18. It is found that the dimensions are rather close to those of the orthorhombic HDPE, seen in Table 2-2. Recalling that the melting point of unbranched ADMET PE is equal to that of HDPE, one can readily conclude that the chain packing behavior and morphological property of ADMET PE are similar to those of commercial HDPE, due to the complete lack of branching in both types of structures.

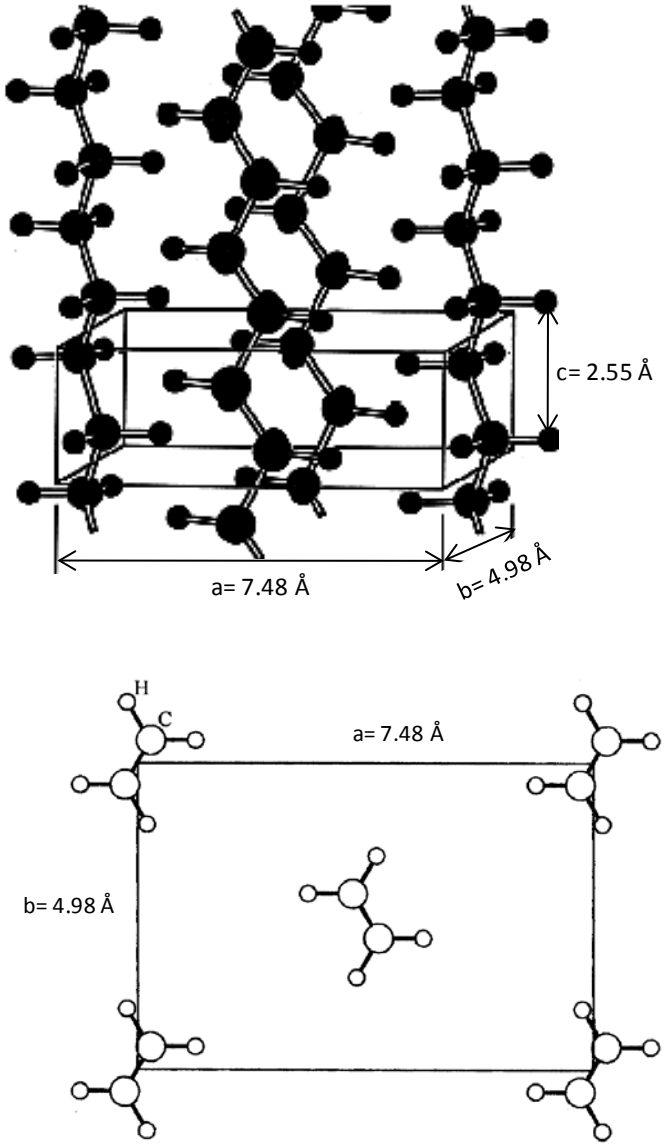

Figure 2-18. Orthorhombic crystal structure of linear ADMET PE: a = 7.48 Å, b = 4.98 Å, c = 2.55 Å. Top is the orthogonal view, bottom is the view along the *c* axis.

Table 2-2. Unit cell dimensions of HDPE and ADMET PE

Polymer	Unit Cell	a, Å	b, Å	c, Å
HDPE	Orthorhombic	7.42	4.95	2.55
HDPE	Monoclinic	8.09	4.79	2.55
HDPE	Hexagonal	8.42	4.56	<2.55
ADMET PE	Orthorhombic	7.48	4.98	2.55

In short, ADMET polymers can function as ideal structural models for commercial polyethylene-based materials by avoiding the complications arising from the collection of organizational structures at both the micro- and macro-molecular scales. Upon introducing heterogeneity into the simple ethylene sequence, the carbon backbone in 3D structure is able to adopt various orientations and motions. It can fold, vibrate, twist, rotate, or entangle. All these morphological related behaviors can to be deciphered using ADMET chemistry and suitable physical measurements.

CHAPTER 3
SOLID STATE NMR SPECTROSCOPY AND X-RAY SCATTERING TECHNIQUES

3.1 Polymer Characterization Methods

Polymer characterization techniques have been developed for decades and are quite established.[2, 21, 67-72] With the development of modern analytical instrumentations, material's structural, dynamic, morphological, thermal, rheological, optical, electrical, mechanical information, etc. are able to be identified and acquired.[4, 68, 73-79] Frequently used characterization methods used in this dissertation are listed in Table 3-1.

Among them, solution nuclear magnetic resonance (NMR) spectroscopy, infrared (IR) spectroscopy, and mass spectrometry (MS) are widely used to determine the compositional structure of polymeric samples. Gel permeation chromatography (GPC), also termed as size exclusion chromatography (SEC) is used to achieve molecular weight and polydispersity (PDI). Transmission electron microscopy (TEM) and atomic force microscopy (AFM) are mainly used to obtain lamellar thickness of the semi-crystalline samples. As for the thermal analysis, differential scanning calorimetry (DSC) is the major tool.

Solid state NMR and X-ray scattering techniques are famous for their powerful characterization abilities and diverse applications for condensed matter.[76, 77] Since we are interested in modeling the commercial polyethylene-based materials, the physical properties of precision polyolefins at solid state are of particular interested. Therefore, SS-NMR and XRD have been selected specifically in this dissertation as two major analytical tools in order to investigate structural, dynamical, and morphological properties of ADMET polymers at condensed state. In the following sections, they will be reviewed in detail.

Table 3-1. Polymer characterization methods used in this dissertation

Method	Principle	Sample	Information	Limitation
GPC	Random coil dimensions of polymer chains are in correlation with their molecular weight	solution state	molecular weight and its distribution	sample in solution; quantitative information referenced to standard with known M_w.
MS	Samples are ionized in the gas phase and the ion abundance is measured as a function of mass-to-charge ratio of the ions.	solution or solid state	composition; primary structure; end-group; molar mass	complex spectra; sample to be relatively stable under laser irradiation
NMR	Nuclear spins interact with the external magnetic field.	solution, molten, or solid sample	structure; end-group; molecular weight; stereo-regularity; dynamics; chain alignment	Only non-zero nuclear spins are active.
IR	The frequency of the absorbed radiation matches the vibration frequency of the bond or group.	thin film or solid sample	structure; functional groups; additives	sample to be infrared-active
TEM	Electrons are transmitted through ultra thin sample and form images by interacting with the sample atoms.	ultra thin film	morphology	sample preparation; data acquired by averaging several characteristic areas in the image
AFM	A cantilever probe interacts with the sample surface and the deviation of the cantilever is monitored versus the distance between the probe and the surface.	solid thin film; in solution	topographic images; force	data acquired by averaging several characteristic areas in the image; slow scanning speed
DSC	Heat flux to the sample is monitored against time or temperature.	solid sample	thermal behaviors: T_m, ΔH, T_c, T_g, C_p	low sensitivity compared to DMTA
XRD	X-radiation interacts with sample atoms and scattered signals are monitored.	solid sample	crystalline structure	not sensitive to non-crystalline structure

3.2 Solid State NMR Spectroscopy

3.2.1 Introduction to NMR

Just as Nobel Prize winner Dr. Ernst commented on the Nobel Lecture[80], "Nuclear spin systems possess unique properties that predestine them for studies of molecules…", it has demonstrated that modern NMR spectroscopy is well-suited in studying polymer structures in solution, molten, and solid state. The principle of structure determination by NMR lies in the fact that a nuclear spin's response in the magnetic field is due to the intrinsic properties of nuclear spins and electron spins. The nuclei with non-zero spin not only interact with the applied magnetic field, but also with the chemical environments they encounter. Since the density of the surrounding electron cloud varies with the chemical environment of the material, the degree of shielding of the nucleus of interest is thus dependent on its chemical structure. This offers the fundamentals of NMR spectroscopy as an excellent tool in understanding structures of polymeric materials. Some parameters of an NMR spectrum are used widely, such as chemical shift and chemical shift anisotropy, peak area, coupling constants, and relaxation times.[20, 57, 81] Unitizing NMR techniques, one can not only confirm the molecular structure of interest, but also exact quite a lot useful information including molecular weight, end-group structure, morphology, bond distance, exchanging rate, relative bond alignment, chain packing patterns, interphase, branching, crosslink, isomerization, and segmental dynamics.[67, 77, 79, 80, 82]

Benefited from the development of quantum mechanics, nuclear magnetic resonance (NMR) was first predicted and measured by Isidor Isaac Rabi in 1937,[82] and in 1944 Rabi won the Noble Prize in Physics for his discovery of NMR. The phenomenon of nuclear magnetic resonance in bulk material were first reported by

Edward Purcell[83] and Felix Block[84] independently, who shared the Noble Prize in Physics in 1952 for “their development of new ways and methods for nuclear magnetic precision measurements." On the way to modern NMR spectroscopy, there are many major breakthroughs contributed, including the introduction of pulsed Fourier transform (FT) techniques,[85, 86] the discovery of magic angle spinning (MAS) and cross polarization, the prediction[87] and realization of Overhauser Effect, the emergence of high magnetic field, and the development of modern multi-pulse sequences.

The basic concepts and applications of solid state NMR techniques on macromolecules have been studied and covered in several classic NMR books[77, 79, 82, 88-90] and review papers[91, 92]. Afterwards basic concepts, theories, and pulse sequences which are closely related or have been employed in the dissertation herein will be discussed.

3.2.1.1 Resonance and chemical shift

In quantum mechanics, each nucleus spins, like the electrons do. Unpaired particles, such as protons, neutrons, and electrons possess a spin of ½. The total nuclear spin, denoted as *I*, is the sum of proton spins and neutron spins. For instance, with one unpaired proton and one unpaired electron, ^{1}H has the total nuclear spin number of ½ and the total electron spin number ½. However, ^{2}H has a total nuclear spin number *I* of 1, arising from one unpaired proton and one unpaired neutron. In NMR, it is the unpaired spins matter—the atoms with unpaired spins have signals in the magnetic field. For instance, ^{13}C is NMR-active while ^{12}C is not. Besides ^{1}H, ^{2}H and ^{13}C, ^{15}N, ^{29}Si, ^{31}P, ^{19}F, ^{35}Cl, ^{37}Cl are NMR-active nuclei and are widely used for structural and dynamic investigations.

When an atom with non-zero nuclear spins is placed in a magnetic field B_0, the spin vectors of the particle align themselves to the direction of the external magnetic field, which is typically the +*z* direction. In modern NMR spectroscopy, upon absorbing energy from a pulse with appropriate radio frequency (RF), a spin is capable of jumping to a higher energy level; when the RF signal is switched off, the spin relaxes back to its lower energy state (a process termed as "procession" in NMR), and energy is emitted simultaneously. This process is called nuclear magnetic resonance. The signals in NMR spectroscopy result from the energy difference between the absorption and the emission; this energy difference is proportional to the spin population difference between the high and low energy levels, which are normally termed as "spin up" and "spin down" for a spin of quantum number ½. Therefore, NMR obtains its sensitivity from the resonance, or exchange of energy at a suitable frequency, referred to as Larmor frequency ω^0, which is determined by the nature of nuclear spin and the strength of the magnetic field obeying the following equation:

$$\omega^0 = -\gamma B^0 \tag{3-1}$$

where γ is the magnetogyric ratio (often termed as gyromagnetic ratio), a constant for each nucleus; B^0 is the magnetic field at the site of the particle.

In this dissertation, three nuclei are focused: ^{1}H, ^{2}H, and ^{13}C. Their spin numbers, natural abundance, and γ values are shown in Table 3-2.

Table 3-2. List of three nuclei investigated in this dissertation.

Nucleus	Ground state spin	Energy levels	Natural abundance	Gyromangnetic ratio γ, rad s^{-1} T^{-1}
^{1}H	1/2	2	99.9885%	$267.5552*10^6$
^{2}H	1	3	0.115%	$41.066*10^6$
^{13}C	1/2	2	1.07%	$67.283*10^6$

A nucleus encounters not only the external electromagnetic field but also the localized magnetic fields induced by the surrounding electron clouds, illustrated in Figure 3-1. The change of the local magnetic field results in a change of resonance frequency termed as chemical shift δ. The sum of applied external field and the induced field generated by the electrons is the local magnetic field that a certain nucleus feels:

$$\boldsymbol{B}^{local} = \boldsymbol{B}^{0} \pm \boldsymbol{B}^{induced} \quad (3\text{-}2)$$

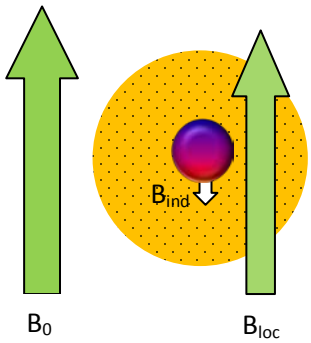

Figure 3-1. Schematic illustration of chemical shift mechanism. B^0 indicates the external magnetic field; B^{ind} is the induced magnetic field due to the surrounding electrons in the applied field; B^{loc} is the localized magnetic field of the nucleus by subtracting/addition of B^{ind} from B^0. The inner circle illustrates the nuclear spin while the outside yellow circle is the surrounding electron cloud.

Although the induced field $B^{induced}$ is only around 10^{-4} of the applied field B^0,[88] it is large enough to give rise to measurable chemical shifts. Since the induced electronic field is directly proportional to the strength of the external magnetic field, the local resonance frequency is related to B^0 as well. However, chemical shift δ is independent on B^0, based on its definition:

$$\delta = \left(\frac{\omega^0 - \omega^0_{TMS}}{\omega^0_{TMS}}\right) \quad (3\text{-}3)$$

where ω^0_{TMS} is the Larmor frequency of the same nucleus in a reference compound (f.g. tetramethylsilane) exposed to the same applied field. Chemical shift is dimensionless.

The induced filed, $B^{induced}$, has a linear relationship with the applied filed B^0:

$$\boldsymbol{B}^{induced} = \boldsymbol{\sigma}^j \cdot \boldsymbol{B}^0 \tag{3-4}$$

where $\boldsymbol{\sigma}^j$ is a 3x3 matrix, termed as *chemical shift shielding tensor* of nucleus site I_j.

The matrix-vector form of Equation 3-4 can be written as:

$$\begin{pmatrix} B_{j,x}^{induced} \\ B_{j,y}^{induced} \\ B_{j,z}^{induced} \end{pmatrix} = \begin{pmatrix} \sigma_{xx}^j & \sigma_{xy}^j & \sigma_{xz}^j \\ \sigma_{yx}^j & \sigma_{yy}^j & \sigma_{yz}^j \\ \sigma_{zx}^j & \sigma_{zy}^j & \sigma_{zz}^j \end{pmatrix} \cdot \begin{pmatrix} 0 \\ 0 \\ B^0 \end{pmatrix} = \begin{pmatrix} \sigma_{xz}^j B^0 \\ \sigma_{yz}^j B^0 \\ \sigma_{zz}^j B^0 \end{pmatrix} \tag{3-5}$$

where the applied static field $\boldsymbol{B}^0$ is assumed to be along the *z*-axis of the laboratory frame. The components of induced filed in the *x*-, *y*-, and *z*-direction are represented by $\sigma_{xz}^j B^0$, $\sigma_{yz}^j B^0$,and $\sigma_{zz}^j B^0$, respectively. Equation 3-5 explains the fact that the induced filed is usually in a different direction to the applied filed. Therefore, the chemical shift at a given nuclear site depends on the molecular orientation with respect to the external field, as well as the location of the nuclear spin within the molecule.

3.1.1.2 Chemical shift anisotropy

Based on the mechanism of chemical shift, the full form Hamiltonian of chemical shift of spin I_j can be represented as:

$$\begin{aligned} \hat{\boldsymbol{H}}_j^{CS} &= -\hat{\boldsymbol{\mu}}_j \cdot \hat{\boldsymbol{B}}_j^{induced} = \hat{\boldsymbol{\mu}}_j \cdot \boldsymbol{\sigma}^j \cdot \boldsymbol{B}^0 \\ &= -\gamma_j \sigma_{xz}^j(\Theta) B^0 \hat{I}_{jx} - \gamma_j \hat{\sigma}_{yz}^j(\Theta) B^0 \hat{I}_{jy} - \gamma_j \sigma_{zz}^j(\Theta) B^0 \hat{I}_{jz} \end{aligned} \tag{3-6}$$

where the symbol Θ is molecular orientation used to emphasize the spatial orientation-dependent of the chemical shift; $\hat{I}_{jx}$, $\hat{I}_{jy}$, and $\hat{I}_{jz}$ are operators for the three components of nuclear spin I_j angular momentum at *x*, *y*, and *z* directions.

Since applied field $\boldsymbol{B}^0$ is much stronger than the chemical shift interaction, Equation 3-6 can be simplified by applying the secular approximation:

$$\widehat{\boldsymbol{H}}_j^{CS} \cong -\gamma_j \sigma_{zz}^j(\Theta) B^0 \hat{I}_{jz} \tag{3-7}$$

where σ_{zz}^j is the experimental measurable shielding tensor when the applied filed pints to *z* direction. Its quantity can be obtained from the following equation[79]:

$$\sigma_{zz} = \sigma_{iso} + \frac{1}{2}\Delta\sigma \cdot (3cos^2\theta - 1 + \eta \cdot sin^2\theta \cdot sin^2 2\phi) \tag{3-8}$$

where σ_{iso} is the isotropic chemical shift, $\frac{1}{2}\Delta\sigma \cdot (3cos^2\theta - 1 + \eta \cdot sin^2\theta \cdot sin^2 2\phi)$ is the anisotropic part with shielding anisotropy $\Delta\sigma$ and asymmetric parameter η, θ and ϕ are the Euler angles,[93] as illustrated in Figure 3-2.

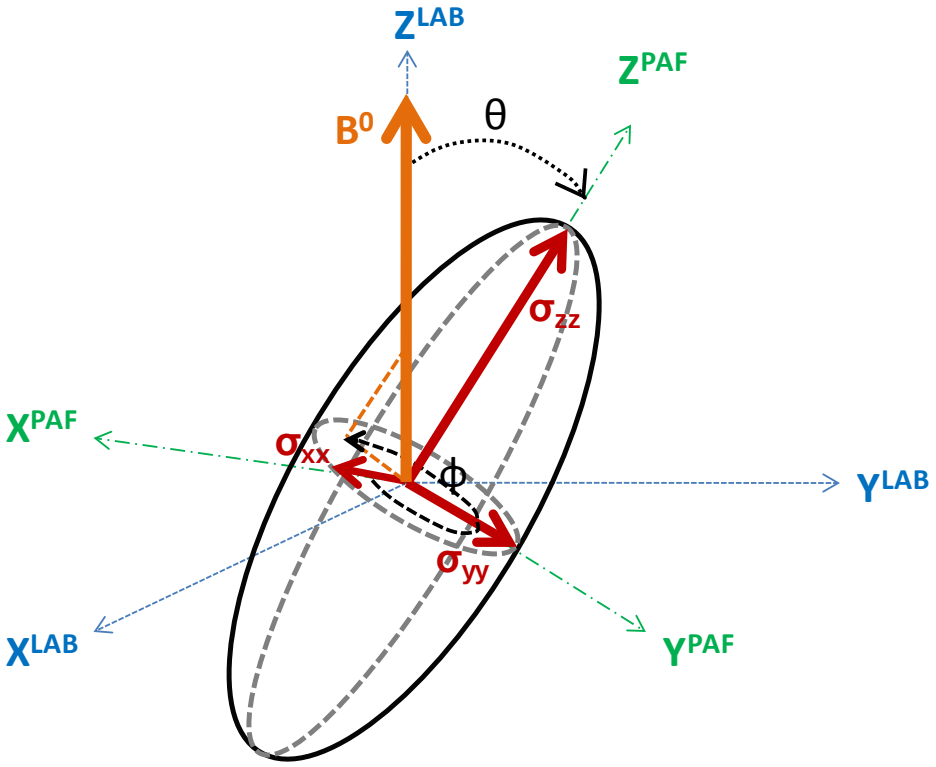

Figure 3-2. The definition of tensor orientation in different coordinate systems. LAB stands for laboratory frame. PAF stands for principal axis frame. θ is the angle between the *z*-axis of PAF and external field $\boldsymbol{B}^0$. ϕ is the angle between the X^{PAF} and the projection of $\boldsymbol{B}^0$ in the *x*-*y* plane of PAF.

The three principal values σ_{iso}, $\Delta\sigma$, and η are defined as follows:

$$\sigma_{iso} = \frac{1}{3}\left(\sigma_{xx} + \sigma_{yy} + \sigma_{zz}\right) \quad (3\text{-}9)$$

$$\Delta\sigma = \sigma_{zz} - \sigma_{iso} \quad (3\text{-}10)$$

$$\eta = \left(\sigma_{yy} - \sigma_{xx}\right)/\sigma_{zz} \quad (3\text{-}11)$$

where σ_{xx}, σ_{yy}, and σ_{zz} are tensor components in the principal axis frame (PAF), as shown in Figure 3-2. Since the chemical shift interaction is related to the spatial orientation with respect to the applied magnetic field, the introduction of PAF largely simplifies the problem by offering a diagonal tensor.

The spectral lineshapes of semi-crystalline polymers are typically called “powder pattern” because of the random orientation of chemical microstructures. CSA patterns are characteristic of nuclear spin’s spatial orientation and its chemical environment, and are sensitive to segmental motions. Figure 3-3 shows three special CSA lineshapes:

(a) The three shielding components are different from each other, $\sigma_{xx} \neq \sigma_{yy} \neq \sigma_{zz}$. However, the asymmetry parameter $\eta = \frac{\left(\sigma_{yy} - \sigma_{xx}\right)}{\sigma_{zz}} \cong 1$, corresponding to static motion or hop of nuclear spin between two spatial orientations.

(b) When a chemical shift tensor has axially symmetry, the CSA lineshape can be signified as Figure 3-3 (b). For this case, $\sigma_{\parallel}$ and $\sigma_{\perp}$ refer to the shielding along and perpendicular to the principle z-axis, where $\sigma_{\perp} = \sigma_{xx} = \sigma_{yy}$, $\sigma_{\parallel} = \sigma_{zz}$, and $\eta = \sigma_{\parallel} - \sigma_{\perp} \neq 1$. This unique CSA spectrum can be assigned to an axial motion of the nuclear spin at site.

(c) When the three components of chemical shift tensor are identical, $\sigma_{xx} = \sigma_{yy} = \sigma_{zz}$, the anisotropy part disappears and the spectrum

collapses to an pure isotropic lineshape with one middle peak left at σ_{iso} frequency. This CSA pattern represents the isotropic motion of the nuclear spin at site.

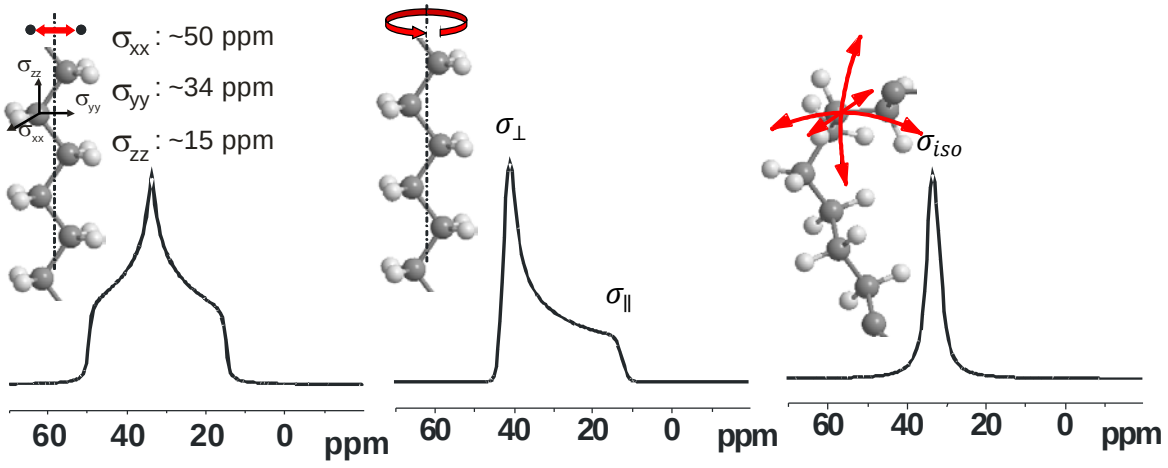

(a) (b) (c)

Figure 3-3. Special CSA lineshapes: (a) static or 180º hopping; (b) axial rotation; and (c) isotropic motion

3.1.1.2 NMR interactions

In NMR, the total Hamiltonian can be expressed as following:

$$\hat{H}_{spin} = \underbrace{\hat{H}_z + \hat{H}_{RF}}_{\hat{H}_{ext}} + \underbrace{\hat{H}_J + \hat{H}_D + \hat{H}_{CS} + \hat{H}_Q}_{\hat{H}_{int}} \quad (3\text{-}12)$$

where Zeeman interaction $\hat{H}_z$, and the interaction with radio frequency (RF) pulses $\hat{H}_{RF}$, belong to external interactions. Indirect spin-spin coupling (*J*-coupling) $\hat{H}_J$, dipole-dipole interaction $\hat{H}_D$, chemical shift $\hat{H}_{CS}$, and quadrupole interaction $\hat{H}_Q$, can be classified as internal interactions.

$\hat{H}_z$ describes the Hamiltonian of an isolated spin in the static, uniform magnetic field, and is much stronger than other interactions when a high magnetic field is applied.

It is $\widehat{H}_z$ that causes the energy splitting into $2I + 1$ energy levels. Arising from the time-dependent RF electromagnetic radiation $\widehat{H}_{RF}$ is unitized to manipulate the internal spin interactions in NMR. Based on this, NMR is capable of provide a wealth of information about the structures, dynamics, interactions, etc. Representing the indirect interaction of nuclear spins through bonding electrons, $\widehat{H}_J$ in SS-NMR is quite small and obtains not many attentions herein. $\widehat{H}_D$, in contrast, is the direct interaction of nuclear spins through space without involving the electron clouds. $\widehat{H}_Q$ describes the quadrupole interaction for all nuclei with a spin number $I > 1/2$, such as ^{2}H. It is generated from the interaction of nuclear quadrupole moment with the gradient of its surrounding electric field at the nucleus site.

For molecules in solution, due to the rapid tumbling of the molecules, the CSA and dipolar interactions are rarely to be observed and line peaks can be obtained. However, in the case of solid samples, the motionally-averaged spin Hamiltonian are dominantly governed by the much stronger short-range dipolar interaction, chemical shift anisotropy, and quadrupole coupling (for $I > 1/2$), which give rise to the undesired line broadening in SS-NMR spectra. Therefore, numerous techniques have been explored to reduce the spectra line width in SS-NMR.

3.1.1.3 Cross-polarization and magic angle spinning

To achieve high quality spectra for solid samples, the spin and space manipulations of NMR interactions are usually adopted. The most useful spin manipulation technique is the cross polarization (CP), while a popular space manipulation method is the usage of magic angle spinning (MAS). The experiment by

combination of these two techniques, CP/MAS, is widely used in SS-NMR for polymeric samples.

For dilute spins, such as ^{13}C, it is hard to obtain NMR signals without any manipulation due to the problems arising from its low natural abundance: low signal-to-noise ratio and very long relaxation time. These problems can be solved by CP. The rich magnetization in the abundant ^{1}H spins can be transferred to the X spins in the sample via the dipole-dipole coupling between ^{1}H and X spins. Since dipolar interaction is distance-dependent, CP is more efficient for spins in the crystalline regions than those in the amorphous regions.

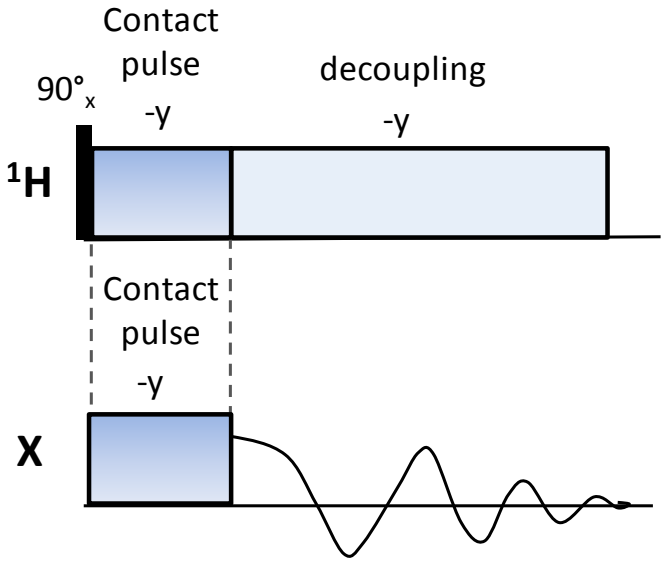

Figure 3-4. The cross-polarization pulse sequence.

Magic Angle Spinning (MAS) is a routinely used method in the vast majority of SS-NMR experiments. It involves rotating the solid sample in a cylindrical rotor at high frequency. The spinning axis is oriented at the magic angle, $\theta_M = 54.7°$, with respect to the applied magnetic field B^0, as shown in Figure 3-5. The major tasks of MAS are to

eliminate the chemical shift anisotropy and heteronuclear dipolar coupling effects, and thus to reduce a powder pattern to a single line at the isotropic chemical shift.

The magic angle of $54.7°$ is calculated from the anisotropic Hamiltonian according to the perturbation equation.[88] For a sample spinning uniformly at an angle θ relative to the applied field, the theoretic anisotropic interaction contains the second Legendre Polynomial factor $P(\theta) = \frac{1}{2}(3cos^2\theta - 1)$ in the constant term.[77] Such a mathematic expression provides a simple but efficient way to eliminate the anisotropy broadening by setting $\theta = 54.7°$ to satisfy $cos^2\theta - 1 = 0$. This angle $54.7°$ is the so-called magic angle. Spinning rate should be fast on the NMR timescale, i.e., the change of molecular orientation has to be fast relative to chemical shift anisotropy, dipolar coupling, etc.[77, 90]

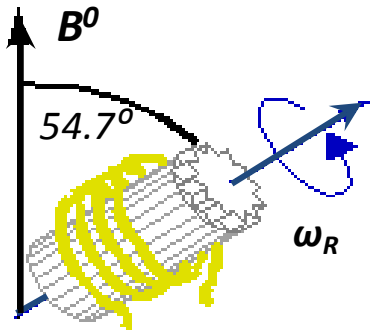

Figure 3-5. The magic angle spinning experiment setup. The angle between the spinning axis and applied field is set to $54.7°$, the magic angle.

3.1.2 NMR Spectrometer

NMR spectrometer has now become a very sophisticated instrument, which has been used widely in chemistry, material science, biology, physics, etc. As Figure 3-6 illustrated, the spectrometer consists of several important components:

- A strong, homogeneous and stable magnetic field—the perfectly uniform magnetic field contributes to the high quality signals by avoiding inhomogeneous broadening and allowing the small changes of Larmor frequency to be resolved. Modern NMR magnet is usually accomplished by using persistent superconducting materials, typically alloys of Nb and Sn. The superconducting coil is immersed in a bath of liquid He which is isolated by a liquid N_2 reservoir. The positional and temporal inhomogeneity can be compensated by the shim coils.
- A *probe*—the probe is inserted into NMR though the centre of the magnet, which is called *bore*. Inside of the probe, the sample is surrounded by a RF coil. RF pulses are exerted on the coil as currents to generate a transient field on the sample, and the response from the sample is then detected by the coil as well. The thermal noise from the RF coil is the major noise in a well-designed NMR spectrometer.
- An *RF transmitter*—it is the RF transmitter that generates controlled RF pulses, either short but high-powered, or long but low-powered.
- A *pulse programmer*—it is used to produce precisely timed pulses and delays;
- A sensitive *RF receiver*—since the NMR signal from the RF coil is in the order of μV, RF receiver is used to capture and amplify the NMR signals.
- A *digitizer* —it is an analogue-digital converter, used to convert the NMR signals (oscillating electrical current) into digital form (a sequence of ‘ones’ and ‘zeros’) which can be stored in computer memory.
- A computer—as the heart of NMR spectrometer, it controls all the components and processes the data.

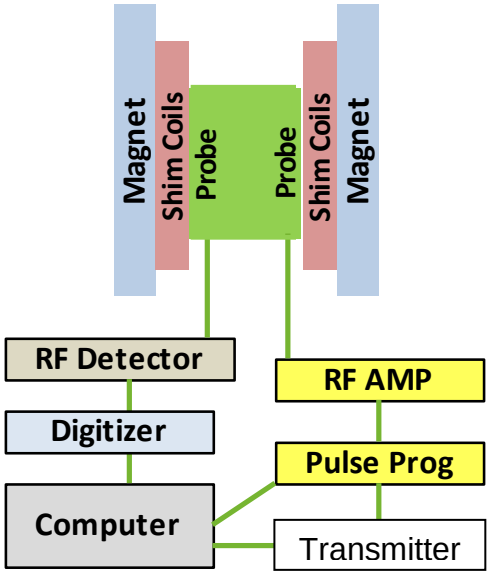

Figure 3-6. Schemetic overview of a NMR spectrometer

The magnets for solution and SS-NMR are the same. It is the probe that determines the state of the samples that can be examined. Typical probes used in SS-NMR include various magic angle spinning probes, static wideline probe, etc.

3.1.3 Introduction to Deterium Solid State NMR

Deuterium is the isotope of hydrogen with extremely low natural abundance and a spin number of one. Like other nuclei with spin number *I* greater than ½, ^{2}H NMR lineshapes are mostly dominated by the quadrupole interaction, which arises from the interaction of the nuclear electric quadrupole moment with the surrounding electric field gradient (EFG) at the nucleus. Powder NMR spectra of ^{2}H of static samples consist of doublet patterns which arise from the two spin transitions: $+1 \leftrightarrow 0$ and $0 \leftrightarrow -1$. These doublet are called Pake patterns with their horns split by $\frac{3}{4}[e^2qQ/h]$, falling in the range of 105-165 kHz for organic samples. The Pake patterns and the doublet splitting are shown in Figure 3-7.

The quadrupole splitting between the doublets is given by:

$$\omega_Q = \frac{3}{2}[e^2qQ/h]\left[\frac{1}{2}(3cos^2\theta - 1) - \frac{1}{2}(\eta\, sin^2\theta \cdot cos2\phi)\right] \qquad (3\text{-}12)$$

where e^2qQ/h is the quadrupole coupling constant, in the range of 140-220 kHz for organic compounds; θ and ϕ are the Euler angles which define the principle axis frame of the EFG relative to the laboratory frame at the deuteron site; and η is the quadrupolar asymmetry parameter of the EFG.

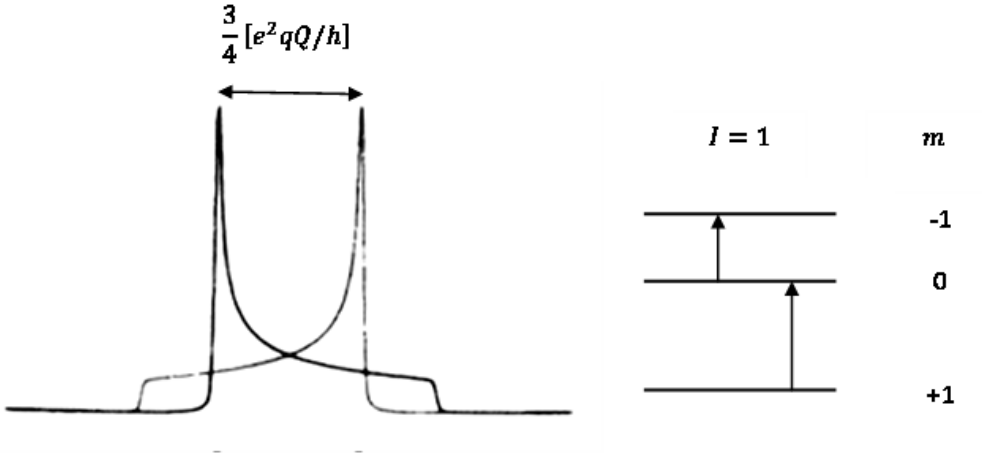

Figure 3-7. Pake pattern of ^{2}H NMR. The doublet splitting is due to the two allowed spin transitions. Their horns are split by ¾ of the quadrupole coupling constant.

^{2}H NMR is particularly well-suited for investigation of molecular dynamics. In polymer chemistry, by isotope labelling of the specific site of interest, ^{2}H NMR can be very informative in terms of molecular motions. The C-D bonds give birth to the electron filed gradient, which is axially symmetric around the C-D bond. Such a fact allows the molecular motions to be monitored through the orientation of an individual C-D bond, largely simplifying the NMR data interpretation. Moreover, the moderate width of powder patterns, as compared to other quadrupole nuclei, and the high dynamic range of 10^4 to

10^6 Hz, make ^{2}H NMR extensively effective and applicable in dynamics studies, via spectra lineshape analysis, relaxation time measurements, and exchange experiments.

3.1.4 Pulse Sequences

The success of NMR as a powerful characterization tool for polymer chemistry is undoubtedly related to the highly developed pulse sequences. Some of the ones that turn out to be quite useful for polymer studies will be discussed in below.

3.1.4.1 Quadrupole echo

The quadrupole echo, also termed as “solid echo”, is the most common pulse sequence used in ^{2}H NMR measurements. As a result of the strong quadrupole coupling, deuterium spectra acquired with one pulse excitation can have extremely broad lines which display fast decaying free induced decays (FIDs). Due to the occurrence of the receiver “dead time” (a delay of measurement after a pulse), the loss of signal arising from the rapidly delaying FID accounts for a significant part in the total FID, which leads to severely distorted spectral lineshapes. This phenomenon is negligible in solution NMR because the FID decays much more slowly. On the contrary, in solid state NMR, this effect cannot be ignored. Fortunately, an “echo” sequence can resolve this problem. Quadrupole echo is such a method.

Quandrupole echo has been widely used to study slow motions of polymers at condensed state.[79, 91, 94, 95] Its pulse sequence can be seen in Figure 3-8. The magnetization dephasing due to the quadrupolar interaction can be refocused by the second 90º pulse and hence form a quadrupolar echo. By taking the standard Fourier transform of the data starting at the echo maximum, there is no signal loss due to a dead time delay.[77, 91]

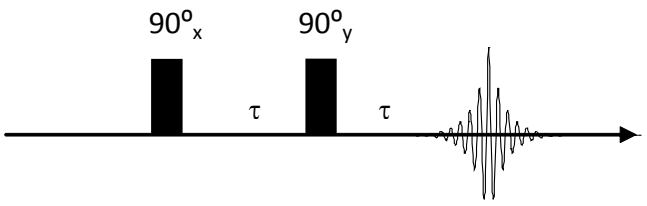

Figure 3-8. The Quandrupole echo pulse sequence. Two 90º pulses are applied; experimental signals are acquired after echo delay τ.

3.1.4.2 SUPER

SUPER, which stands for "Separation of Undistorted Powder patterns by Effortless Recoupling", is a newly developed recoupling technique used to obtain undistorted, quasi-static CSA powder patterns under magic angle spinning.[96] The pulse sequence is shown in Figure 3-9. SUPER can be conducted under CP condition as Figure 3-9 illustrated, or single pulse excitation (SPE) (not shown here). The latter can be easily realized by removing the CP part without affecting the nature of SUPER pulse sequence.

As mentioned previously, high resolution NMR in solids can be achieved via MAS by spatially averaging anisotropic spin interactions, which actually contain valuable dynamical and structural information. To avoid this sacrifice, recoupling techniques, which can selectively reintroduce anisotropic interactions while maintaining high resolution via MAS, have been explored. Among them, SUPER attracts researcher's attention because of its robustness: being insensitive to pulse-length related imperfections, being compatible to a wide range of hardware, and works effectively under standard power levels and spinning rates.[96]

SUPER pulse sequence is derived from a similar sequence reported by Tycko and co-workers.[97] By replacing the 180º pulses with the 360º pulses, SUPER yields two dimensional spectra with one dimension providing recoupled chemical shift anisotropy (CSA) information and the other dimension providing the high resolution spectrum. Using SUPER, isotropic and anisotropic chemical shifts can be separated effectively.

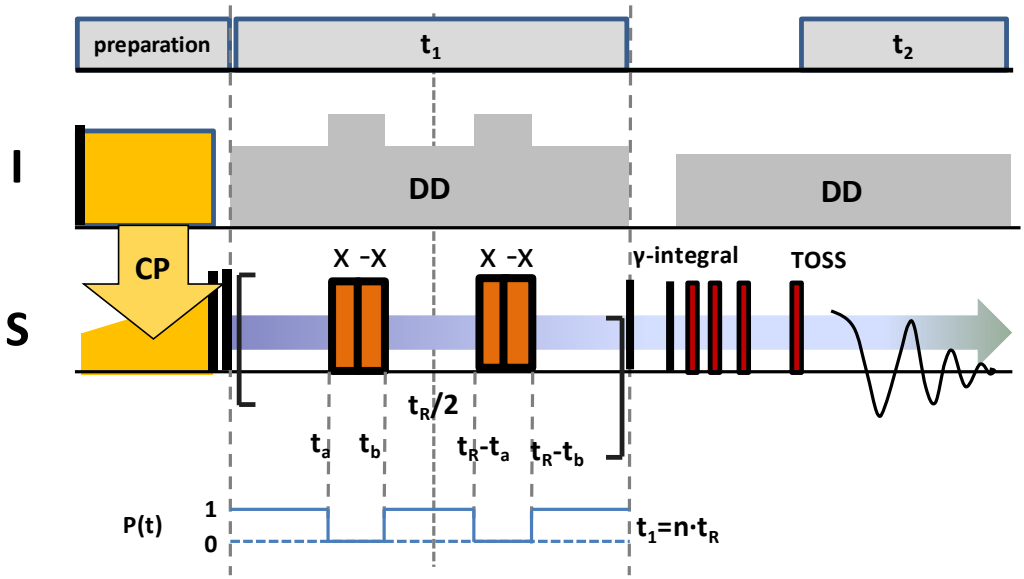

Figure 3-9. The SUPER pulse sequence under CP condition: DD stands for dipole decoupling; CP indicates cross polarization; x and -x are 360º pulses. TOSS (total suppression of spinning sidebands) and γ-intergral are used to suppress the sidebands up to the fourth order.[98]

3.1.4.3 REDOR

Like SUPER, REDOR (rotational-echo double resonance) and REREDOR (rotor-encoded REDOR) are recoupling techniques used to selectively reintroduce anisotropic interactions including dipole-dipole coupling under magic angle spinning. The difference between SUPER and REDOR lies in that the former provides CSA information while the latter studies dipole-dipole interaction. The pulse scheme of REDOR is shown in Figure

3-10. The major idea of this technique is to use a series of well-spaced 180º pulses to prevent the heteronuclear dipolar coupling from being averaged to zero of by MAS. Since the dipole-dipole coupling depends on the interspin-distance, REDOR is widely used to investigate molecular structure, especially the heteronuclear distance and angle determination.

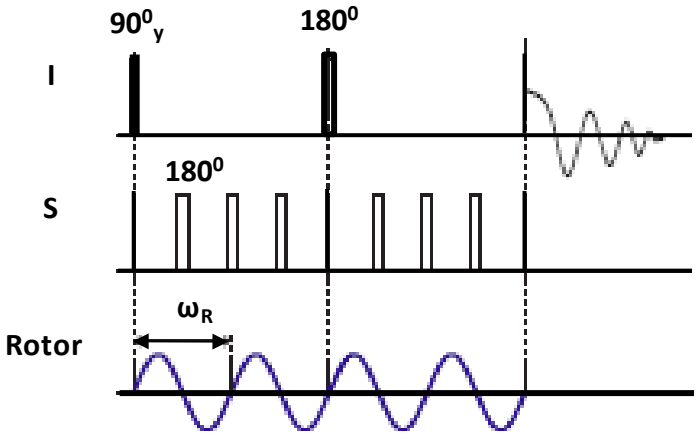

Figure 3-10. The rotational-echo double resonance (REDOR) pulse sequence.

3.1.4.4 REREDOR

REREDOR (rotor-encoded rotational-echo double resonance) originates from the REDOR sequence but is more sensitive in determination of heteronuclear ^{1}H-X dipolar couplings. The improved sensitivity arises from the dipolar coupling.

It is a two-dimensional NMR experiment with high resolution spectrum in the direct dimension and spinning sideband patterns in the indirect dimension. Usually a fast MAS with rate of 25 kHz or higher is performed to offer the desired spectral resolution as well as informative sidebands. The scheme of REREDOR pulse sequence is shown in Figure 3-11. Starting with the preparation of initial S magnetization via CP transfer

(single pulse excitation also works), REREDOR sequence is composed of two REDOR blocks followed by indirect dimension t_1 after each block. After recoupling, spin S magnetization will gain several phase factors, which are related to the recoupling constant and can be calculated from signal intensity of spin S. The quantitative dipolar coupling information can be extracted from the spinning sideband fitting.

Under very fast MAS, REREDOR is capable of studying the dipole-dipole coupling of XH_n groups in either rigid or mobile systems, where X can be isotopically dilute, such as ^{13}C. This makes REREDOR a useful technique for investigation of the molecular structure in polymeric materials.

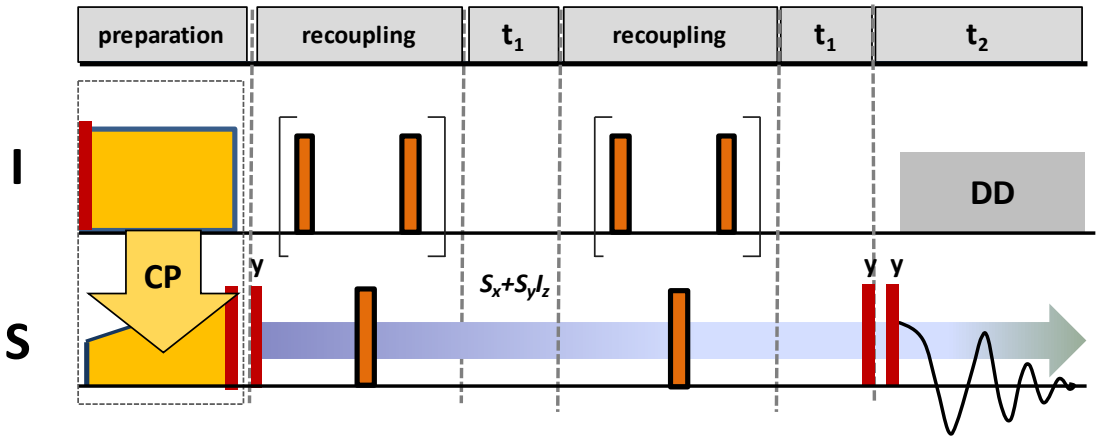

Figure 3-11. The pulse sequence of CP-based Rotor encored REDOR (REREDOR)

3.2 X-ray Scattering Techniques

3.2.1 Introduction

X-ray diffraction (XRD) technique can be dated back to the time of Bunn.[11] Nowadays, it has become one of the mature tools used to investigate morphological properties of polymeric materials. Like light scattering and neutron scattering, X-ray scattering is a technique utilizing the X-ray as the incident media to study the inner

structure of interphase orientation of various materials, such as metals, ceramics, alloys, and polymers. Both qualitative and quantitative information can be obtained from XRD, including dimensional parameters of unit cells, degree of crystallinity, lamellar periodicity, and degrees of orientation.

X-rays, like light, are electromagnetic radiation with wavelength in the range of 0.1 Å to 100 Å. When X-rays pass though a substance their energy is dissipated by the ejection of orbital electrons and by scattering, resulting in the loss of the X-ray intensity. The interaction of incident X-ray and sample atoms can be complex with several processes competing: elastic scattering, inelastic scattering, fluorescent X-ray, photoelectron releasing, and heat accumulation. The elastic scattering (also named *Thomson scattering*), which has the scattered X-rays with the same energy, i.e., wavelength as the incident radiation, is the main type of scattering involved in XRD and this dissertation. Since the emitted X-rays contain characteristic structural information, XRD has been widely used in polymer science and industry.

3.2.2 WAXS and SAXS

Wide angle X-ray scattering (WAXS), sometimes termed as wide angle X-ray diffraction (WAXD), defines the scattered X-rays occurring at the angle of 2θ within the range of $5°\sim120°$, where 2θ (the so-called *scattering angle*) is the angle between the incident and scattered X-rays, as shown in Figure 3-12. In the case of PE, the most useful information extracted from the 2θ range of $5°\sim50°$, corresponding to the atomic spacing ranging from $20\sim2$ Å, if Cu *Kα* radiation is used. WAXS measurement can provide information of atomic spacing (*d*-spacing), unit cell parameters, as well as the degree of crystallinity.

Small angle X-ray scattering (SAXS) is the twin of WAXS by sharing many similarities such as the scattering theories and the instrumentation schemes. The basic difference of these two methods lies in the scattering angle 2θ: SAXS detects the 2θ value smaller than $5°$. Typical 2θ for Cu *Kα* radiation falls in the range of $0.2°\sim2°$, corresponding to atomic spacing of $440\sim44$ Å, which is much larger than the dimension that WAXS can detect. Consequently, SAXS equipment is much more sophisticated than WAXS resulted from the small scattering angles.

Besides WAXS and SAXS, there are several other XRD methods existing, such as medium angle X-ray scattering (MAXS), ultra small angle X-ray scattering (USAXS), classified by the scattering angle as well.

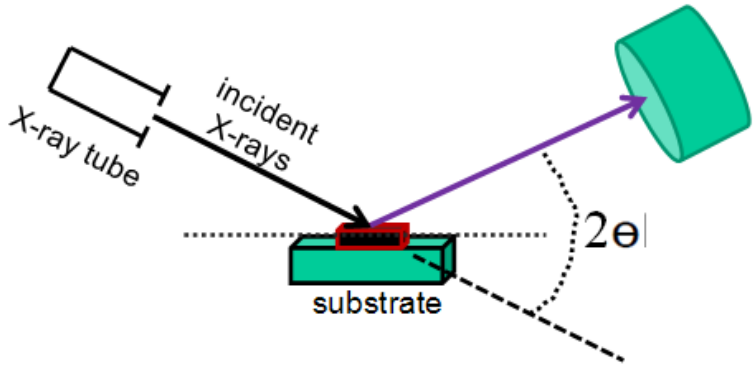

Figure 3-12. Schematic illustration of X-ray scattering for solid samples

3.2.3 Bragg's Law

In crystallography, Bragg's law is widely used. Since the incident X-rays are always in phase and parallel, when they interact with the sample atoms, the scattered X-rays interfere constructively and the differences in the beam travel path equals to some integer multiples of the wavelength. The occurring of such constructive interference ensures the X-ray beams to be diffracted at the same angle as the incident

beam with respect to the atomic plane. This condition is summarized in Figure 3-13, named as Bragg's law:

$$n\lambda = 2d \cdot \sin\theta \tag{3-13}$$

where λ is the wavelength of incident radiation, d is the distance between the adjacent parallel crystallite planes, and n is the integer indicating the order of diffraction.

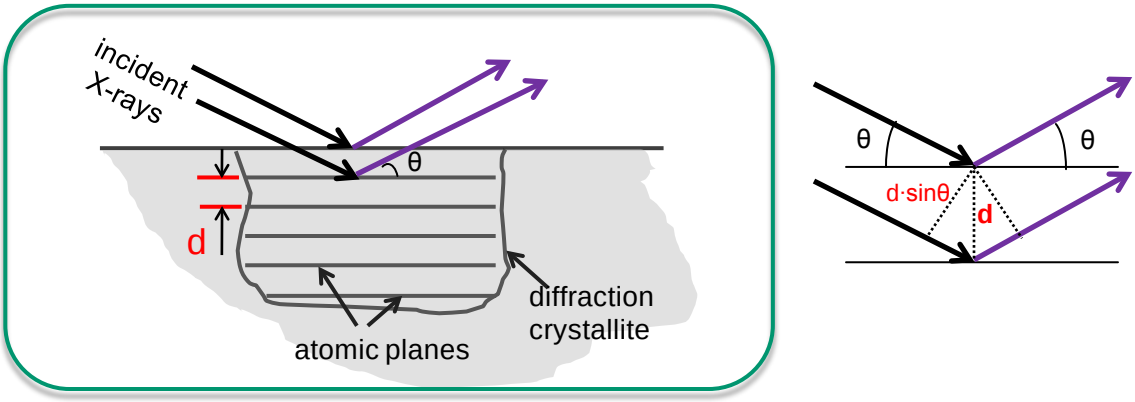

Figure 3-13. Scheme of Bragg's Law

CHAPTER 4
INFLUENCE OF BRANCH FREQUENCY ON DYNAMICS AND STRUCTURE OF PRECISION POLYMERS

4.1 Introduction

The precision polymers exhibit significantly different thermal behaviors compared to the commercial polyethylenes, as described in Chapter 2. It is believed that the branch identity and branch frequency influence not only inter- but also intra-chain packing and the corresponding macroscopic properties. Herein, the branch identity is fixed while the branch frequency varies. To simplify the study, a series of methyl branched polymers possessing various branch concentration has been chosen in order to investigate how and why the branch frequency will influence the microscopic properties of precision polyolefins, therefore to help us understand the structure-property-performance relationship in commercial PE-based materials.

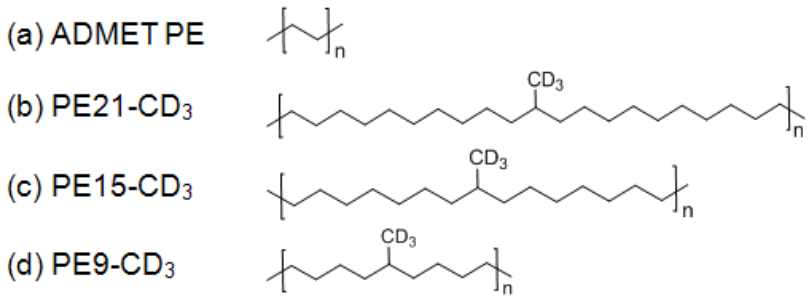

Figure 4-1. Structure of precisely branched polymers: (a) linear ADMET PE, with no branches; (b-c) PEn-CD_3, with deuterated methyl group on each and every n^{th} carbon.

Four precise polyolefins including three perdeuterated polymers were prepared to study the conformational defects: **ADMET PE**, **PE21-CD_3**, **PE15-CD_3**, and **PE9-CD_3**, in which the number after "PE" indicates the spacing of two adjacent CD_3 branches along the backbone. For instance, **PE21-CD_3** specifies the ADMET polyethylene with CD_3

group regularly displaced on each and every 21st carbon along the ethylene backbone, seen in Figure 4-1.

4.2 Polymer Synthesis

4.2.1 Monomer Synthesis

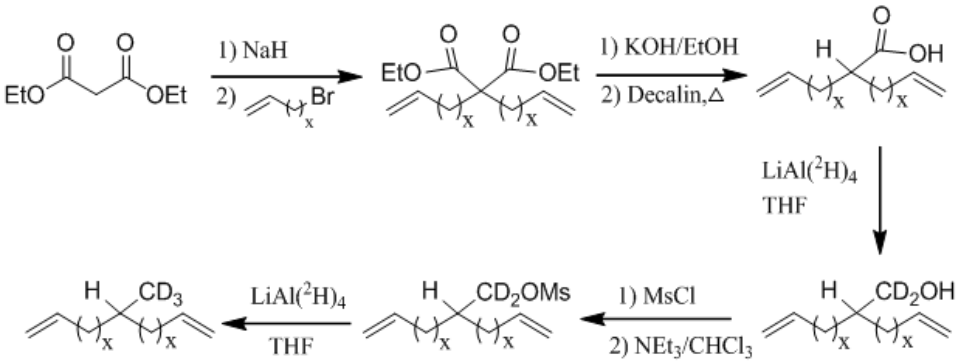

x	Monomer	Polymer
3	1	PE9-CD_3
6	2	PE15-CD_3
9	3	PE21-CD_3

Figure 4-2. Synthetic methodology used to produce perdeuterated monomers: when x=9, monomer 1 for PE21-CD_3; x=6, monomer 2 for PE15-CD_3; and x=3, monomer 3 for PE9-CD_3.

The model polyolefins were synthesized via ADMET step polymerization using a modification of the procedure described before.[26, 31] Synthesis of the three symmetric diene monomers containing precisely displaced deuterated methyl branches was achieved based on a modification of the synthetic methodology in literature, described in Figure 4-2. Basically, the synthesis started with the diethylmalonate being disubstituted with an alkenyl bromide possessing the appropriate methylene spacing. The resulting diester was then saponified and decarboxylated to yield the corresponding

monoacid. Upon selective reduction of the acid with lithium aluminum deuteride, the acid was able to be reduced to the primary alcohol, which was mesylated and then reduced via deuteride displacement to offer the symmetrical diene of interest. The frequency of the CD_3 branches can be varied by choosing starting alkenyl bromides possessing various methylene spacing, e.g. when 5-bromo-1-pentene (x=3) is used, the resulting symmetric diene is the monomer of PE9-CD_3.

4.2.2 Polymer Synthesis

The precision polymers sampled for this study were synthesized by ADMET step polycondensation chemistry. In general, the α,ω-diene monomer is polymerized in the presence of Schrock's or Grubbs catalyst under mild step polymerization conditions to form the unsaturated precision polymer, which is then exhaustively hydrogenated to offer the saturated precision polymer, as shown in Figure 4-1. For linear ADMET PE, 1,9-decadiene was used as the starting compound for polymerization.[28]

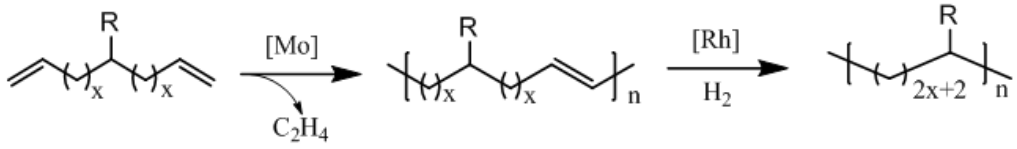

R	X	Polymer
H		ADMET PE
CD_3	9	PE21-CD_3
CD_3	6	PE15-CD_3
CD_3	3	PE9-CD_3

Figure 4-3. Synthetic methodology used to produce precision polyolefins via ADMET chemistry.

4.3 Characterization of Deuterated Polymers

The sample polymers were characterized using various analytical methods. Besides the normal characterization methods, such as thermal analysis, molecular

weight determination, and structure confirmation, the morphology and dynamics were investigated by solid state NMR spectroscopy and scattering techniques.

4.3.1 Basic Characterization

The basic characterization data of the deterated precision polymers studied herein are presented in Table 4-1.

Table 4-1. Basic characterization data of deuterated and protonated precision polymers

Model Polymer	Methyl Branches/ 1000 Backbone Carbons	M_w [a] (kg/mol)	PDI [b]	T_m [c] (K)	ΔH_m [c] (J/g)	T_g [d] (K)
ADMET PE	0	68	2.7	407	205	---
PE21-CD_3	48	56	1.9	335	101	---
PE15-CD_3	67	53	1.9	312	79	---
PE9-CD_3	111	56	1.8	264	30	---
PE21-CH_3	48	34	1.7	335	103	229
PE15-CH_3	67	29	1.7	312	82	229
PE9-CH_3	111	30	1.7	259	28	230
PE7-CH_3	143	13 [e]	---	213	19	---
PE5-CH_3	200	28 [e]	---	amorphous		208

a. Gel permeation chromatography (GPC), polystyrene standards
b. Polydispersity index (M_w/M_n), from GPC
c. Determined by differential scanning calorimetry (DSC)
d. Glass transition temperature from literature[99]
e. number-averaged molecular weight data[28]

4.3.2 Morphology Measurement

The morphology and packing behaviour of HP15 and HP21 (protonated formats of PE15-CD_3 and PE21-CD_3) have been published earlier.[99, 100] The results by X-ray scattering and electron microscopy in previous literature[99] support our rotational model extracted from solid state NMR measurements in this study. The lamellar thickness (between 10 and 20nm) and powder scattering patterns of the two precisely displaced polymers show that some of the methyl branches are incorporated into the crystalline

region, i.e., the methyl side group functions as conformational defect within the crystal lattice. As expected, the shorter spaced PE15-CH_3 exhibits higher degree of conformational disorder. However, the motion and torsion angle of this disorder are uncertain by scattering and microscopy measurements.

The deuterium labelled versions were also investigated by microscopy and scattering techniques to compare with the previous results from protonated ones. Consider that the sizes of deuterium and hydrogen atoms have no significant difference within the scale involved herein; the lamellar size and the chain packing behaviour should be identical for protonated and deuterated ones. TEM measurements of CD_3-branched precision polymer show no different morphological behaviour in contrast to CH_3-branched one, indicating the reproducibility of ADMET synthesis and correctness of the hypothesis concerning no significant effect of deuterium on packing behaviour.

Modern transmission electron microscopy is famous for its capability of imaging fine structures at nano scales, which is well-suited for analyzing the lamellar structures formed in semi-crystalline polymeric samples.

TEM measurements were conducted at Max Planck Institute for Polymer Research (MPIP), Mainz, Germany. White powder-like of ADMET precision polymer PE21-CD_3 as achieved from synthesis was dissolved in O-xylene with a concentration of 10mg/10ml; the mother solution was then 10 times diluted. TEM sample was prepared by putting one drop of diluted solution on carbon coated grid and stored in the refrigerator at around 7 ºC for single crystals to grow. The O-xylene was evaporated while the grid remained in the refrigerator.

The solution-grown single crystal for PE21-CD_3 shows lamellar crystal structure, illustrated in Figure 4-4. Images in (a), (b), and (c) of Figure 4-4 were taken from the crystals as developed from O-xylene solution. Clear lamellar type crystals can be observed. The thickness of the lamellar was measured using various techniques including Pt-shadowing, Electron Energy Loss Spectroscopy (EELS), and Atomic Force Microscopy (AFM), as seen in Appendix A. The thicknesses determined by these three methods are in agreement with each other: 10-13 nm from TEM (Pt-shadowing), 8 nm from TEM (EELS), 9 nm from AFM. The 10 nm averag lamellar thickness confirmed the previous result about thickness dimension for PE21-CH_3.

Figure 4-4 (d) and (e) are TEM images of the so-called “edge-on” lamellar structures, which were prepared by shearing the molten sample between two glass slides and consequently the edges of the lamellar structures can be readily imaged. Directly measuring the dimension of the lamellar edges provides an averaged thickness of around 16 nm. It is worth noticing that the lamellar thickness from the “edge-on” structure is not comparable with solution-grown single crystals because in the former case, a crystalline nucleation thread (shish) is formed and thus thicker crystals are expected. The structures shown in (c) and (d) in Figure 4-4 can be easily identified as the famous shish-kebab morphology in crystallography.

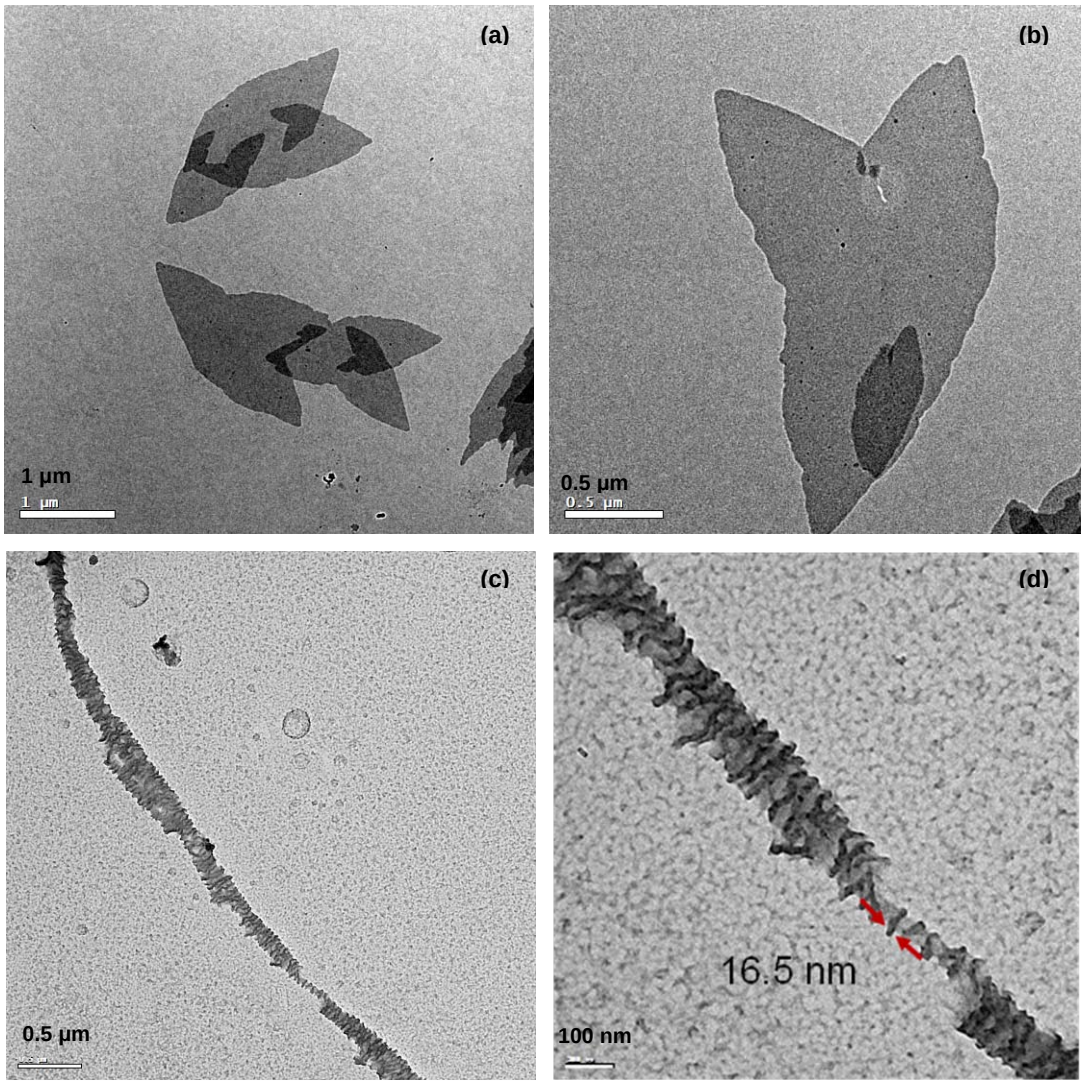

Figure 4-4. TEM images for ADMET precision polymer PE21-CD_3: (a) and (b) solution-grown single crystals as prepared, no contrast enhancement; (c) and (d) "edge-on" lamellar structures. The red arrows in (d) indicate an edge of a lamellar with size of 16.5nm.

4.3.3 Deuterium Solid State NMR Measurement

Molecular motions are of utmost importance for the macroscopic properties of polymers.[21, 101] In linear polymers like polyethylene (PE), branches change the mobility and have pronounced effects on the mechanical properties[102, 103], processablity and drawability and has, therefore, been studied in detail.[9, 104, 105] In the systems studied

previously and in particular in merchandized PE, the side chains are irregularly distributed along the main chain, which results in complexity and uncertainty of the defect influence. Therefore, it is highly desirable to study the effect of branching on molecular motions in polyolefins with exactly defined branches both with regard to the chemical nature of the branch and the distance between the branches along the chain. Once such samples are available, both rate and amplitude of chain motions can be studied site selectively with advanced solid state NMR methods.[79] Moreover, due to the sensitivity of ^{13}C chemical shifts on conformation and torsional angles,[20, 106] NMR can also probe structure and dynamics of the chain defects imposed by the branch. The effect of branching on mobility is particularly interesting in the crystalline regions of the semi-crystalline polymer, provided the branches can be incorporated. This suggests methyl groups as branches. Combining state-of-the-art synthetic chemistry and NMR spectroscopy we can then address the following questions: What is the nature of the motion of the branches? How do the branches alter the geometry and mobility of adjacent chain segments? Does the motion of one branch influence the motion of neighboring branches (collective motion, rotator phase)? Can gauche conformers be incorporated in the crystalline regions? Indeed, such precisely defined polyolefins have recently been prepared by acyclic diene metathesis (ADMET) polycondensation[26, 31, 46], where the primary structure, i.e. branch identity and spacer, can be controlled. Moreover, the methyl branches can be selectively deuterated, such that the mobility of the branches themselves can conveniently be studied by ^{2}H NMR.[91, 107-109]

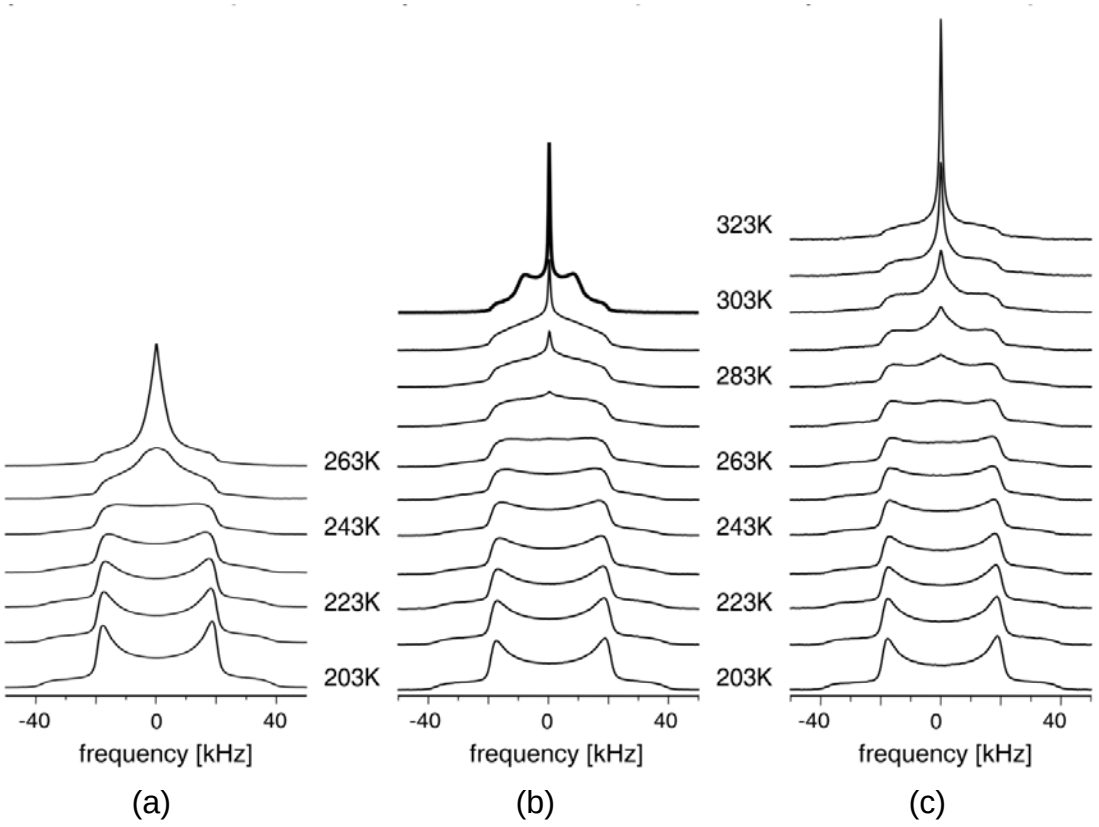

Figure 4-5. Temperature dependence of ^{2}H spectra for (a) PE9-CD_3; (b) PE15-CD_3; and (c) PE21-CD_3. Spectra were acquired on a Bruker Avance 400MHz NMR spectrometer using quadrupolar echo pulse sequence with an echo delay of 30μs, a 90^o pulse width of 2.5 μs, and a recycle delay of 1s. Samples were heated above melting points to remove the thermal history prior to collecting data every 10K. The special line shape of PE15-CD_3 at T = 303 K, plotted bold, indicates the presence of fast axial rotational dynamics.

Governed by the quadrupolar interaction, ^{2}H NMR is well suited for studies of local molecular dynamics. The ^{2}H NMR line shapes are very sensitive to segmental motions.[91, 107-109] Figure 4-5 displays temperature dependent ^{2}H NMR spectra for the three polymer samples with deuterated methyl branches. It's easy to see that the trend of line shape with temperature is similar for all of them and shows the gradual build-up of molecular dynamics. At low temperatures Pake patterns indicative of an axially symmetric tensor with fixed C_3-axes of the branches are observed. With increasing

temperature, the singularities of the Pake pattern broaden and the ^{2}H NMR line shape changes via an almost rectangular shape to a pattern resembling an asymmetric tensor (asymmetry parameter η=1). Since the ^{2}H NMR spectra contain signals from chains in crystalline and non-crystalline regions of the sample, which for the CD_3-groups cannot be separated by the standard procedures,[91, 108] we mention that such patterns can also result from branches undergoing large angle motions on intermediate time-scales. Upon further increasing the temperature, a rather narrow component in the centre of the spectrum emerges. Remarkably, only in **PE15-CD_3** at T = 303K, does the ^{2}H NMR spectrum show a regular Pake pattern (η=0) with half the static line width, indicating the presence of axial rotation sufficiently fast to average the ^{2}H line shape not observed in linear PE itself.[91, 107-109] Therefore, we attribute this behaviour to motions of methyl groups embedded in the crystalline regions. The highly asymmetric ^{2}H line shape observed in all cases is usually interpreted as evidence for a 'kink motion,[91, 108] but is also consistent with ill-defined rotations around the local chain axis (*all-trans* in the crystallites) with amplitude about ± 40°, seen in section 4.3.6. The detailed interpretation of the deuterium NMR lineshapes is aided by fitting to spectra lineshape simulations, which are presented in chapter 5.

An attempt measuring 2-dimentsional ^{2}H exchange NMR indicates that there has no slow orientation on the exchange time scale due to absence of off-diagonal intensities, as shown in Appendix B.

4.3.4 ^{13}C Solid State NMR Measurement

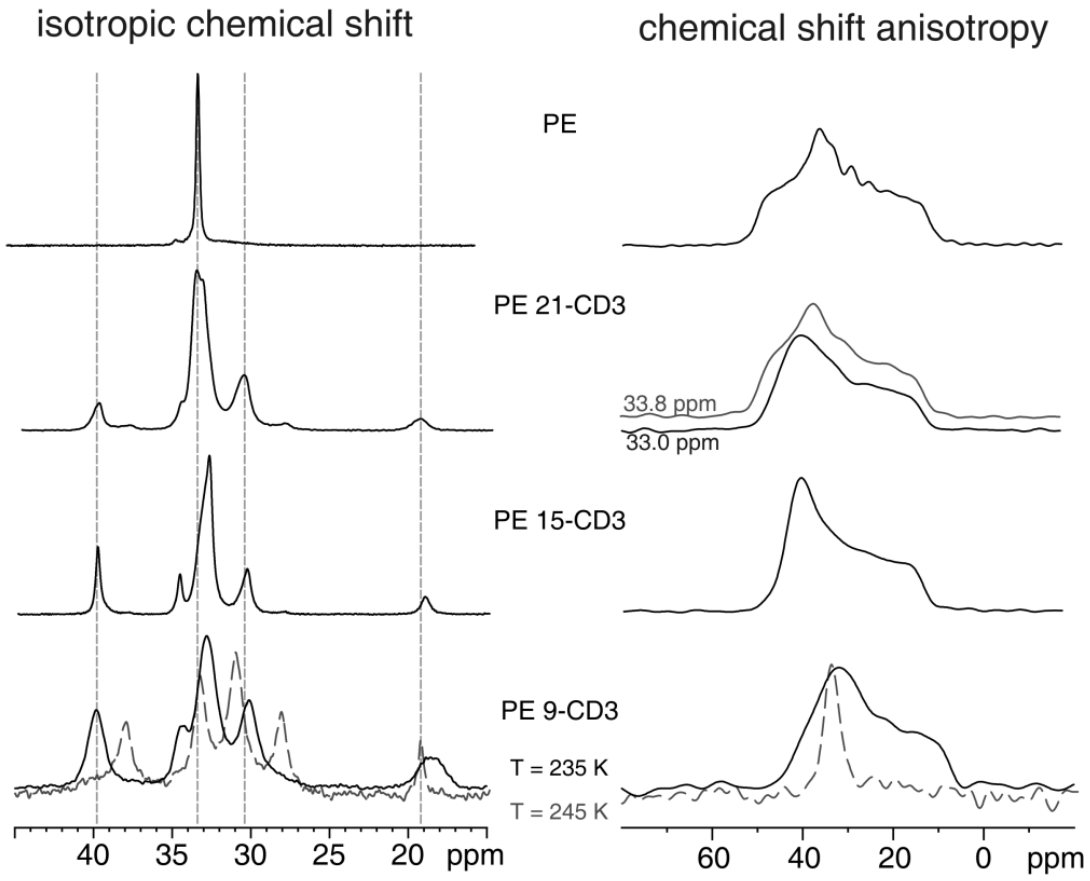

Figure 4-6. ^{13}C isotropic and anisotropic chemical shifts for precise polymers: (from the top) ADMET PE at 300K, PE21-CD_3 at 300K, PE15-CD_3 at 300K, PE9-CD_3 at 235K and 245K. Spectra were acquired on a Bruker Avance III NMR spectrometer at 213 MHz ^{13}C Larmor frequency (850 MHz for ^{1}H) using the SUPER[96] pulse sequence with a spinning rate 4125 Hz and an initial CP set to improve ^{13}C spin polarization.

^{13}C NMR experiments, observing randomly distributed ^{13}C sites along the chain, provide a direct picture of the chain dynamics. The isotropic chemical shift in a magic angle spinning (MAS) NMR spectrum[79] indicates the local conformation[20, 106] and the motionally averaged chemical shift anisotropy (CSA), that can be site-selectively recorded by two-dimensional NMR,[79] reflects local reorientations of CH_2 groups of the

polymer backbone. Figure 4-6 displays both the isotropic and anisotropic chemical shift patterns of the three samples and a linear PE sample prepared by ADMET synthesis, acquired by separation of undistorted powder patterns by effortless recoupling (SUPER).[96] For linear **PE** without methyl branches, the ^{13}C isotropic chemical shifts in Figure 4-6, left column, show a strong signal at around 33.5 ppm, characteristic of the *all-trans* stems in the orthorhombic phase and a minor monoclinic contribution at around 35 ppm, as well as a very broad amorphous signal with low intensity at 33-29 ppm. In the following, only the signals originating from the stems in the crystalline regions will be discussed. The ^{13}C static line shape for the orthorhombic signal of **ADMET PE** exhibits a CSA tensor with η=0.67 and principal axes values of 13 ppm along the chain, and 37 ppm and 51 ppm perpendicular to it, as previously discussed in the literature.[110]

Introducing regularly spaced methyl side groups along the polyethylene backbone changes the morphology[99] and the molecular dynamics. In the ^{13}C MAS NMR spectra, Figure 4-6, two new signals are observed in all cases, assigned to the methyl group(~ 19 ppm) and the methine carbon (~40 ppm). Moreover, changes are observed for the signals assigned to the regular CH_2 units located in crystalline and non-crystalline regions of the samples along the PE main chain. In **PE21-CD_3** the NMR signal at 33.5 ppm known from linear PE and assigned to *all-trans* conformations in the crystalline regions splits into two signals at 33.6 ppm and 33.2 ppm, which are resolved in our 850 MHz NMR spectrometer. The CSA line shapes for the MAS NMR signal at 33.6 ppm shows a CSA tensor line shape similar to that of PE. The CSA powder line shape of the MAS NMR signal at 33.2 ppm, however, displays the lineshape of an almost axially symmetric CSA tensor, where the principal value of 13 ppm along the crystalline c-axis

persists and the two other values are largely averaged. Remarkably, the averaging observed is consistent with rotations of the trans segments around the chain axis with the same amplitude (± 40°) as deduced from ^{2}H NMR for the branch (see section 4.3.6). It should be noted that the isotropic chemical shift of the averaged tensor is shifted by 0.8 ppm towards the gauche containing signals in the non-crystalline regions. As ^{13}C chemical shifts of polymers are sensitive even to small changes in torsional angles,[106] we assign this small shift to local deviations from the regular *all-trans* geometry, resulting from chain twists in the vicinity of the methyl branch. This will minimize the spatial requirements for incorporating the methyl branch in the crystals. The isotropic shift observed actually reflects an average over twisting motions of the defected chain units close to the methyl branch. Finally, the ^{13}C NMR signal at 30 ppm in the spectrum of **PE21-CD$_3$** is assigned to non-crystalline PE. This line is considerably narrower and more intense compared to linear PE. These differences, however, can be attributed to the different crystallinities of the two samples (30 % in **PE21-CD$_3$** vs. 85% in **ADMET-PE**) and the non-quantitative CP-MAS method used to efficiently record the ^{13}C MAS NMR spectra.

For **PE15-CD$_3$**, the signal assigned to CH_2 sites in the crystalline regions is observed at 32.9 ppm with a shoulder of about half the signal height at 33.5 ppm. Remarkably, all ^{13}C signals in the NMR spectrum of **PE15-CD$_3$** show the powder line shape of well defined axially symmetric CSA tensors, even at 33.5 ppm, the isotropic chemical shift characteristic of undistorted *all-trans* units. Thus, whereas in **PE21-CD$_3$** the CH_2 groups in proximity to the lattice perturbing methyl branches perform local motions like in pinned defects, the rotation in **PE15-CD$_3$** at T = 303 K involves all CH_2

groups along a given polymer chain and thus shows collective behavior like in a rotator phase, also deduced from X-ray data.[99]

The ADMET precision polymer PE9-CD_3, with the shortest spacer of only 8 CH_2 units between subsequent methyl branches, exhibits at T = 235 K (about 20 K below its melting point) a ^{13}C MAS NMR spectrum very similar to that of PE21-CD_3 and PE15-CD_3, see Figure 4-6. All known carbon signals are observed close to the chemical shifts from the other spectra, but the line width of the NMR signals is 2-4 times larger. This increased line width at low temperatures is attributed to a substantial conformational disorder in the crystalline regions of the sample, induced by the dense distribution of methyl branches along the polymer backbone. At T = 235 K, the static powder line shape of the crystalline component observed at 32.8 ppm, resembles the pattern of an incompletely averaged CSA tensor of the chain defects in PE21-CD_3. At T = 245 K, however, only 10 K higher and 10 K below the melting point, all ^{13}C MAS NMR peaks become much sharper and all signals except the methyl signal are shifted towards higher fields. Moreover, instead of static CSA powder patterns, isotropic lines are observed under CSA recoupling, as seen in the spectrum plotted as a dotted line in Figure 4-6. The findings at T = 245 K thus indicate substantial pre-transitional conformational disorder in PE9-CD_3, which hampers the comparison of this sample with the other two. Therefore the results obtained for PE9-CD_3 have not been used to develop a model for the molecular dynamics in the regular methyl-branched polyethylene samples.

4.3.5 Motional Model

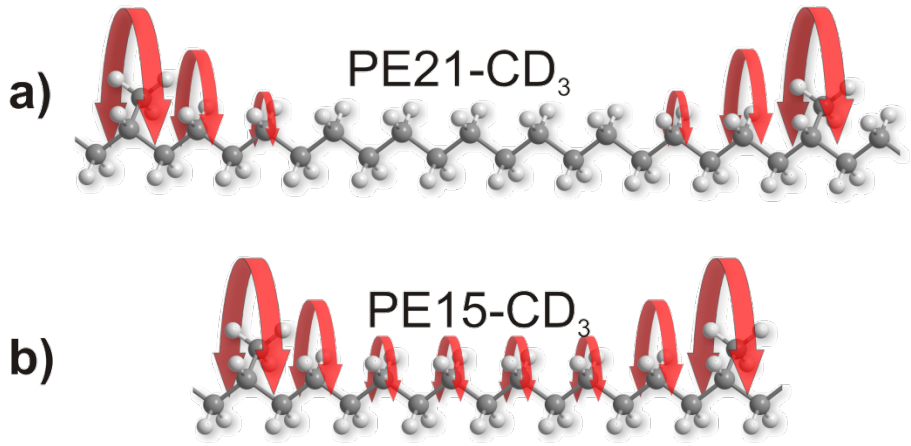

Figure 4-7. Schematic model for rotational dynamics in (a) PE21-CD_3, ADMET precision polymer with deuterated methyl branch on every 21st carbon along the backbone and (b) PE15-CD_3, ADMET precision polymer with deuterated methyl branch on every 21st carbon along the backbone

Combining the results for **PE15-CD_3** and **PE21-CD_3** obtained from ^{2}H and ^{13}C NMR, which probe the branch and the neighbouring chain defect separately, we propose a simple model for the molecular dynamics of the regular methyl-branched polyethylene in the crystalline regions as shown in Figure 4-7: In the crystalline regions of **PE15-CD_3** and **PE21-CD_3**, the lattice perturbing methyl-branches undergo axial oscillations around the polymer backbone. In both samples, this motion of the methyl branches gains in amplitude and rate with increasing temperature. However, in the case of **PE21-CD_3**, this dynamic mode is restricted to CH_2 groups in close proximity to the methyl branch in a twist defect, whereas the CH_2 groups remote from the methyl branches are not involved in this motion as demonstrated by the regular PE CSA pattern observed at 33.6 ppm, but may undergo 180° flips as known for crystalline PE.[110] The relative intensities of the isotropic lines corresponding to the axially

symmetric and the η=0.67 CSA pattern is approximately 1:2. From this, the number of CH_2 units involved in the dynamic twist defect is estimated as 3-4 CH_2 units on either side of the branch. Based on this picture of a localized dynamic perturbation of the crystal lattice caused by the methyl branches, one would expect a 1:1 ratio between rotating and rigid units for **PE15-CD_3**. While MAS NMR signals indicate undistorted trans-conformers, see Figure 4-6, all sites along the chain are found to exhibit similar rotational dynamics. In other words, the localized rotational motion observed in **PE21-CD_3** turns into collective dynamics due to the higher density of defect sites in **PE15-CD_3**.

The main results of our study can then be summarized as:

Nature of the motion of the branches: The ^2H spectra, Figure 4-5, clearly show that the branches perform angular restricted rotations reaching amplitudes of about ± 40° around the long axis of *all-trans* PE chains close to the melting point.

Influence of the defects on the adjacent chain segments in the same molecule: The methyl-branches lead to a twist of the adjacent chain segment, Figure 4-7, manifesting itself as a component at lower ^{13}C-chemical shift. From the intensity of this line, compared to that of the *all-trans* segments, the length of the defect is readily estimated to involve about 3-4 CH_2-groups at either side of the branch.

Local vs. cooperative axial motion: The chemical shift anisotropy patterns, Figure 4-6, right column, clearly show axial motions of the twisted segments similar to those of the branch itself, whereas the CH_2-groups of the undistorted *all-trans* segments in the sample with long chains between the branches, **PE21-CD_3,** are rigid on the timescale of these experiments, as in linear PE itself. Thus, the motion of the branches and the

adjacent chain defects are localized and can be considered as pinned. In **PE15-CD$_3$**, however, the twisted parts are so close that the axial motion imposed by the defect becomes cooperative and also rotates the undistorted trans-segments in between, as in a rotator phase, Figure 4-7 (b).

Incorporation of gauche defects in the crystals: Incorporation of gauche defects is only observed in **PE9-CD$_3$**, the sample with the highest branch density, at temperatures close to the melting point.

4.3.6 Analysis of NMR Powder Line shapes

In static solid state NMR spectra of quadrupolar nuclei such ^{2}H or nuclei with a substantial chemical shift anisotropy (CSA) the line shape is governed by these angle dependent interactions. Both, the first order quadrupole coupling as well as the chemical shift anisotropy are second rank tensorial interactions, which can be described in terms of their anisotropy δ and their asymmetry parameter η. The orientation dependence of the resonance frequencies for a set of polar coordinates (θ,ϕ) between the zz-component of the principal axes system of the tensor and the magnetic field is given by[79]

$$\omega(\theta,\phi) = \tfrac{1}{2}\delta\left[3\cos^2\theta - 1 - \eta\sin^2\theta\cos(2\phi)\right] \qquad (4\text{-}1)$$

Rotational motions in the fast motion limit lead to a new tensor with averaged principal values and different principal axes. The angular dependence of the NMR frequency can then still be described by an equation similar to Equation (4-1), but with averaged principal values and new polar angles:

$$\overline{\omega}(\beta,\alpha) = \tfrac{1}{2}\overline{\delta}\left[3\cos^2\beta - 1 - \overline{\eta}\sin^2\beta\cos(2\alpha)\right]. \qquad (4\text{-}2)$$

Processes of different geometries can give identical principal values. Moreover, in case of ^{2}H the spectrum neither does nor reveals the sign of δ, increasing the ambiguity [1]. In the current case, however, we are interested in the chain motion in the crystalline regions only, where the isotropic chemical shift ^{13}C tells us that we look at motions of extended *trans* units, which can only rotate around their local chain axis, the crystallographic c-axis of the PE. Therefore, in order to analyse the static NMR line shapes in terms of dynamics, we assume Gaussian distributed rotational fluctuation around the crystallographic c-axis of the PE samples. The unique axes of the tensorial interaction, i.e. q_{ZZ} for ^{2}H and CS_{ZZ} for ^{13}C form angles of 90° and 0°,[110] respectively, with the c-axis. Assuming, that the molecular dynamics close to the melting point of the crystallites is in the fast motional limit, the NMR line shape can conveniently be computed using the NMR Weblab.[109]

Along these lines, the quadrupole and CSA line shapes obtained for a systematic variation of the width σ of the Gaussian distributed rotational fluctuations are given in figure 4-8. In the case of the ^{2}H NMR, the strength of the quadrupole coupling, $\bar{\delta}$ reduces down to ½ δ and $\bar{\eta}$ increases with the spread of the distribution, reaching $\bar{\eta}$ = 1 for σ = 42.5° and then reduces again for broader fluctuation distributions until for σ ~ 80° an axially symmetric averaged quadrupole tensor with unique axis parallel to the rotation axis results. In the case of ^{13}C NMR CSA powder line shapes for CH_2 groups of extended trans conformers these fluctuations keep CS_{ZZ} constant and reduce $\bar{\eta}$. Rotational fluctuations with σ > 40° lead to a powder line shape which is difficult to distinguish from that of an axial rotation as $\bar{\eta}$ almost vanishes already. Moreover, it should be noted that the experimental line shapes not only reflect these geometrical

aspects of the local molecular dynamics. For NMR spectra recorded in a temperature range 0-50 K above the glass transition temperature the time scale of the dynamic processes will be another crucial parameter and distortions of the NMR line shapes due to the intermediate motional effects will have to be taken into account to obtain agreement between experimental and computed spectra.

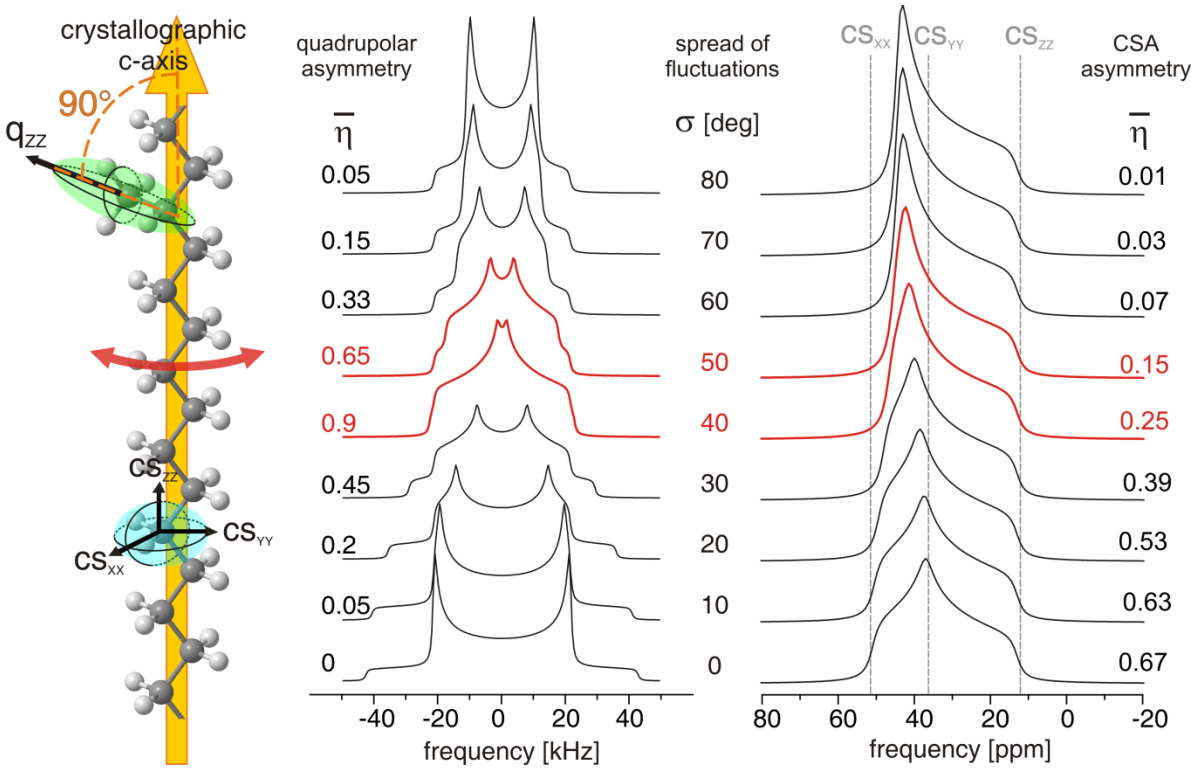

Figure 4-8: Computed ^{2}H NMR and ^{13}C NMR powder line shapes for a Gaussian distributed rotational fluctuation of the width σ around the crystallographic c-axis of crystalline PE according the motional model presented in Figure 4-7.

From Figure 4-8 it is clear that the only motional mode that is consistent with *both* the observed ^{2}H and ^{13}C NMR line shapes recorded at temperatures close to the melting point, where the fast motion limit is a good approximation, involves fluctuations of the order of ± 40° used to develop our model of twisted defects.

4.4 Conclusion of Branch Frequency Effect

Reflecting the importance for the mechanical behaviour, the nature of chain motions of the stems in the crystals has been under debate for decades. In particular, local conformational defects[21, 101] as opposed to propagating twists[111] were considered as mechanisms for chain transport. Our results clearly favour twists, which require considerably less disturbance of the crystal lattice. Remarkably, recent NMR studies of chain diffusion between the crystalline and the non-crystalline regions of linear ultrahigh molecular weight PE showed that chain transport, involving cooperative motion of the stems, has different temperature dependence than the local mobility of the chains. This indicates increased presence of defects that do not transport the chain at higher temperatures.[112-115] Rotator phases in polymers were deduced from X-ray scattering, thermal analysis, and solid state ^{29}Si NMR.[116, 117] However, for branched polyethylenes, this is the first time that clear evidence of a rotator phase has been found, consistent with the results of scattering and microscopy.[99] Our proof of chain twists also helps to explain the conformational motions of amorphous polymers in the melt, where two-dimensional NMR has clearly shown that conformational transitions do happen, yet they occur with broad distributions of rotational angles.[94] This suggests twisted defects in the chain as also considered theoretically.[118, 119] Clearly, the occurrence of both isolated and cooperative motions in stems of single molecules could only be detected by a combination of innovative synthetic chemistry generating well-defined model systems and state-of-the-art solid state NMR on different nuclei probing structure and dynamics with different interactions. The implications for polymer physics and engineering of merchandized PE are obvious as irregular branching along the chain[9, 104, 105] results in the possibility of all the different motions identified above to occur in the same polymer.

CHAPTER 5
MORPHOLOGY AND DYANMICS BY DEUTERIUM NMR LINESHAPE ANALYSIS

5.1 Introduction

Despite its structural simplicity, polyethylene (PE) is a remarkably versatile material. Branching explains its versatility. While previous studies of branching in PE have been limited to relatively ill-defined primary structures, the methodology now exists to synthesize polyolefins possessing uniformly spaced branches of a specified type, yielding an unequivocal primary structure. Here, we present the first variable temperature deuterium NMR study of -CD_3 branching groups in precision PE, the intent being to understand the effect of precision branch placement on morphology and chain dynamics. Since ^2H NMR spectra are extensively dominated by the quadrupole interaction, it is well-suited to study chain segmental dynamics in bulk. The selectively labeling of methyl branches offers a good opportunity to utilize deuteron as an effective indicator of the polymer main chain motion by studying the C-CD_3 bond.

For methyl-branched ADMET precision polyethylenes, it has demonstrated that the methyl branches are incorporated in the crystalline phase. Therefore, for such semi-crystalline polymers, the magnetization from solid echo experiment, in fact, contains signals from both crystalline region (CR) and non-crystalline region (NCR), which makes the lineshape analysis even more troublesome. Achieving signals from mostly pure homogeneous regions is in need. In this study, it can be realized by T_1 filtration experiment. The quadrupole echo spectra lineshapes are analyzed by least squares fitting to deuterium motion simulations.

5.2 Theories of Lineshape Analysis

Deuterated methyl groups are advantageous for ^{2}H NMR spectroscopy since even at temperatures below the glass transition, where the polymer chain motion is quenched, the fast methyl rotation averages the nuclear quadrupole interaction of the methyl deuterons. In the secular approximation, the transition frequencies are given by

$$\bar{\omega}_{\pm} = \omega_0 \pm \bar{\delta}\left(3\cos^2\vartheta - 1 - \bar{\eta}\sin^2\vartheta\cos 2\varphi\right) \tag{5-1}$$

where $\bar{\delta}$ and $\bar{\eta}$ are the motionally averaged quadrupole coupling and asymmetry parameter, respectively, and ϑ and φ are the Euler angles relating the lab frame to the principal axis system of the (motionally averaged) quadrupole coupling tensor. The fast rotating -CD_3 mimics a -C-D group with a scaled quadrupole coupling constant $\bar{\delta} = \delta / 3$ and $\bar{\eta} = 0$. This results in a three-fold greater signal and a three-fold reduction in the frequency dispersion (in polycrystalline samples), yielding a substantial NMR sensitivity enhancement compared to a single static deuteron with quadrupole coupling constant δ.

Deuterium lineshapes are very sensitive to motions, as shown in Figure 5-1. When at low temperatures, the segmental chain motions are frozen, resulting in the classic Pake pattern (see blue line structure) with characteristic doublet splitting. At elevated temperatures, by absorbing thermal energy, the chains lose part of the motional anisotropy and result in motionally averaged lineshapes. For instance, when a three-bond kink motion is involved, the ^{2}H NMR shows a characteristic lineshape with the appearance of a central peak (see Figure 7-1 (b)). When more chains get involved in the segmental motions, the lineshape varies correspondingly. With such high sensitivity,

deuterium NMR lineshape analysis becomes very attractive for investigation of segmental dynamics within the NMR timescale.

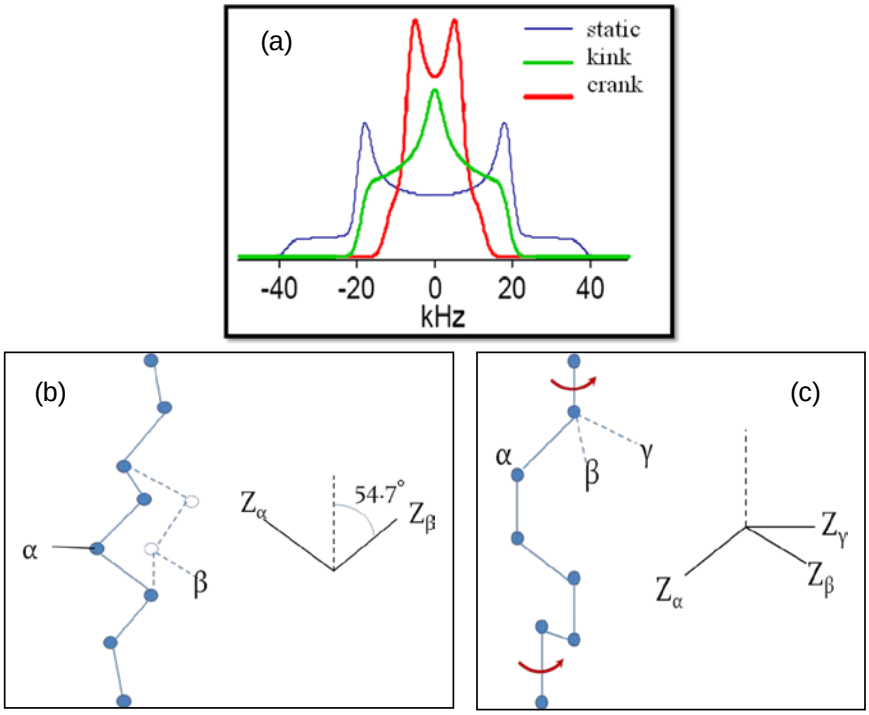

Figure 5-1. Theoretical ^{2}H lineshapes in static and fast motional limits: (a) the blue spectrum corresponds to the static ^{2}H lineshape; the green one indicates the kink motion; the red one refers to the crankshaft motion. (b) 3-bond kink motion. (c) 5-bond crank-shaft motion.

5.3 Experimental

Deuterium NMR measurements were performed on a Bruker Avance NMR spectrometer operating at 61.4MHz (9.4T). Temperature-dependent solid echo experiments used the $90^\circ_x - \tau - 90^\circ_y - \tau$ pulse sequence with τ = 25 and 75 μs, a 90^o pulse width of 2.2 μs, a recycle delay of 1.5 s, and 512 scans. Deuterium spin-lattice relaxation time was determined by using inversion recovery pulse sequence with 1s recycle delay, a 90^o pulse width of 2.2 μs, an echo delay of 30 μs, and 128 scans. A T_1 filter was used to selectively acquire the spectra of the non-crystalline phase. Spectra

were acquired by adding a 5 ms delay following the saturation by a π/2 pulse train.[91] The T_1 filtered spectra were acquired with a 11ms recycle delay, echo delays of either 25 or 75 μs, and 16k scans. The temperature ranges from the melt to well below the glass transition temperature.

5.4 Results & Discussion

5.4.1 Deuterium T_1 Measurement

Inversion recovery is the most commonly used method to extract spin-lattice relaxation time (T_1). In this study, the magnetization at the symmetric center of the lineshape plotted as a function of recovery time in Figure 5-2 to extract T_1 values.

The experimental data were fit to three different functions for best fit:

1. Double exponential function (**EE**) [120]:

$$f = -a_1 b_1 \cdot exp\left(-t/T_{1,NCR}\right) + b_1 - a_1 b_2 \cdot exp\left(-t/T_{1,CR}\right) + b_2 \quad (5\text{-}2)$$

where b_1 is the initial magnetization from non-crystalline regions (NCRs) when $t = 0$, b_2 is the initial magnetization from crystalline regions (CRs) when $t = 0$, a_1 is a constant, $T_{1,NCR}$ is the spin-lattice relaxation time of NCRs, and $T_{1,CR}$ is the T_1 of CRs. This function considers the presence of two phases in semi-crystalline polymers: crystalline and non-crystalline phases with distinguishable relaxation times.

2. Kohlrausch, or stretched exponential function (**K**) [121-125] :

$$f = -ab \cdot exp(-t/T_1)^{1-n} + b \quad (5\text{-}3)$$

where *n* is the stretching parameter (when *n*=1, the usual exponential decay is recovered), which describes the stretched exponential decay in disordered systems.

3. Exponential-Kohlrausch function (**EK**):

$$f = -a_1 b_1 \cdot exp\left(-t/T_{1,NCR}\right) + b_1 - a_1 b_2 \cdot exp(-t/T_1)^{1-n} + b_2 \quad (5\text{-}4)$$

where *n, b_1, and b_2* have the physical meanings as in EE and K functions. In fact, EK function is a combination of EE and K functions by taking advantages of both. EK contains not only the normal morphological parameters (crystalline and non-crystalline phases) but also the possible distribution of relaxation times.

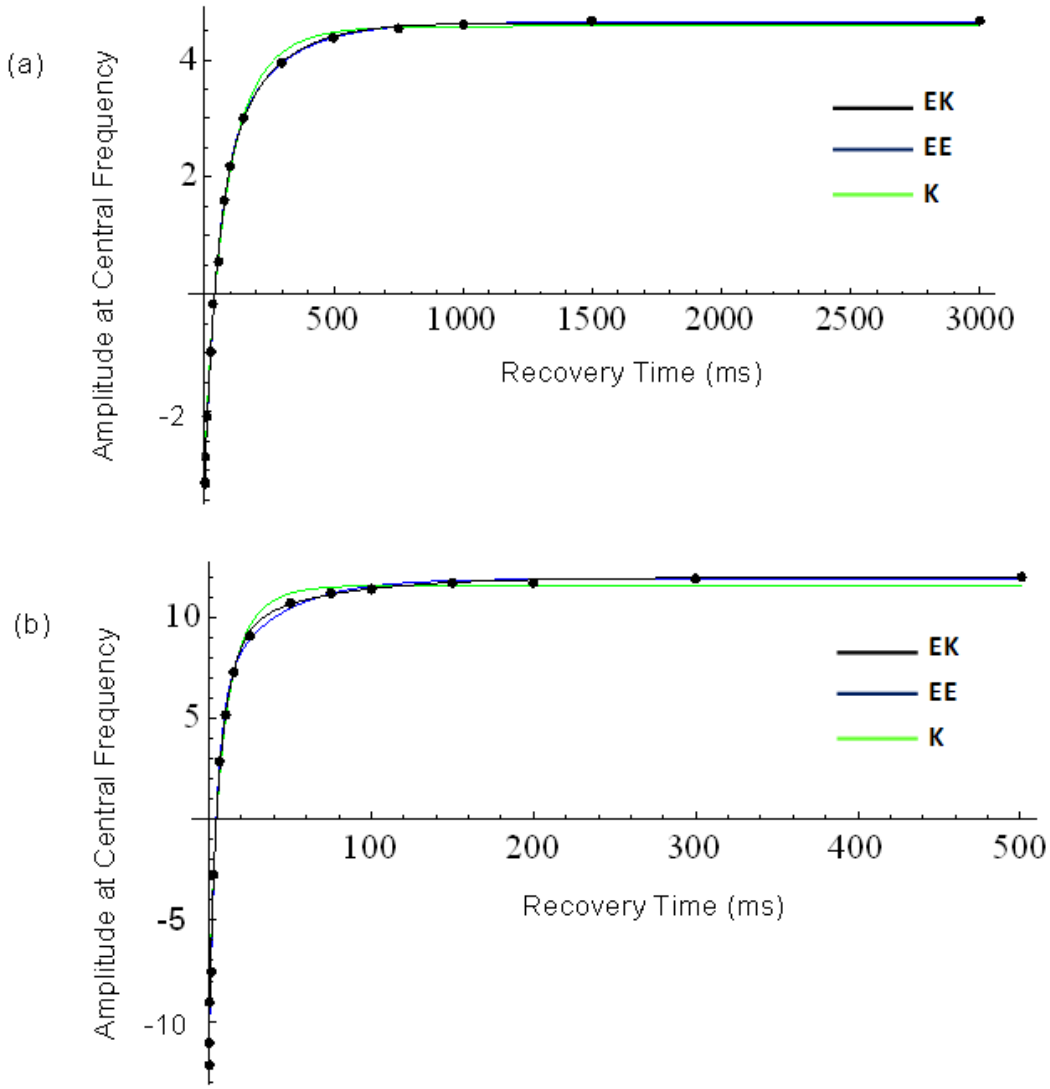

Figure 5-2. T_1 determination from inversion recovery using various fit functions: (a) 298K, and (b) 118K. EK: Exponential Kohlrausch function. EE: Double exponential function. K: Kohlrausch function.

Fitting of the deuterium T_1 data was performed for spectra at each temperature using three functions separately. Figure 5-2 sampled the fit results at two temperatures:

298K (a) and 118K (b). It can be seen the bimodal fitting function EK provides the best fit. Double exponential function EE favors the high temperature while the Kohlrausch function K works better at low temperature. Fitting at other temperatures (not shown here) also supports this conclusion. Therefore, the bimodal fitting function EK is chosen to extract the deuterium T_1 data for precision polymer PE21-CD_3. The relaxation time data are shown in Figure 5-3. As expected, the T_1 value arising from the non-crystalline region is much shorter than that from the crystalline region: the former is less than 40 ms while the latter exceeds 100 ms at temperatures above T_g. Both T_1 values undergo a minimum at around 170 K.

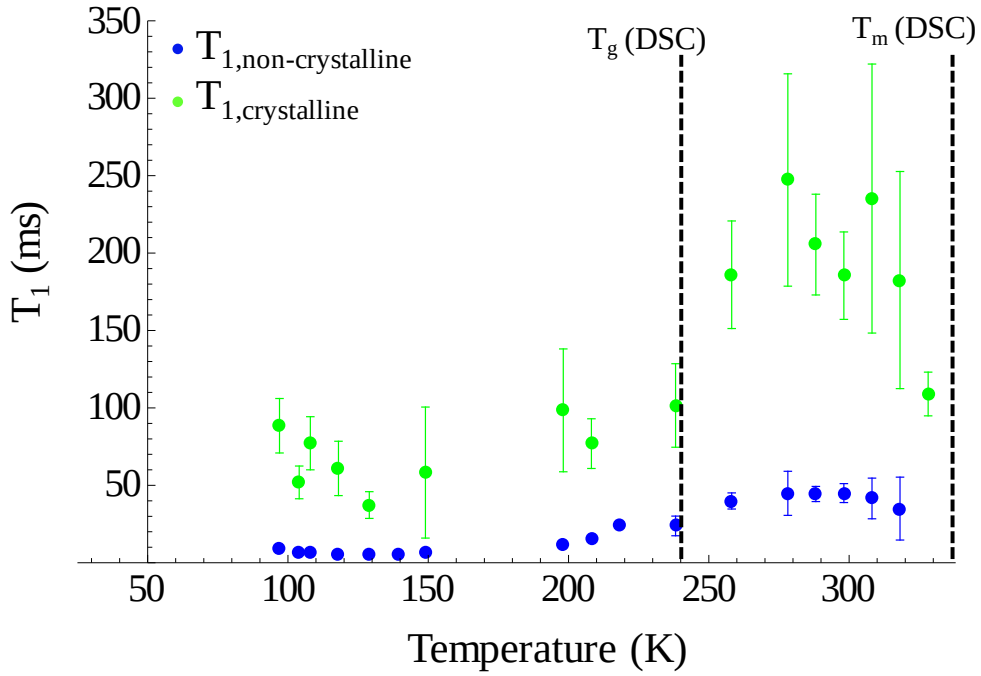

Figure 5-3. Spin lattice relaxation data for ADMET precision polymer PE21-CD_3 at various temperatures. Data were acquired from the EK bimodal fitting function.

From the EK bimodal fitting function, the stretching parameter *n* is obtained in addition to the spin-lattice relaxation time. Stretching parameter *n* indicates the width of

the distribution of relaxation times: the smaller the *n*, the narrower the distribution. Figure 5-4 shows the Kohlrausch stretching parameter as a function temperature for fits to EK function. At temperatures below the glass transition, *n* reaches a maximum value of about 0.2, indicating a distribution of micro-environments of the methyl branch. Above the glass transition, molecular exchange between these different microenvironments can occur on a time-scale short compared to T_1. Therefore, an average relaxation time is observed. As the temperature is increased, *n* decreases and approaches zero at the melting temperature. Under these conditions, each spin relaxation becomes effectively homogeneous throughout the non-crystalline phase.

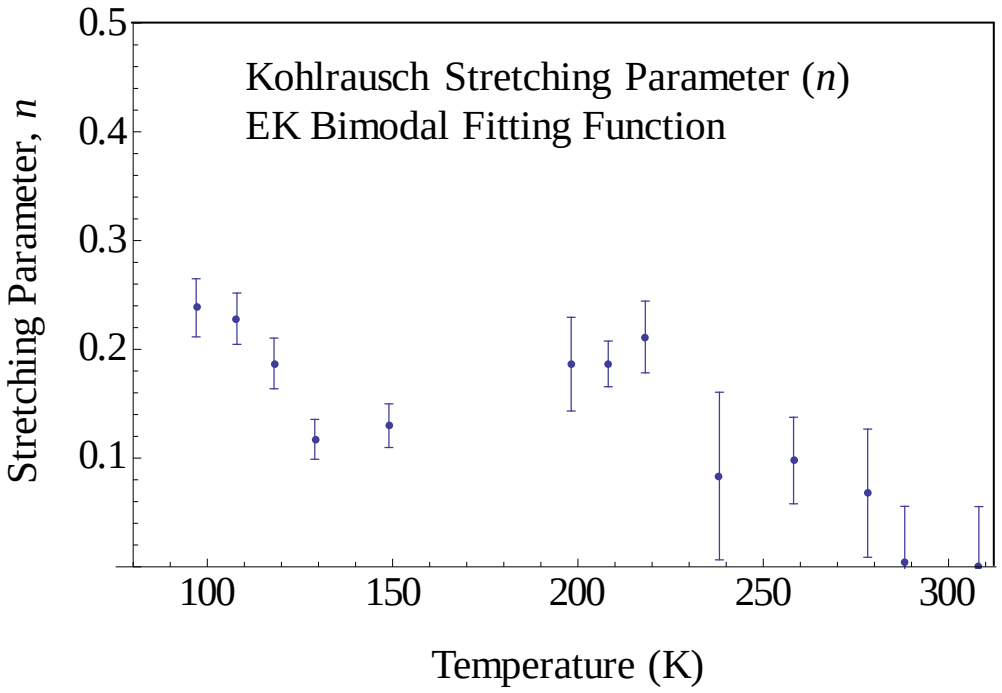

Figure 5-4. Stretching parameter *n* at various temperatures for PE21-CD_3, achieved from the EK bimodal fitting function.

Parameters b_1 *and* b_2 have significant physical meaning: the initial magnetization from non-crystalline and crystalline regions. Therefore, the degree of crystallinity X_c can be calculated from these two parameters by using the equation:

$$X_c = \frac{b_2}{b_1+b_2} \times 100\% \quad (5\text{-}5)$$

In Figure 5-5, the non-crystalline fraction, $1 - X_c$, is plotted as a function of experimental temperature. These results are in agreement with the degree crystallinity acquired from wide-angle X-ray diffraction measurements (see Figure 5-6).

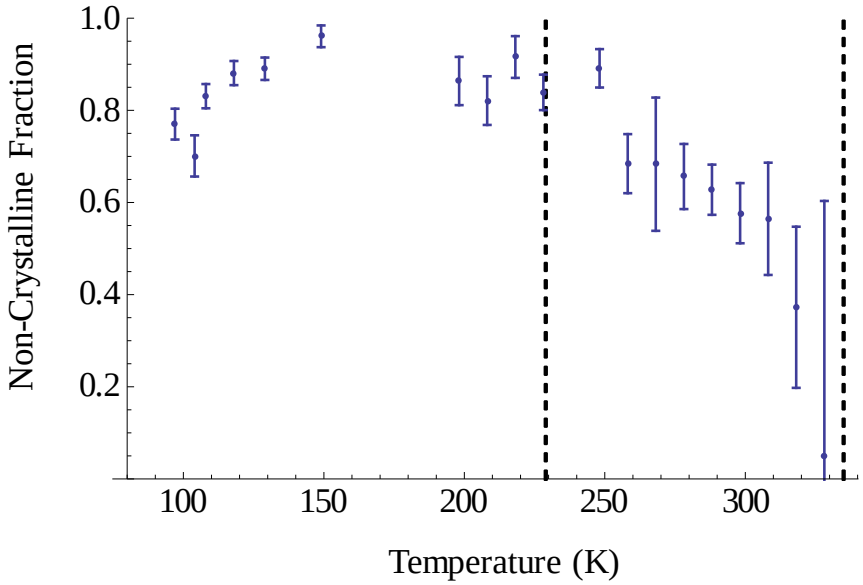

Figure 5-5. Non-crystalline fraction acquired from bimodal function EK at various temperatures for polymer PE21-CD_3.

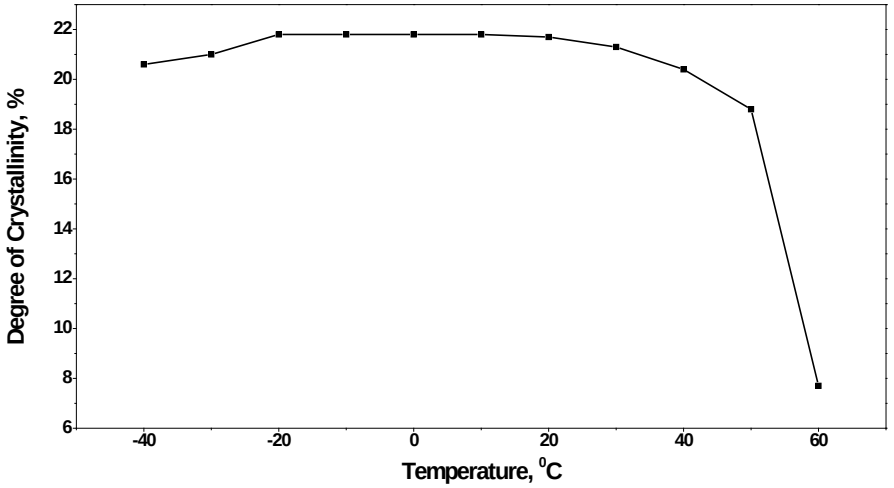

Figure 5-6. Degree of crystallinity acquired from WAXS at various temperatures for polymer PE21-CD_3.

5.4.2 Fully-Relaxed and Amorphous ^{2}H NMR Measurements

Herein, the segmental dynamics of ADMET polymer was explored on the 10^{-7}-10^{-2} s time-scale using variable-temperature ^{2}H quadrupole-echo NMR. Typically the temperature ranged from the melting temperature to well below the glass transition temperature. For each temperature, spectra were acquired at different echo delay time τ in order to compare the evolution of quadrupolar relaxation in the spectral lineshape simulations. The fully relaxed experimental spectra clearly demonstrate that there is a mobile and a rigid fraction in the sample, which have different contributions to the line shape. The more mobile fraction is observed as the narrow signal in the center of the spectrum and has a shorter T_1 relaxation time (c.a. < 40 ms).

The amorphous spectra were acquired by T_1 filtration experiments, as described above. The crystalline spectra, which are more difficult to measure directly, are calculated by subtracting the experimental amorphous signals from the fully-relaxed spectra. Experimentally acquired fully-relaxed and amorphous spectra, as well as calculated crystalline spectra at various temperatures are shown in Figure 5-7.

At two extreme conditions, near melting and well below the glass transition, the amorphous and crystalline spectra are not appreciably different. At -75 ºC, the crystalline and amorphous spectra show nearly identical Pake patterns evidenced with “horns” at $\pm$20 kHz. The solution-like narrow peaks at 55 ºC indicated the isotropic motions are dominant in both phases. However, at any temperature in between, one can distinguish the two spectra easily. A fairly broad feature in the amorphous spectra begins to appear at -75 ºC and is apparent at -15 ºC. Such a feature does not arise in the crystalline spectra until 15 ºC, when the Pake powder pattern is still dominant. At 25

ºC, the powder pattern in the amorphous spectra collapses to a broad peak, which gets narrower at elevated temperatures due to accelerated segmental motion.

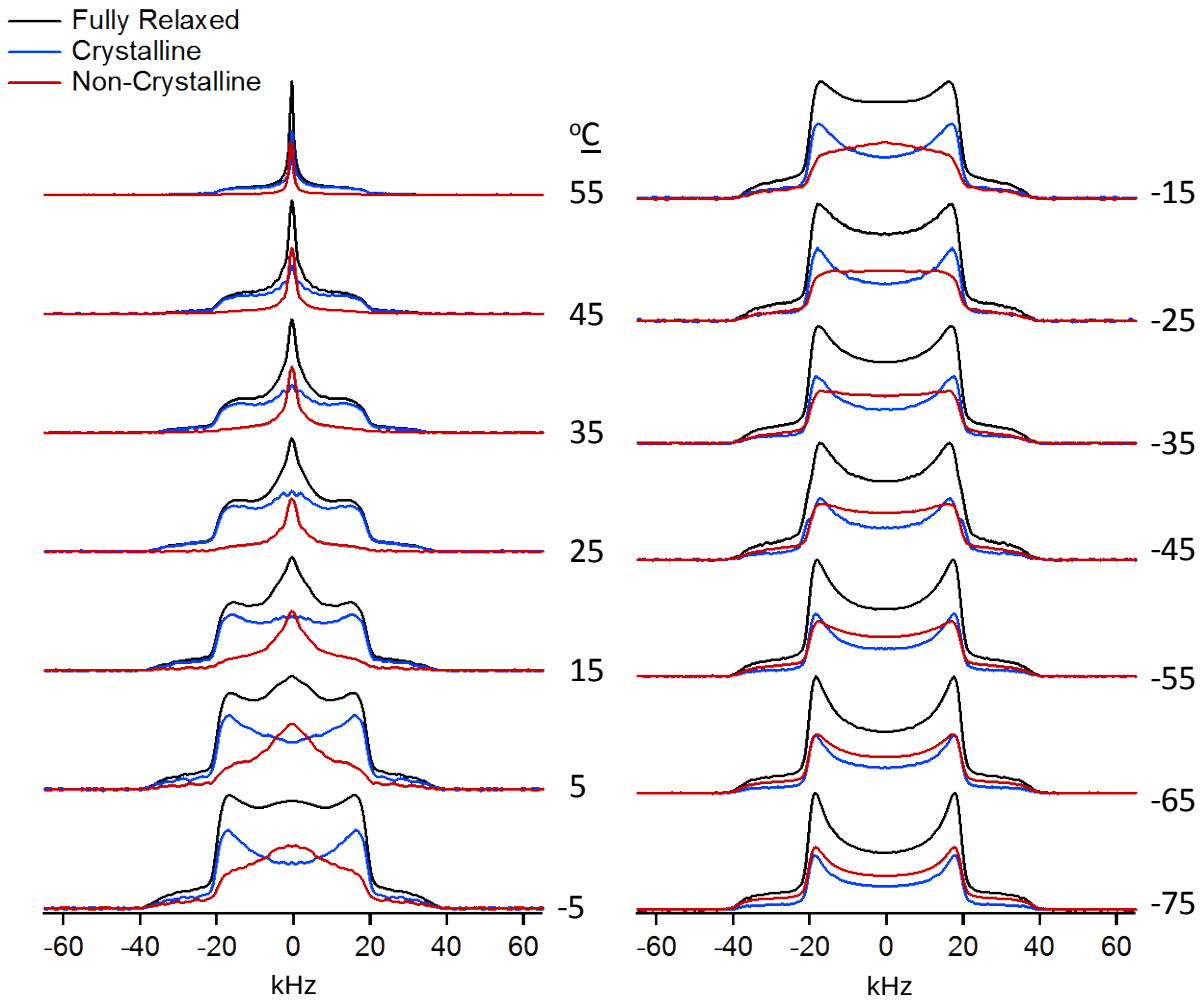

Figure 5-7. Plot of temperature-dependent fully-relaxed (experimental, in black), amorphous (experimental, in red), as well as crystalline spectra (calculated, in blue)

From the separated spectra shown in Figure 5-7, one may conclude that the rigid crystalline component having a longer T_1 relaxation time has a great contribution to the "horns". The mobile amorphous component gives birth to the central broad peak. The

next step is to use deuterium NMR line shape simulations to characterize the segmental motions in the crystalline and non-crystalline domains.

5.4.3 Theoretical Lineshape Fitting

To simulate the motions in CD_3 branched PE, we look to the NMR literature of PE, where ^1H, ^2H and ^{13}C NMR have been employed to study chain dynamics in both the amorphous and crystalline phases.[126-130] Various α-processes have been considered, including *two-site* rotational jumps, a special case of which is the well-known 180º *flip-flop* motion associated with the translational diffusion along the chain axis, and rotational *oscillations*. Although flip-flops cannot be directly detected by ^2H quadrupole echo NMR,[131] their occurrence, together with small angle rotational oscillations of 8º, were first deduced from a 2nd moment analysis of the proton lineshape in crystalline PE at 100 ºC.[128-130] Flip-flops have also been confirmed by ^{13}C NMR.[131] An early ^2H NMR study reported an increase in the amplitude of rotational oscillations from 5º to 12º over the 40-100 ºC temperature range (T_m=123 ºC).[127] VanderHart reported a narrowing of the ^{13}C-^{13}C dipolar satellites in crystalline PE at temperatures above 100 ºC, consistent with much larger rotational motions.[132] However, no distinction between continuous or discrete jump models could be made from this data. Rotational oscillations can be classified as harmonic, statistical or Gaussian, where the probability for angular displacements from the equilibrium positions in the crystal lattice is given by a normal distribution.[128-130] In addition, rotational diffusion about the chain axis should also become a plausible motional mode when the potential energy barrier to rotation is low, such as in a rotator phase,[116] in the amorphous phase,[114] or near the melting point in the crystalline phase of the precisely branched polymers studied here.

Fits to the ^{2}H SS-NMR spectra of PE21-CD_3 were performed using Eastman's Deuterium Fitting Program (DFP).[133] To explore the dynamic information in the complicated polymer system, several motional models are employed and compared: diffusion, abbreviated as "***Dif***", describes the diffusion of deuterium atoms on a sphere; rotation, abbreviated as "***Rot***", describing the rotation about axis perpendicular to C-CD3 bond; and kink motion, denoted as "***Kink***", describing the three-bond kink motion (refer to Figure 5-1).

Since the amorphous spectra contain mostly highly mobile signals, it is reasonable to speculate the motions to be nominally isotropic in character. In the ***Dif***, C-CD3 bond undergoes rotational diffusion which is modelled by discrete jumps between nearest neighbor vertices of a polyhedral approximation to a sphere. The results of fitting of the experimental spectra of the non-crystalline domains using various motional models are shown in Figure 5-8. Single ***Dif*** versus ***Dif+ Dif*** (two discrete rotational diffusive motions with different rates) model are compared. It is clear that the ***Dif+ Dif*** model provides a better fitting, evidenced by the nearly overlapping experimental and simulated lineshapes. The goodness-of-fit parameter, chi-square as shown in Figure 5-9, offers quantitative support of this conclusion. The rather small chi-square value of ***Dif+ Dif*** model indicates the correctness of this double diffusive model. Recalling the rather small values of stretching parameter ***n*** related to the distribution of spin relaxation, this double diffusion model is consistent with structural heterogeneity in the amorphous phase. Such heterogeneity is inevitably averaged at elevated temperatures. Even the fits by the single diffusion motion ***Dif*** are acceptable at high temperatures, due to the averaged dynamics in the amorphous phase.

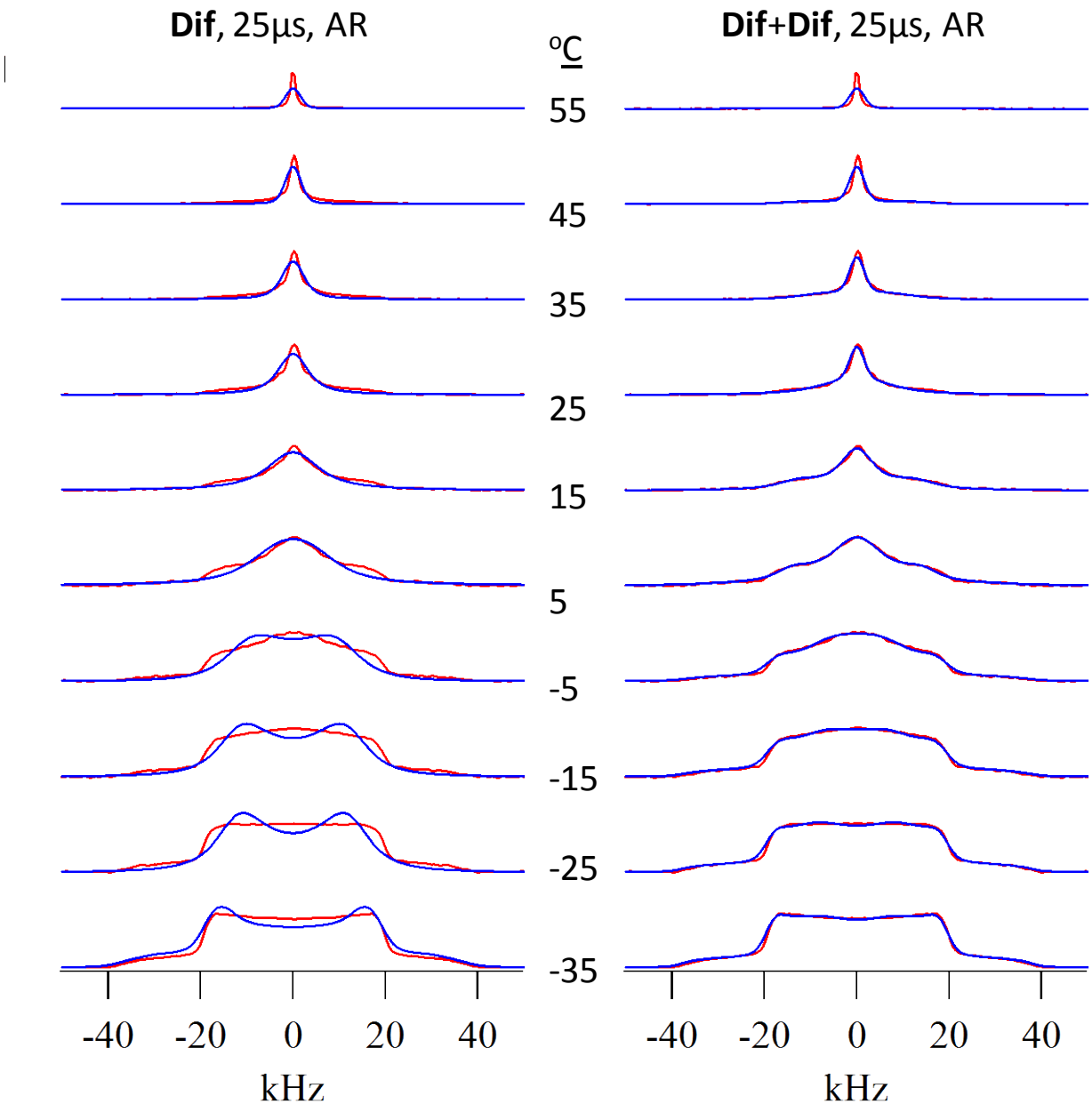

Figure 5-8. Fitting of experimental amorphous spectra using various motional models: single diffusion model (left) and two diffusion models. Echo delay is 25 µs. The experimental spectra are in red and the fits are in blue. Polymer sample is PE21-CD_3.

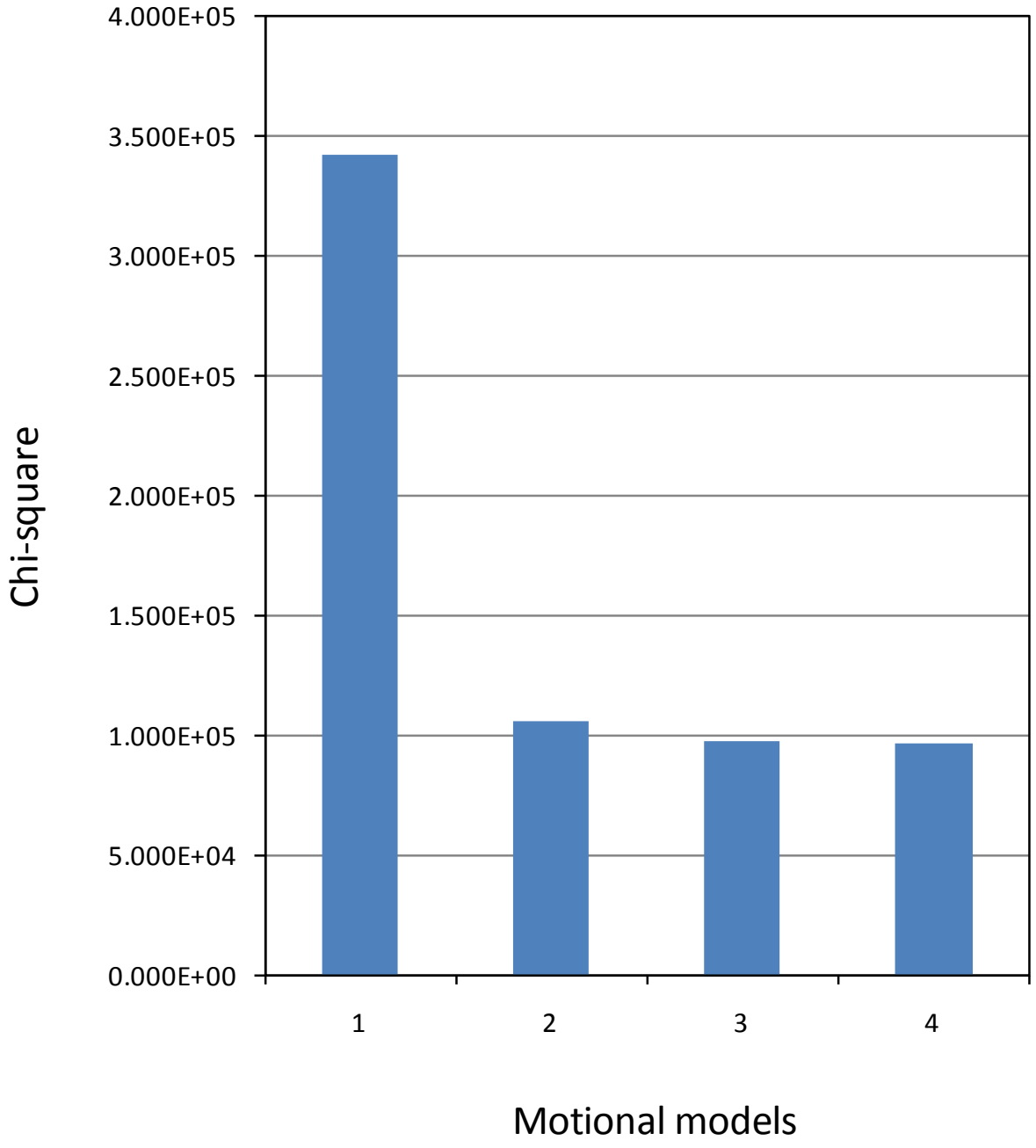

Figure 5-9.Chi-square value as a function of fitting models for amorphous spectra. Model “1” denotes a single ***Dif***. “2” is ***Dif*** + ***Dif***. “3” is ***Dif*** + ***Dif*** + ***Dif***. “4” is ***Dif*** + ***Dif*** + ***Dif*** + ***Dif***.

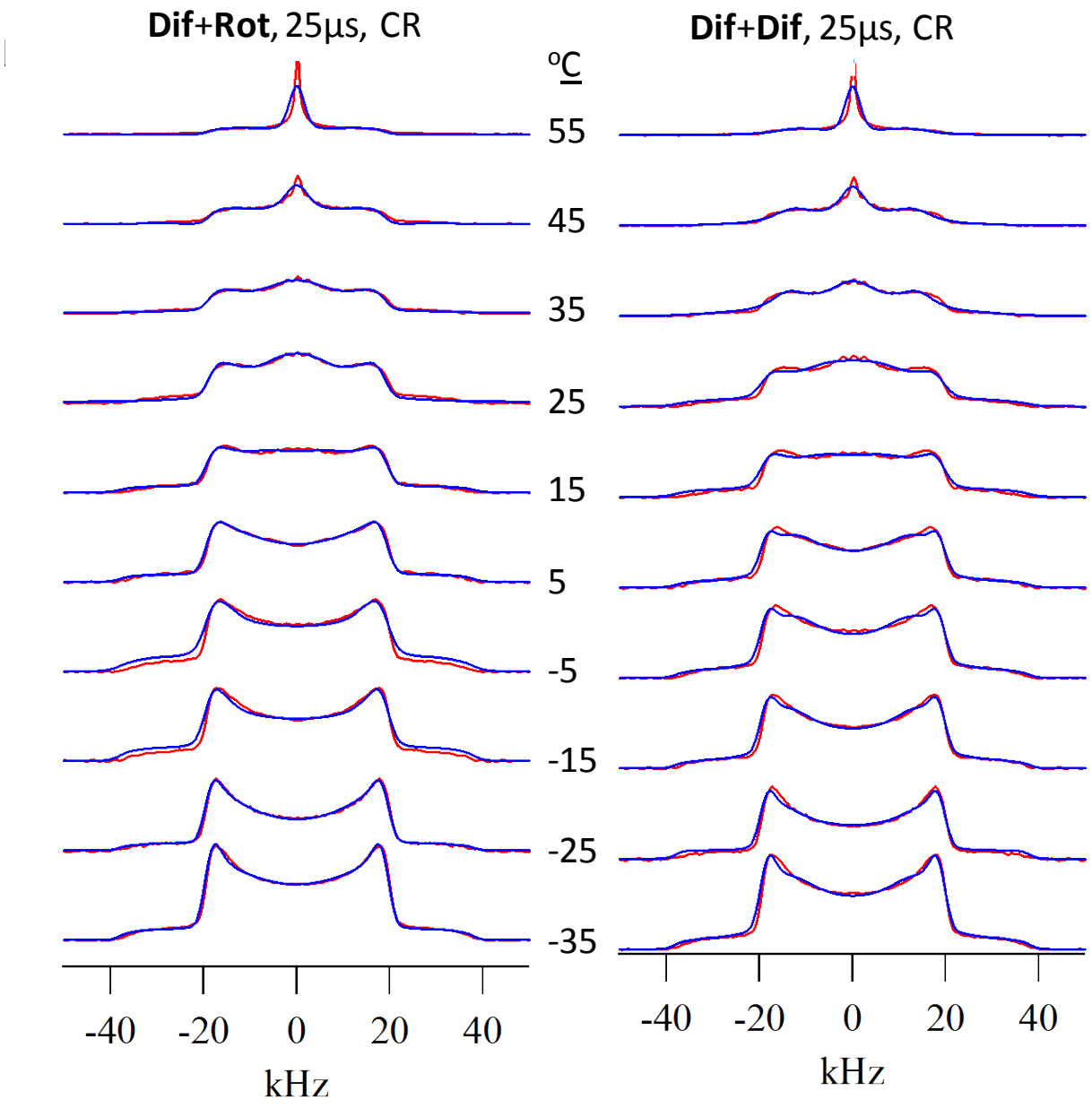

Figure 5-10. Fitting of calculated crystalline spectra using various motional models: diffusion+rotation model (left) and two diffusion models. Echo delay is 25 µs. The experimental spectra are in red and the fits are in blue. Polymer sample is PE21-CD_3.

Figure 5-10 shows the fitting to the calculated crystalline spectra. Inspired by the simulation results of amorphous spectra, fitting models involving more than one type of motional models are compared: ***Dif*+*Rot*** (diffusional and rotational dynamics with

different rates and fractions) versus ***Dif***+***Dif*** (two diffusional dynamics). As expected, the former model offers slightly better fits compared to the latter one, indicated by the smaller chi-square values. The fitting results to the CR phase indicate that the motion in the chains can be described by rotational diffusion about the chain axis and isotropic diffusive motion of the C-CD_3 bond. The necessity to include a ***Dif*** component could arise from the inability to achieve a complete separation of the non-crystalline and crystalline sub-spectra due to the occurrence of the interphase or due to the tail in the distribution of T_1 relaxation times for the amorphous phase.

Based on the lineshape simulation results of the amorphous and crystalline spectra, the fully-relaxed spectra can be readily fit into a three-component model: ***Dif***+***Dif***+***Rot***. Figure 5-11 shows the fitting results.

The fits (in red) are superimposed on top of the experimental spectra (in black). As the temperature increases through the glass transition, the onset of dynamics becomes evident with the broadening of the singularities of the Pake pattern, with intensity building in the center. Changes in the ^2H spectra are consistent with the thermodynamic data indicating that the CD_3 branches introduce disorder. Upon further increasing the temperature in PE21-CD_3, a narrow liquid-like Lorentzian shaped peak appears, representing the relatively mobile regions of the amorphous phase.

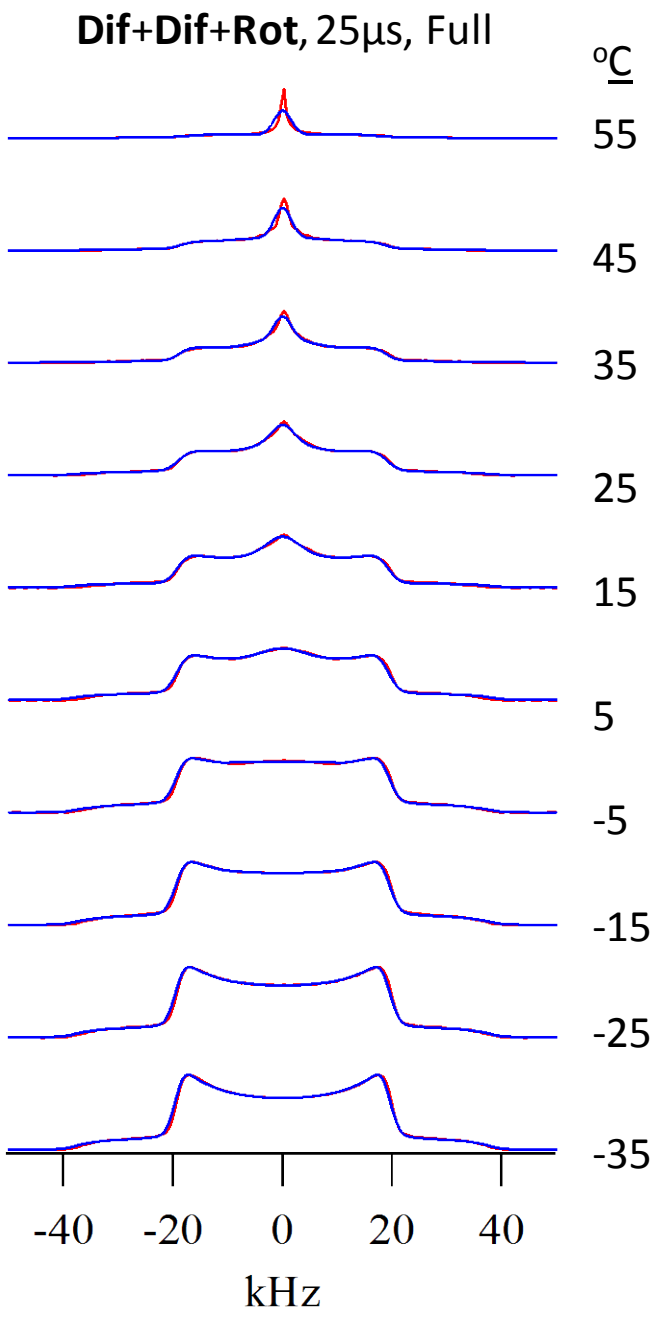

Figure 5-11. Fitting of fully-relaxed spectra using a combination of three motional models: diffusion+diffusion+rotation model. Echo delay is 25 µs. The experimental spectra are in red and the fits are in blue. Polymer sample is PE21-CD_3.

5.4 Conclusion

To conclude, deuterium solid state NMR has been proven to be well-suited in investigation of conformational dynamics. By applying T_1 filtration, the amorphous spectra can be separated from the fully-relaxed ones. The crystalline spectra can be simply calculated by subtracting the amorphous signals from the total. Lineshape simulation by using combinations of motional models provides new insights into the microscopic details of the segmental dynamics in PE. The experimental lineshapes are found to be compatible with a model in which rotation about the local chain axis occurs by a diffusive process. However, other modes of rotational motion – i.e., two-site jumps or harmonic oscillation – still cannot be excluded, and such processes could involve either specific rotation angles or distributions. Thus, further studies with selectively labeled, precisely branched polyethylene, are needed to more fully characterize the chain dynamics in these systems.

CHAPTER 6
EFFECTS OF BRANCH IDENTITY ON THE MORPHOLOGY OF PRECISION POLYOLEFINS WITH ALKYL BRANCHES

6.1 Introduction

The densities of commercial PE-based materials are determined by the size of the branches— low density of LDPE is due to the presence of both short-chain and long-chain branches while relatively high density of LLDPE comes from the existence of only short-chain branches. Meanwhile, the density itself origins from the different packing behavior, which in turn is constrained by the size of the branches. For ADMET polymers, the size of branches also counts. Herein the influence of branch identity on several properties including thermal property and morphology is discussed. ADMET precision polyethylenes with various alkyl branches *R* on each and every 21st carbon on the backbone, denoted as PE21-R, are sampled.

Table 6-1. Basic characterization data of PE21-R, including the M_w data and the thermal analysis results[29, 134]

Polymer	Branch identity	Mw,[a] g/mol	PDI [b]	T_m, ºC	ΔH_m, J/g	X_c [c], %
ADMET PE	H	15 k	2.6	134	204	70
PE21-Methyl	methyl	20.2 k	1.7	63	104	35
PE21-gemMethyl	gem-methyl	76 K [d]	-	45	62	21
PE21-Ethyl	ethyl	50.2 k	1.9	24	65	22
PE21-Propyl	propyl	41.4 k	1.7	12	60	20
PE21-isoPropyl	*iso*-propyl	46.0 k	1.7	11	37	13
PE21-Butyl	butyl	40.3 k	1.7	12	57	19
PE21-secButyl	sec-butyl	42.6 k	1.9	9	43	15
PE21-tertButyl	tert-butyl	32.1 k	1.7	13	50	17
PE21-Pentyl	pentyl	45.8 k	1.8	14	58	20
PE21-Hexyl	hexyl	46.1 k	1.7	12	49	17
PE21-cycloHexyl	cyclo-hexyl	33.6 k	1.6	9	37	13
PE21-Adamantyl	adamantyl	64.7 k	1.7	-8 & 17	2 & 8	0.1 & 2

[a] M_w acquired by GPC in THF (40 ºC) referenced to PS
[b] Polydispersity index = M_w/M_n
[c] Degree of crystallinity = ΔH_m / 293 J/g [135]
[d] Number averaged data: M_n from literature[134]

The synthesis of this series of polymers is mature and has been reported in literatures.[26, 28, 29, 31, 34, 37] The polymers studied in this chapter are mainly synthesized via the cyanide chemistry because of its short steps and quantitative yield.[28, 37]

Table 6-1 lists the basic characterization data of PE21-R, including M_w and thermal data. Note that the weight averaged molecular weight of each PE21-R polymer is larger than 15,000 g/mol, after which the molecular weight expose negligible influence on polymers' behaviours.[26]

6.2 Thermal Properties

The thermal analysis of precision ADMET polymer series PE21-R was accomplished via TGA and DSC.[28, 29] Plot the melting temperature data listed on Table 6-1 as a function of the branch identity, seen in Figure 6-1. At the first glance, one can easily find that the T_m decreases when introducing methyl and ethyl branches, surprisingly levels off when branch identity switches to the propyl group. This level-off indicates the melting temperature is no longer affected by the branch identities from the point of the propyl group. One realistic explanation will be that the bulkier groups are no longer present in the crystalline phase. In fact, this hypothesis can be reasonable, according to the famous Thompson-Gibbs equation:

$$T_m = T_m^o \left(1 - \frac{2\sigma_e}{l\Delta h_f}\right) \quad (6\text{-}1)$$

where T_m denotes the real melting temperature of a polymer, $T_m{}^o$ is the ideal equilibrium melting temperature, σ_e is the free energy for each unit area of the fold surface of the crystal, l is the crystal thickness, Δh_f is the enthalpy of the phase transition from melt state to crystalline phase. In general, this rule tells us the actual melting temperature is proportional to the thickness of the crystal. The similar melting

points of bulkier group branched PE21-R indicates the similarity in crystal sizes of these polymers. If the bulkier branches were incorporated, the crystal size would have been changed with the size of branches, and consequently the melting temperature will change as well. Nevertheless, this is not the fact. Melting temperatures of PE21-Propyl, PE21-Butyl, PE21-Hexyl, ect. Remain constant. It seems that the bulkier branches are indeed cannot exist in the crystalline phase. X-ray and SS-NMR in the next two sections will be employed to investigate this hypothesis.

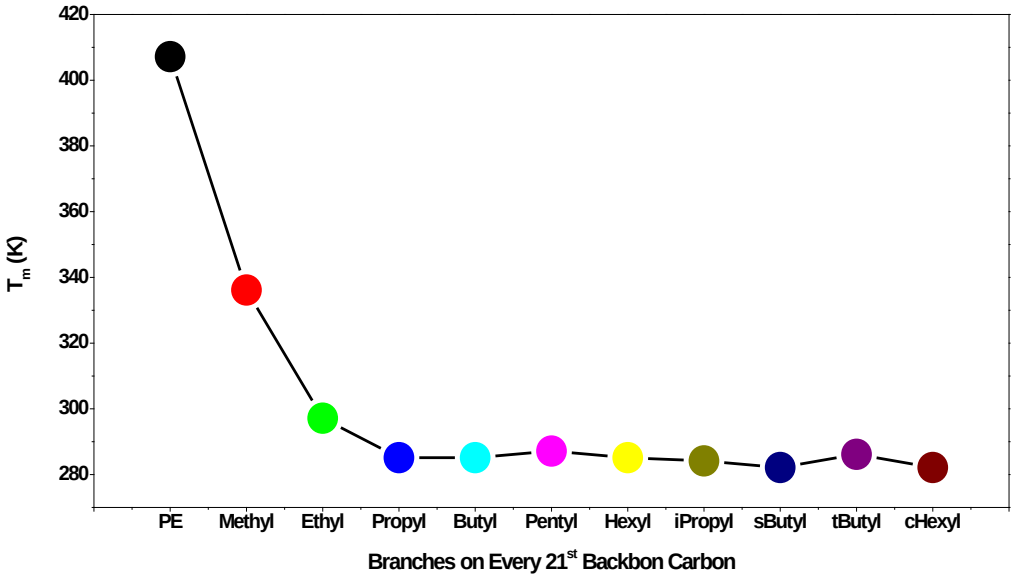

Figure 6-1. Plot of melting temperature as a function of branch identity. T_m was acquired by DSC at a rate of 10 ºC/min.

6.3 Branch Displacement Determination by WAXS

Thermal analysis displays that the alkyl groups larger (including) propyl group on longer affect ADMET polymers' melting temperature. Base on that observation, a hypothesis is proposed, saying that the bulkier alkyl groups are excluded from the crystalline regions. Therefore, changing the branch identity doesn't change the chain

packing behavior in crystalline phase, and thus has no effect on the melting temperature. WAXS is a powerful technique in studying crystal structures and is applied herein to investigate the branch displacement in 3D structure.

6.3.1 Experimental

Wide angle powder X-ray diffraction (WAXD) data were obtained on a Bruker D8 diffractomer equipped with liquid N_2 cooling system, using copper K_α radiation with λ=1.54 Å. The solid polymers (T_m > room temperature), such as linear ADMET PE and methyl branched PE, were filled into a copper container of 10 by 10 mm^2 with a depth of 1mm. Prior to measurement, these solid samples were melted to remove any thermal history. As for liquid polyolefins (T_m < room temperature), i.e., polymers with branches longer than the ethyl group, samples were put on top of a flat copper substrate to form a thin layer with ~1mm thickness. During the measurements, in order to reduce scattering from air and avoid chemical degradation by oxygen at elevated temperatures, medium vacuum was applied to the sample chamber. XRD data were collected at the experimental scattering angle 2θ ranging from 5º to 45º, with a step of 0.1 º/min. Temperature dependent measurements were addressed at temperatures varying from below glass transition temperature to above melting points, with cooling or heating rate of 1 ºC/min.

6.3.2 Results and Discussion

Wide-angle X-ray diffraction (WAXD) measurements further support the observation of a change in polymer morphology as a function of branch size. Six such WAXD diffractograms are shown in Figure 6-2; these patterns indicate that the introduction of branches leads to the lattice distortion and local conformational disorder,

where the type of crystal structure and polymer morphology is strongly dependent on the branch identity.

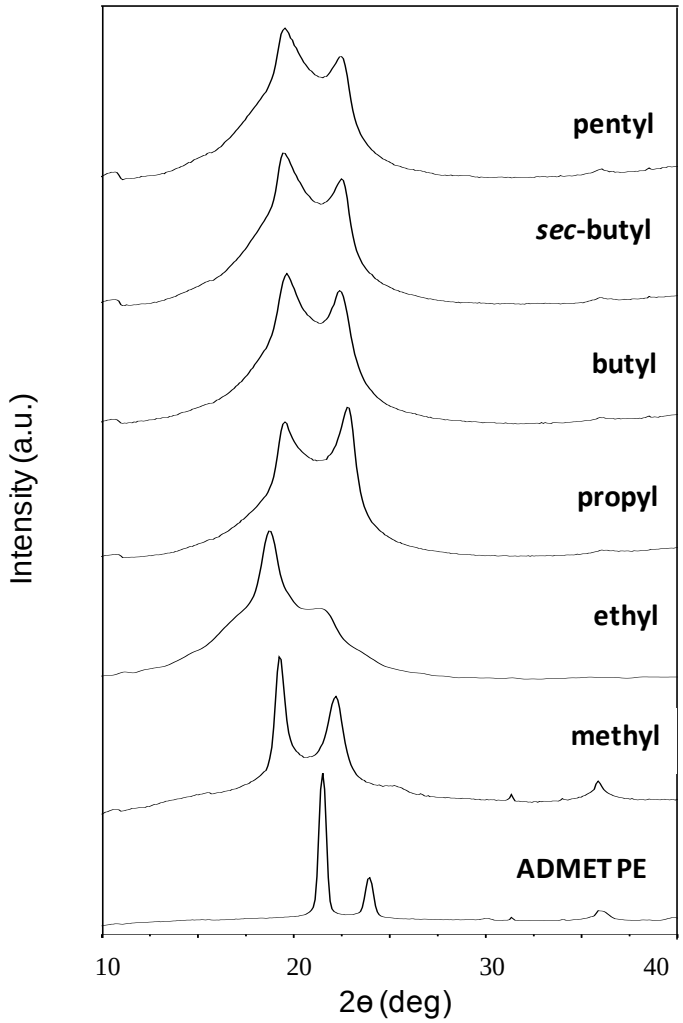

Figure 6-2. WAXS results of PE21-R, referenced to linear ADMET PE: **ADMET PE** at 27 ^{o}C (no branch, T_m= 134 ^{o}C), **PE21-Methyl** at 27 ^{o}C (methyl branch, T_m= 63 ^{o}C), **PE21-Ethyl** at room temperature (ethyl branch, T_m= 24 ^{o}C), **PE21-Propyl** at 0 ^{o}C (propyl branch, T_m= 12 ^{o}C), **PE21-Butyl** at 0^{o}C (butyl branch, T_m= 12 ^{o}C), **PE21-secButyl)** at 0 ^{o}C (sec-butyl branch, T_m= 9 ^{o}C), **PE21-Pentyl)** at 0 ^{o}C (pentyl branch, T_m= 14 ^{o}C). Prior to measurements, all samples were heated to above melting temperature in order to remove thermal history, and then cooled to specific temperature at a rate of 1 ^{o}C/min.

For the sake of comparison, **ADMET PE** is displayed at the bottom of Figure 6-2 exhibiting the typical orthorhombic crystal form with two characteristic crystalline peaks

superimposed with the amorphous halo, exactly the same as for high-density polyethylene made by chain propagation chemistry. The more intense peak at scattering angle 21.5° and the less intense one at 24.0° correspond to reflection planes (110) and (200), respectively. Upon introducing precisely placed branches of known identity, the crystal structure loses its symmetry with the unit cell shifting from orthorhombic to triclinic. Moreover, in contrast to linear polyethylene, scattering occurs at relatively lower scattering angles and with broad reflections being displayed, suggesting the decrease of crystallite size and crystallinity.

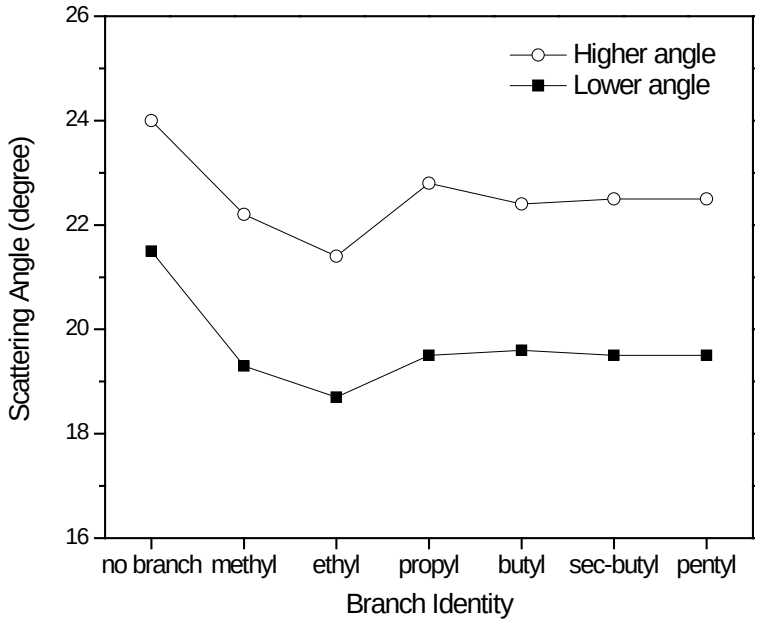

Figure 6-3. Plot of scattering angle of two strong reflections as a function of branch identity. The top line is for the reflection at higher angle while the bottom one is for the reflection at lower angle.

In the case of the methyl-branched polymers **PE21-Methyl**, two reflections representing a triclinic crystal orientation occur at scattering angle 19° with the Miller index (100) and 22° with the Miller index (010). Transmission electron microscopy (TEM)

shows the lamellar thickness to be quite small, between 10 and 20 nm. Since such a thickness is much larger than the length of 20 CH_2 units, indicating that the methyl side chains are incorporated in a triclinic lattice.

Similar changes in crystalline unit cell identity were observed in the ethyl branched polymer, **PE21-Ethyl**. Two strong reflections shift to lower scattering angles (18° and 21°) compared to the methyl-branched polymer (19° and 22°). On the basis of Bragg's law, this observation allows us easily to draw the conclusion that the ethyl branch is incorporated in the crystal region. In contrast to the **PE21-Methyl**, the introduction of the ethyl side chain perturbs the crystal structure more and requires larger space to be incorporated. As a consequence, the reflections shift to lower scattering angles, which correspond to larger *d*-spacing. For the polymers possessing bulkier branches (propyl or larger), the WAXD diffractograms (the top four graphs in Figure 6-2) show nearly identical scattering patterns, indicating that the crystal structure is independent of the branch identity. Moreover, these patterns are obviously different from those of polymers possessing smaller branches like methyl or ethyl branches, exhibiting larger scattering angles and even broader reflections.

To understand these observations, the scattering angles of two strong diffraction peaks as a function of branch identity are illustrated in Figure 6-3. We see two trends: the decrease of scattering angles for smaller branches, followed by leveling-off of the scattering angles for bulkier branches. The former trend is easily understood. The methyl/ethyl side chains function as defects in the crystal lattice and result in the increase of *d*-spacing, thus decreasing scattering, where the ethyl results in a smaller scattering angle. Distinct difference is the case for the bulkier branches, where the

angles for bulkier branchedpol ymers, **PE21-Propyl**, **PE21-Butyl**), **PE21-Pentyl**, and **PE21-*sec*Butyl** increase to higher degrees, 19.5° and 22.5°. Recall the X-ray scattering theory: scattering angles are determined by the type of unit cell while the peak intensities are based on the atom arrangements within the lattice. *With this in mind, we conclude that the packing behaviors of precision polymers possessing sizes equal to or larger than propyl are different from those of the methyl- and ethyl-branched polymers. In all cases, the bulkier branch is excluded from the unit cell into the amorphous region.* The morphology and packing behavior of these precision polymers with bulky branches are independent of the size of the branch. This assessment is in agreement with the thermal data in Table 6-1, where essentially identical melting temperatures are observed for all the branched polymers.

Note that the reflection occurring at ~19.5° is much broader and less symmetric than peaks for the methyl-branched polymer **PE21-Methyl** or ethyl-branched polymer **PE21-Ethyl**. The asymmetry suggests the presence of more than one crystal lattice besides triclinic; broadening is due to a decrease in the degree of crystallinity.

Of particular interest is the fact that the WAXD scattering patterns for these precision polyolefins are noticeably different from those for randomly branched polymers: the precision structures result in varying crystal lattice identity and relatively sharper scattering peaks.[10, 32, 136-138] The random ethylene-propylene (EB) copolymer with 20% comonomer content exhibits a dominant hexagonal crystal form,[136] compared to the triclinic form present in our precision **PE21-Ethyl** polymer. As for the random ethylene-butene (EB) copolymer, it shows orthorhombic crystal structure with low crystallinity.[136, 137] In contrast, the precision ethylene-octene (EO) polymer **PE21-Hexyl**

exhibits an additional hexagonal mesophase besides the orthorhombic crystalline phase.[138]

6.4 Investigation of Dynamic by SS-NMR

The X-ray investigation for precisely sequenced polymers with alkyl branches has concluded that the smaller groups can be incorporated in the unit cell while the larger ones are excluded from the unit cell. The cut-off of the branch identity is the propyl group, whose size is too large to be integrated in the crystalline phase. ^{13}C SS-NMR measurement leads to same conclusion as WAXS based on the knowledge that segments of polymer chains move slower in crystalline region than them in amorphous phase.

6.4.1 Experimental

The polymer samples are the same as used in X-ray studies, i.e., ADMET precision polyethylenes with alkyl branches. The synthesis of these polymers has been described in section 6.1.1 as well as literatures.[28, 29]

SS-NMR was carried out at Max Planck Institute for Polymer Research (MPIP), Mainz, Germany, utilizing a Bruker spectrometer equipped with a Bruker Avance II+ console working at ^{1}H Larmor frequency of 850 MHz. Polymer samples were tightly and evenly packed in 2.5 mm rotors and measured in 850 MHz spectrometer using 2.5 mm MAS ^{1}H-X double resonance probe, which is suitable for NMR experiments under fast MAS conditions.

The segmental dynamics were studied via REREDOR pulse sequence, a sensitive approach to determine ^{1}H-^{13}C dipolar decoupling constants by spinning sideband pattern analysis. The detailed introduction of this modern SS-NMR technique can be found in section 3.1.5.4.

6.4.2 Results and Discussion

The slices from REREDOR experiments are shown in Figure 6-4. The peaks are assigned and highlighted with different colors. For methyl-branched polymer, the methyl branch marked in yellow shows up at 20.3 ppm; the peak at 28 ppm is contributed from β carbon in amorphous phase; two strong peaks at 30.4 ppm and 33.8 ppm represent the *all-trans* CH_2 (δ carbon) in crystalline phase and gauge backbone CH_2 (δ carbon) in amorphous phase, respectively; the small peak appearing at 35 ppm (in green) can be assigned to the methine carbon. Interestingly, a clear splitting of chemical shift occurs for α carbon at around 40 ppm and 38 ppm; moreover, the ratio of the α peak heights is identical to the ratio of δ peak heights. This similarity allows the two alpha peaks to be assigned as α_c (α carbon in crystalline region, 40 ppm) and α_a (α carbon in amorphous region, 38 ppm). Such an assignment indicates the presence of α carbon in both crystalline and amorphous phases, an observation in agreement with WAXS data. The spinning-sideband analysis also supports this conclusion, seen in Table 6-2.

The dipolar recoupling constant, D_{ij} of α_c by simulation is determined to be 14 kHz, corresponding to a slow motion, while the D_{ij} of α_a is simulated to be 7.5 kHz, implying a fast motion in amorphous phase due to less structural constrains from surrounding atoms. Note the D_{ij} of δ_c and δ_a are 14 kHz and 6.5 kHz separately, which confirm the correctness of peak assignment and reverse relationship between D_{ij} and segmental dynamics.

It is worth mentioning the difficulty in simulating the spinning-sideband of methyl branch for PE21-Methyl. By all means, the sideband pattern of methyl group is impossible to fit by any single dipolar coupling constant. However, when fitting it to one large and one small D_{ij} values, the problem is solved. Combined with the results from

WAXS and α carbon sideband analysis, one can readily come to the conclusion that the methyl branches are present at both crystalline and amorphous phase.

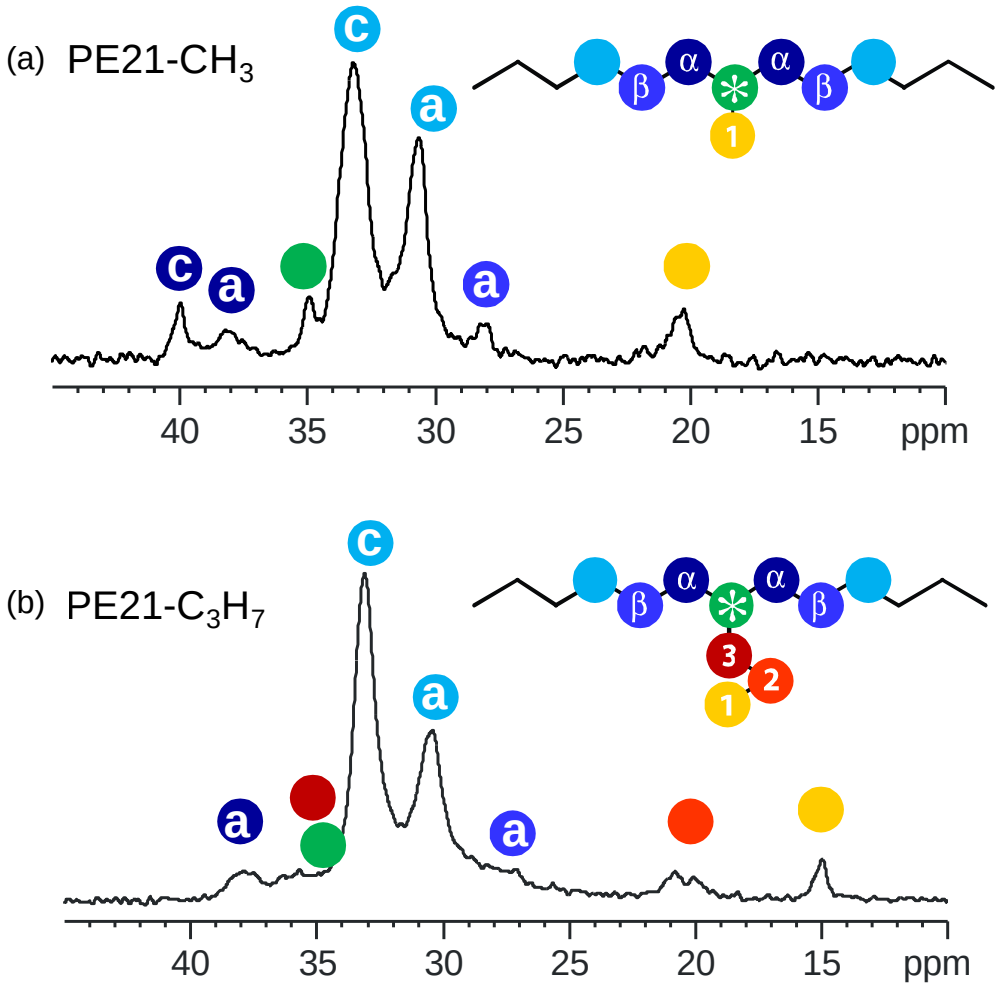

Figure 6-4. Peak assignment of slices from REREDOR spectra for (a) methyl-branched and (b) propyl-branched ADMET precision polymers

As for the case of PE21-Propyl, seen in Figure 6-4 (b), the peak assignment are as follows: methyl group in the propyl branch (carbon 1) shows up at 15 ppm (in yellow); CH_2 group in the propyl branch (carbon 2) appears at 20.5 ppm (in orange); the relatively broad and short peak at 27 ppm is contributed from β carbon in amorphous phase (in blue); the two strong peaks at 30.5 ppm and 33.5 ppm correspond to the *all-*

trans CH_2 (δ carbon) in crystalline phase and gauge backbone CH_2 (δ carbon) in amorphous phase, respectively; the trace peak shows at around 35 ppm may comes from the methine carbon (in green) or carbon 3 (CH_2 of the propyl branch). Apparently both of them are overlapped under the strong peak of crystalline *all-trans* CH_2 groups. The peak at 38 ppm is easily attributed to α carbon.

The simulation results of the spinning sideband patterns for PE21-Propyl is shown in the second half of Table 6-2. Backbone CH_2 carbons display two dipolar decoupling constants of 14 kHz and 6.8 kHz, corresponding to the *all-trans* CH_2 in the crystalline region and gauge conformation of CH_2 in the amorphous region. The D_{ij} of α carbon at 38 ppm is determined to be 6.5 kHz, a typical value indicating fast motion. So are the values of carbon 1 and 2: 6.5 and 3.7, indicating the presence of the propyl groups only in the amorphous phase.

Table 6-2. Recoupling constants derived from REREDOR experiments for methyl-branched and butyl branched ADMET precision polymers with branch spacer of 21.

polymer	site	D_{ij}, kHz	S_{ij}	Conclusion
PE21-Methyl	α_c (α carbon in CR)	14	0.7	slow, CR
	α_a (α carbon in AR)	7.5	0.35	fast, AR
	δ_c (backbone CH_2 in CR)	14	0.7	slow, CR
	δ_a (backbone CH_2 in AR)	6.5	0.3	fast, AR
	$1_{c/a}$ (CH_3 in CR/AR)	6.8/3.5	~0.2	fast, AR / slow, CR
PE21-Propyl	α_a (α carbon in AR)	6.5	0.3	fast, AR
	δ_c (backbone CH_2 in CR)	14	0.7	slow, CR
	δ_a (backbone CH_2 in AR)	6.8	0.3	fast, AR
	2 (CH_2 of propyl group)	6.5	0.3	fast, AR
	1 (CH_3 of propyl group)	3.7	<0.2	fast, AR

CR: crystalline region
AR: amorphous region

The REREDOR experiments for PE21-Ethyl and PE21-Butyl result in the same conclusion as achieved from that for PE21-Methyl and PE21-Propyl—smaller branches

including the methyl and the ethyl groups are integrated in the ordered 3D array, while the larger ones such as the propyl and the butyl groups are found in the non-crystalline phase only.

6.5 Morphological Models

Combining the results from X-ray and SS-NMR, one can conclude the branch displacement for ADMET precision polyolefins exampled by PE21-R series, illustrated by the flow chart in Figure 6-5.

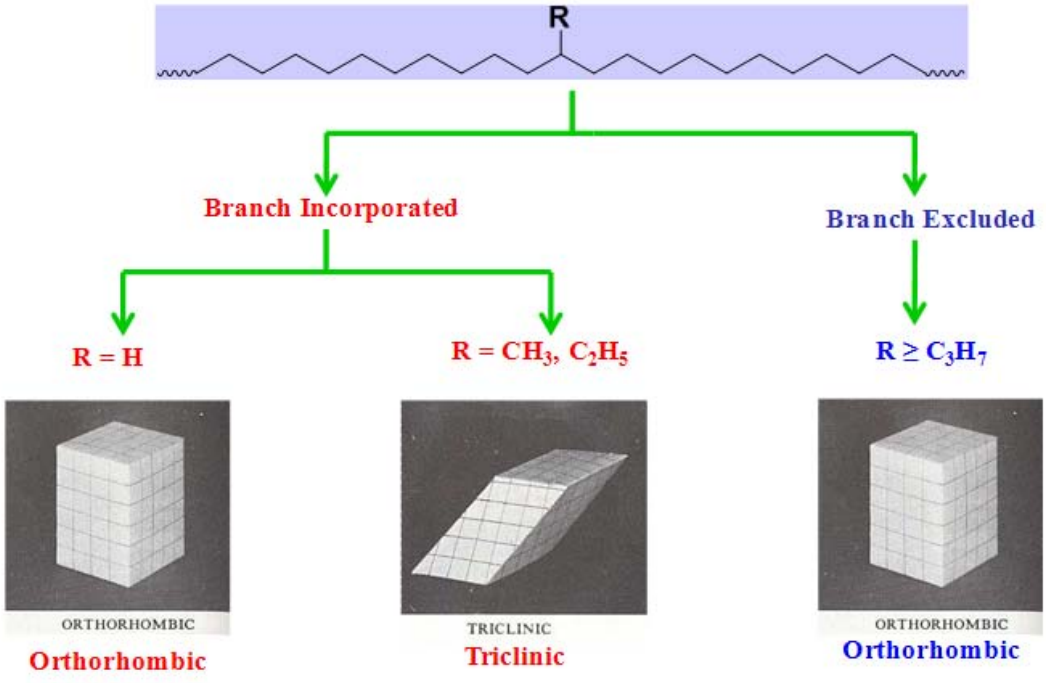

Figure 6-5. Flow chart of Branch displacement in ADMET precision polyolefins PE21-R, where R = alkyl branches on each and every 21st carbon along the ethylene backbone

For high crystallinity linear ADMET polyethylene, i.e., when branch R is in fact the hydrogen atom, the crystal structure deciphered via WAXS is claimed to be orthorhombic, same the crystal form as for commercial PE-based structures. When

small alkyl branches, including the methyl and the ethyl branches are introduced, the symmetric 3D array of crystal structure is disturbed by the “defects” and shifted to triclinic crystal structures due to the incorporation of small side groups in the ordered region. Situation changes when the branches get bigger. The propyl group is the turning point. The alkyl branches as big as or larger than the propyl groups cannot be present in the crystalline region due to the oversized perturbation, seen in Figure 6-5. Therefore, for large alkyl branches, the polymer chains fold to form lamellae devoid of large defects: it is the all-trance polyethylene segments that pack into three-dimensional ordered array, just as the scheme of morphology illustrated in Figure 6-6. However, it is noticeable that the bulkier-branched ADMET polyolefins obtain different unit cell parameters than the unbranched ADMET PE.

Based on the schematic morphology of large defect branches, the size of the lamellae should be determined by the branch spacer, if the polymers crystallize. For instance, if the branch spacer is 21, the lamellae thickness will then be limited by the length of 20 CH_2 sequence in between of two large defects. In fact, the reality should be a little off from the hypothesis, if the substantial size of the branches present at the interphase has to be considered. Due to the connection of polymer structures, the large alkyl branches at the interphase will inevitably disturb the nearby crystal segment’s orientation and packing. Thus, to maintain the ordered structure, the polymer chains will sacrifice some segments by transferring them from the crystalline phase into the interphase, which will result in a lamellar thickness a little bit smaller than the length of CH_2 sequence between two branches. In principle, the bigger the branches are, the large this shrinkage will be.

Moreover, since the melting temperature is directly related to the lamellae thickness for semi-crystalline polymers, one can comment that the melting point of PE21-R series is determined by branch to branch distance- in this case: 20 CH_2 sequences. The fact that branches as big as or bigger than the propyl groups are placed in the non-crystalline regions perfectly explains the similar melting temperatures of PE21-Propyl, PE21-Butyl, PE21-Hexyl, and other PE21-R polymers.

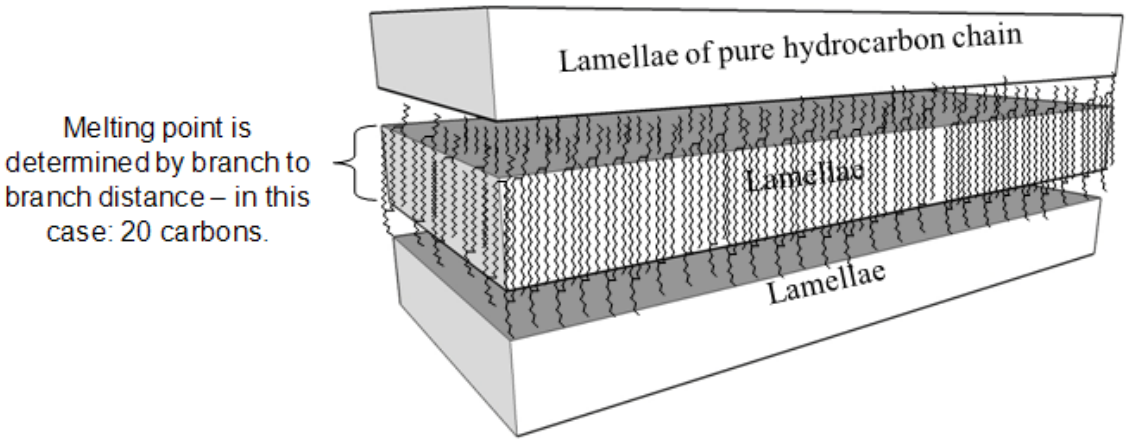

Figure 6-6. Schematic morphology of precision polymers with large defect branches

CHAPTER 7
ADMET PRECISION POLYETHYLENE WITH LOW BRANCH FREQUENCY

7.1 Introduction

As we have demonstrated, the size of the branch as well as the branch content significantly affects the microstructural, thermal, dynamical, morphological properties of the ADMET polyolefins. The manipulation of branching provides an applicable way of modeling the realistic industrial PE-based materials. With high branch content, such as one branch on each and every 21st polyethylene carbon, ADMET polymers are capable of mimicking the structure of linear low density polyethylene. However, for an attempt of understanding metallocene PE, rather low content of branching is needed.[24, 139-145] Recently, a precision ADMET polyethylene possessing quite low frequent branch—a butyl branch displaced on each and every 39th backbone carbon—was made successfully,[36] offering an applicable methodology to produce precision models with up to date maximum precision run lengths between adjacent branches.

7.2 Experimental

Precision polyethylenes with branches on each and every 39th backbone carbon, denoted as PE39-R, were synthesized via polycondensation reaction—ADMET chemistry, followed by exhausted hydrogenation. The key to the successful synthesis involves the preparation of the symmetric diene monomer with reduced branch frequency. Deuterated and protonated methyl-branched precision monomers for polymers PE39-CD_3 and PE39-CH_3 were made via the two methodologies described in Chapter 2. Specifically, the synthesis of these two precision monomers used herein was illustrated in Figure 7-1. The important limitation of this synthesis lies in the

production of commercial unavailable 18-spacer alkenyl bromide,[36] which can be accomplished by dehydrohalogenation of alkyl dibromide.[36, 146]

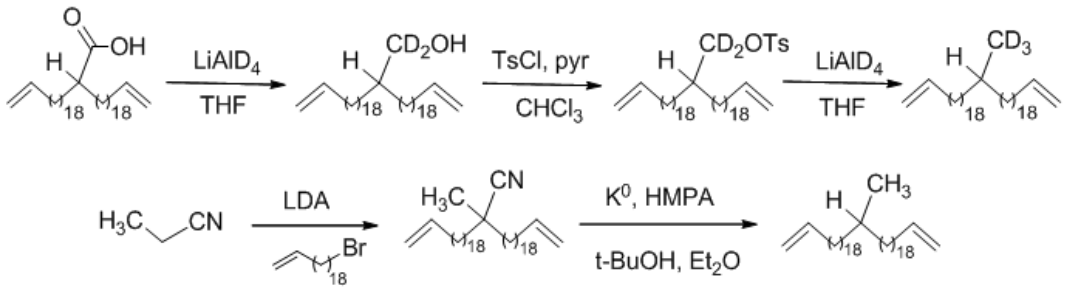

Figure 7-1. Synthetic methodology used to produce precision methyl-branched (18,18) monomers: the top reaction was used to make trideuterated monomer while the bottom one was for the protonated monomer.

Once the pure monomers with desired run length are produced, the precision polymers of interest PE39-CD_3 and PE39-CH_3 can be readily afforded by acyclic diene metathesis polycondensation chemistry and the consecutive hydrogenation under Wilkinson's [Rh] catalyst. The butyl-branched ADMET precision polymer, PE39-C_4H_9, was prepared based on procedures in a recent literature.[36] Table 7-1 lists the basic characterization data of PE39-R, with unbranched ADMET PE as reference. PE39-CH_3-hmw was the high molecular weight version of PE39-CH_3. It was achieved via soxhlet extraction by removing the low molecular weight parts into toluene solution.

Thermal analysis was conducted via a TA Instruments differential scanning calorimetry (DSC) Q1000 equipped with a controlled liquid N_2 cooling setup, at a heating/cooling rate of 10 ºC/min. Molecular weight information was acquired by gel permeation chromatography (GPC) in trichlorobenzene (TCB) at 135 ºC with reference to polystyrene standard. Solid state NMR measurement was performed utilizing the 850 and 700 MHz spectrometers at fast magic angle spinning. 2D X-ray data were obtained

using a rotating anode (Rigaku 18 kW) X-ray beam with a pinhole collimation and a Siemens 2D area detector. Cu-Kα radiation with wavelength 0.154 nm was achieved by a double graphite monochromator. Except for the thermal analysis, GPC, SS-NMR, and WAXS were all measured at Max Planck Institute for Polymer Research, Mainz, Germany.

Table 7-1. Molecular weight and thermal data for ADMET precision polyethylene with branch spacer of 39, referenced to linear ADMET PE.

Polymer	Branch Identity	M_w x10^3, g/mol	PDI	T_m, ºC	ΔH_m, J/g	X_c, %
ADMET PE	n/a	68.4	2.66	134	204	70
PE39-CD_3	CD_3	39.7	2.16	88,91	124	43
PE39-CH_3	CH_3	35.1	2.39	87, 91	175	60
PE39-CH_3-hmw	CH_3	92.7	1.97	92.5	134	46
PE39-C_4H_9	C_4H_9	67.0 [a]	1.44 [a]	75	66	22

a: molecular weight of unsaturated ADMET polymer[36]

7.3 Results and Discussion

7.3.1 Thermal Behavior

It has been evidenced that for semi-crystalline precision ADMET polyolefins, the melting temperature obeys an inverse relationship with the branch frequency. The more the branches are introduced, the more “defects” in the polyethylene microstructures will affect the segmental chains packing into ordered arrays. When the branch frequency exceeds certain limitation, due to the lack of controlled stereochemistry, alkyl branches exhibit random orientation relative to main chain. This heterogeneity of side chain orientation consequently hinders the form of crystalline domains, especially when the run lengths between adjacent defects are so small that packing into ordered structure results in unfavoured conformation with high internal energy. Thus, totally amorphous polymer forms. This is the case for PE5-CH_3 and PE5-C_4H_9, where there is no

crystalline regions exiting. In contrast, with some higher frequency of branches, PE7-CH_3 and PE15-C_4H_9 appear semi-crystalline behaviours.

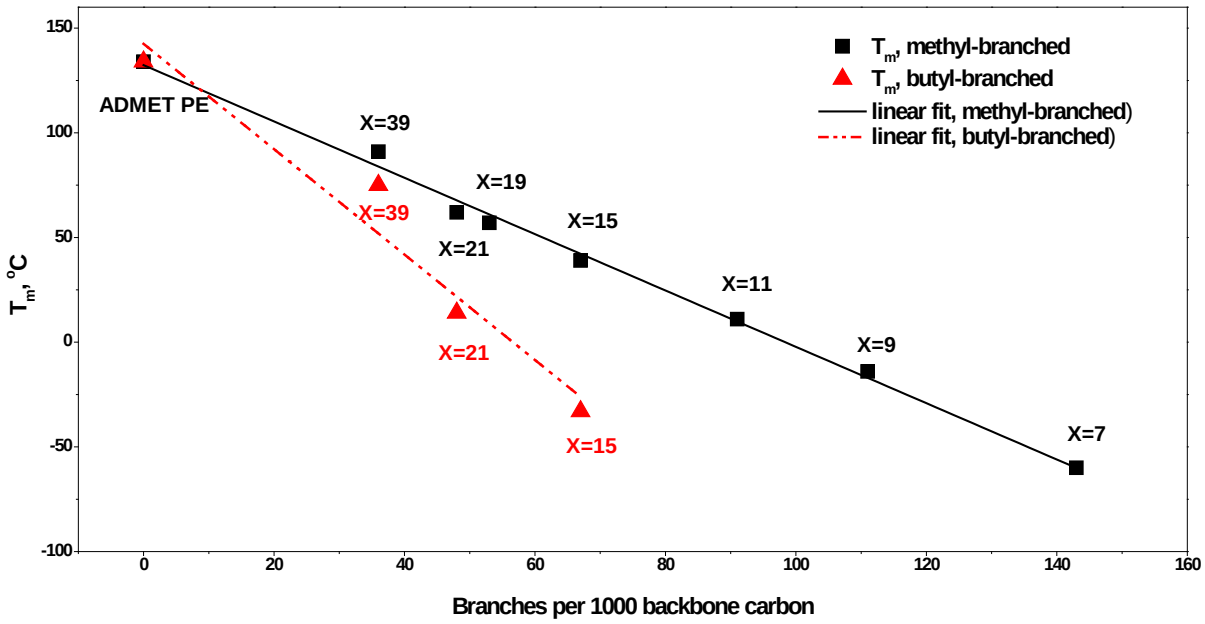

Figure 7-2. Plot of melting point as a function of branch content: black squares and red triangles are the experimental data points acquired from DSC at a heating/cooling rate of 10 ºC/min; linear fits were done via Origin 8.0. T_m data of polymers with lower branch frequency are from literatures.[26, 28, 36, 37]

Figure 7-2 shows the correlation of melting temperature and branch content for methyl-branched and butyl-branched ADMPE precision polyolefins. The experimental data achieved from DSC can be better fit into linear function: $y = 132.34 - 1.3456 * x$ with correlation coefficient R^2 of 0.99480 for PEx-CH_3, where x is the branch spacer; the linear fit for PEx-C_4H_9: $y = 142.5012 - 2.51659 * x$ shows not so perfect fitting with R^2 of 0.93253 due to less data points. Apparently, there is a reciprocal relationship of melting behavior y and branch frequency x, which is in agreement with the conclusion drawn from commercial PE. The fitting functions not only give quantitative relation of

melting points and branch frequency, but also can be utilized for prediction. For instance, from the linear line fit equation, one can deduce the melting temperature of PE75-CH_3 (when methyl branch is displaced regularly on each and every 75th backbone carbon) to be 114 ºC, and T_m of PE75-C_4H_9 to be around 110 ºC. The proximity of these two T_m values can be explained from Figure 7-2 as well: the two linear fits approach same upper limitation—unbranched ADMET PE.

The perfect linearity of melting point as a function of branch frequency for PEx-CH_3 arises from the fact that the crystalline domains incorporate pendant methyl branches as defects. The atactic methyl branches enforce the ideal *all-trans* stem conformation to deviate into conformationally disordered crystal structures. Previous study on PE21-CH_3 and PE15-CH_3 documents that this deviation in turn shortens the chain stems and appears stronger in the lower frequently methyl-branched precision polymer, PE15-CH_3.[99] The shorter chain stems due to the introduction of more frequent branches then give rise to correspondently thinner lamellar structures, which appear in thermal behavior lower melting points.

As for the precision polyolefins with bulkier branches, PEx-C_4H_9, since it has been demonstrated that the butyl branches are present only in the non-crystalline regions, the lamellar thickness is limited by the run length of chain stem in between of two adjacent butyl branches. Therefore, T_m of butyl-branched precision polymer is more directly related to the branch spacer, i.e. the chain length of *all-trans* conformation in crystalline phase. Based on Thompson-Gibbs equation listed in chapter 6,

$$T_m = T_m^o \left(1 - \frac{2\sigma_e}{l\Delta h_f}\right) \quad (7\text{-}1)$$

for the family of PEx-C_4H_9, one can reasonably assume that T_m^o (ideal equilibrium melting temperature), σ_e (free energy for each unit area of the fold surface of the crystal), and Δh_f (enthalpy of the phase transition from melt state to crystalline phase) remain constant regarding the difference in branch spacer. Thus, real melting point T_m can be correlated to l_c (crystal thickness) in such a formula:

$$T_m = a - \frac{b}{l_c} \tag{7-2}$$

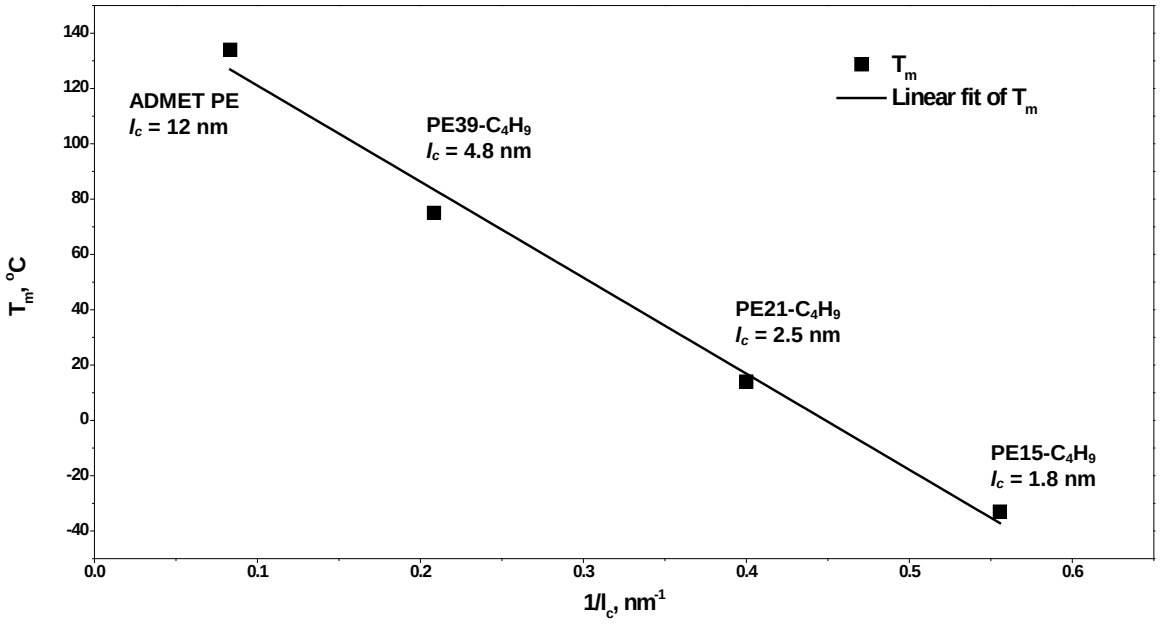

Figure 7-3. Correlation of melting temperature and lamellar thickness for a series of butyl-branched ADMET polymers. The lamellar thickness of unbranched ADMET PE was assumed to be 12 nm, value adopted from the ultra high molecular weight PE.[23, 147] Linear fit formula is: $\boldsymbol{y = 155.7938 - 347.3119 * x}$, with R^2 = 0.986.

The length of *all-trans* chain stem in between two adjacent branches can be calculated from the C-C bond length of 1.54 Å and the CH_2-CH_2-CH_2 tetrahedral angle of 109.47º. According to the morphology model proposed in Figure 6-6 for ADMET precision polyolefins with bulky alkyl branches, one can easily plot the experimental

melting point T_m as a function of reciprocal of calculated lamellar thickness $\frac{1}{l_c}$, as shown in Figure 7-3. The linear correlation of melting points and the reciprocal of lamellar thickness further prove the reality of our morphology model for ADET precision polymers with bulky alkyl side chains. The bulk branch is, indeed, not present in the crystalline domain; the lamellar thickness is limited by the length of ethylene sequence between two branches.

Precision polymers with reduced branch frequency, PE39-R, behave quite differently from those with high branch frequency, not only on the thermal behavior but also on how the polymer chains pack into ordered structure and how the branches orientate in terms of the backbone.

7.3.2 Solid State NMR Investigation

Despite of the low natural abundance, ^{13}C as an interesting nucleus has been proved to be very useful especially when coupled with a high magnetic field. Herein ^{13}C SS-NMR under either CP condition or single pulse excitation was applied on methyl-branched polymers PE39-CH_3, PE39-CH_3-hmw, and PE39-C_4H_9 under fast MAS conditions. The methyl-branched ADMET polymers show some unique observations and will be discussed in details.

The polymer sample PE39-CH_3 was heated to above its melting temperature to remove any thermal history present. The ^{13}C spectrum of the melted polymer is shown in Figure 7-4. The narrow solution-like peaks arise from the accelerated motional averaging at melt state when crystalline structure collapses and the resulting total amorphous polymer exhibits isotropic motions. Based on the chemical shifts and relative intensities, the peaks are assigned to each group with no difficulty. If calculated

roughly from the integrations, one can conclude the degree of polymerization is less than 10, indicating there are quite a few short chains present in the polymer system.

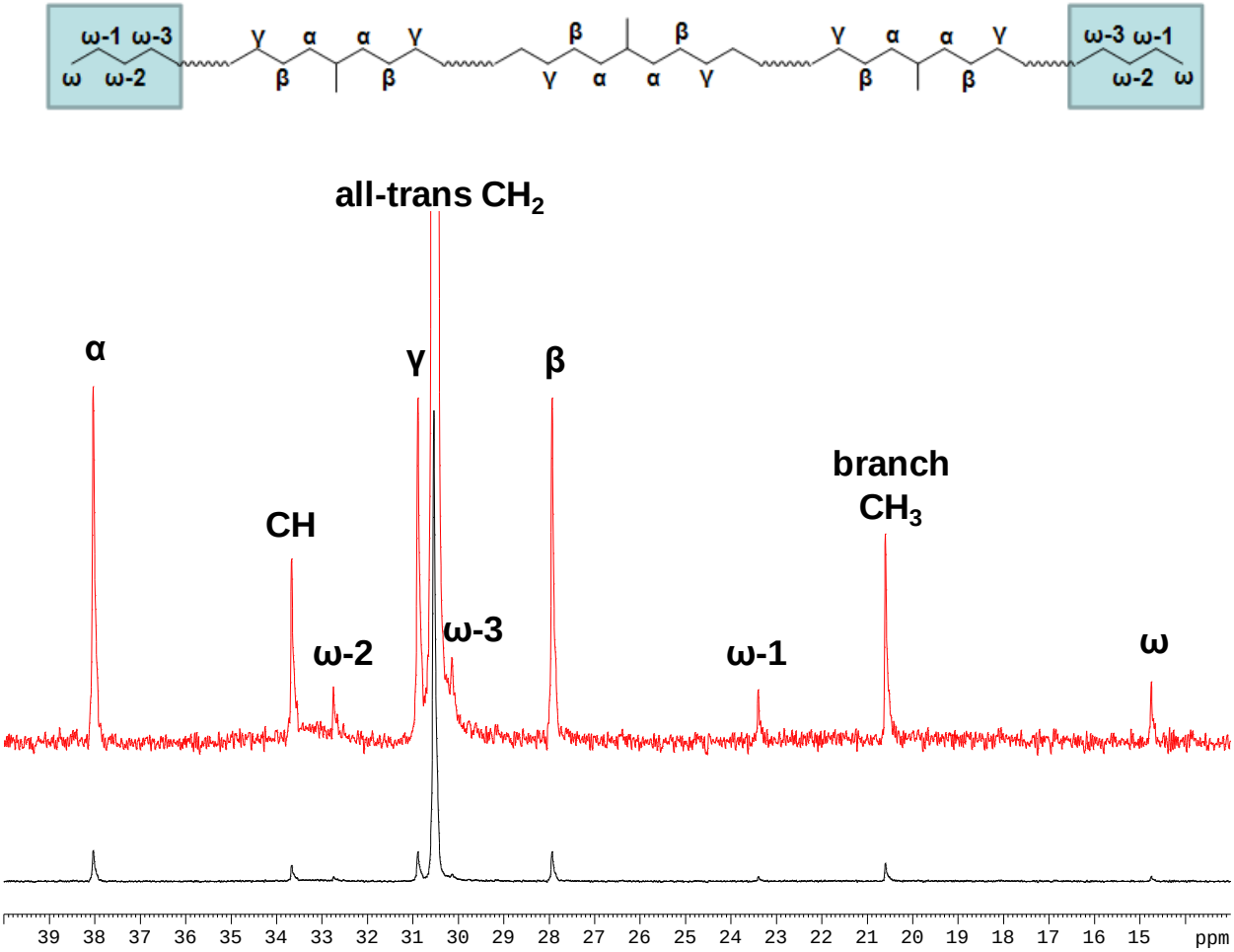

Figure 7-4. ^{13}C SS-NMR spectrum of PE39-CH_3 at melted state: single pulse excitation (SPE) with dipolar decoupling was acquired by a Bruker spectrometer at ^{1}H Larmor frequency of 850 MHz, using 2.5 mm MAS ^{1}H-X double resonance probe, under 8 kHz magic angle spinning, at T=383 K. The top spectrum (in red) is obtained by 10 times magnification of the experimental one (in black).

Slowly cooling down from the melt, temperature dependent spectra were acquired, as shown in Figure 7-5. The effect of anisotropy interactions can be seen clearly at 343K with characteristic line broadening. However, the peaks of methyl branches and α

carbons are surprisingly broad, which is not observed for PE21-CH_3, the ADMET precision polymer with high branch frequency. One possible explanation may arise from the relatively low molecular weight in PE39-CH_3. When there is considerably high ratio of short polymer chains present in the sample, individual polymer chain has less constrains in spatial orientation due to the decrease of chain length. As a consequence, the pendent branches may obtain increased possibility of steric displacements and chemical environments, displaying as wide distribution of chemical shifts in the spectra.

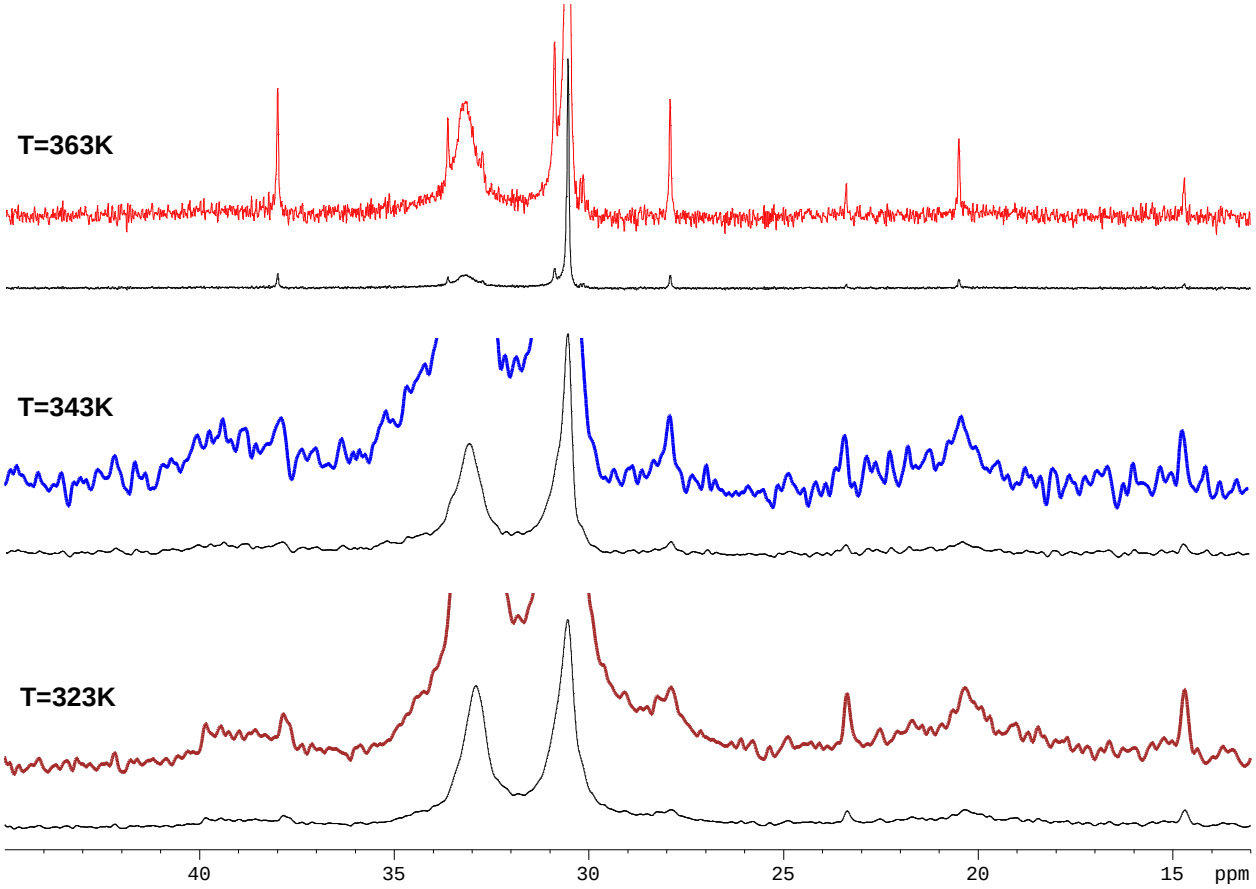

Figure 7-5. Temperature dependent ^{13}C spectra of PE39-CH_3 under SPE: cooling from the melt at a rate of 0.2 ºC/min. The colorful spectra are expanded 10 times of the experimental ones (in black).

To discover whether the unusual line broadening is due to the low molecular weight or not, low molecular weight parts in PE39-CH_3 is removed by using soxhlet extraction to yield PE39-CH_3-hmw, with higher molecular weight and narrower molecular weight distribution, as shown in Table 7-1. Similar experiments were employed on PE39-CH_3-hmw. Interestingly, the unusual line broadening for the methyl branch and α carbon remain the same (see Figure 7-6).

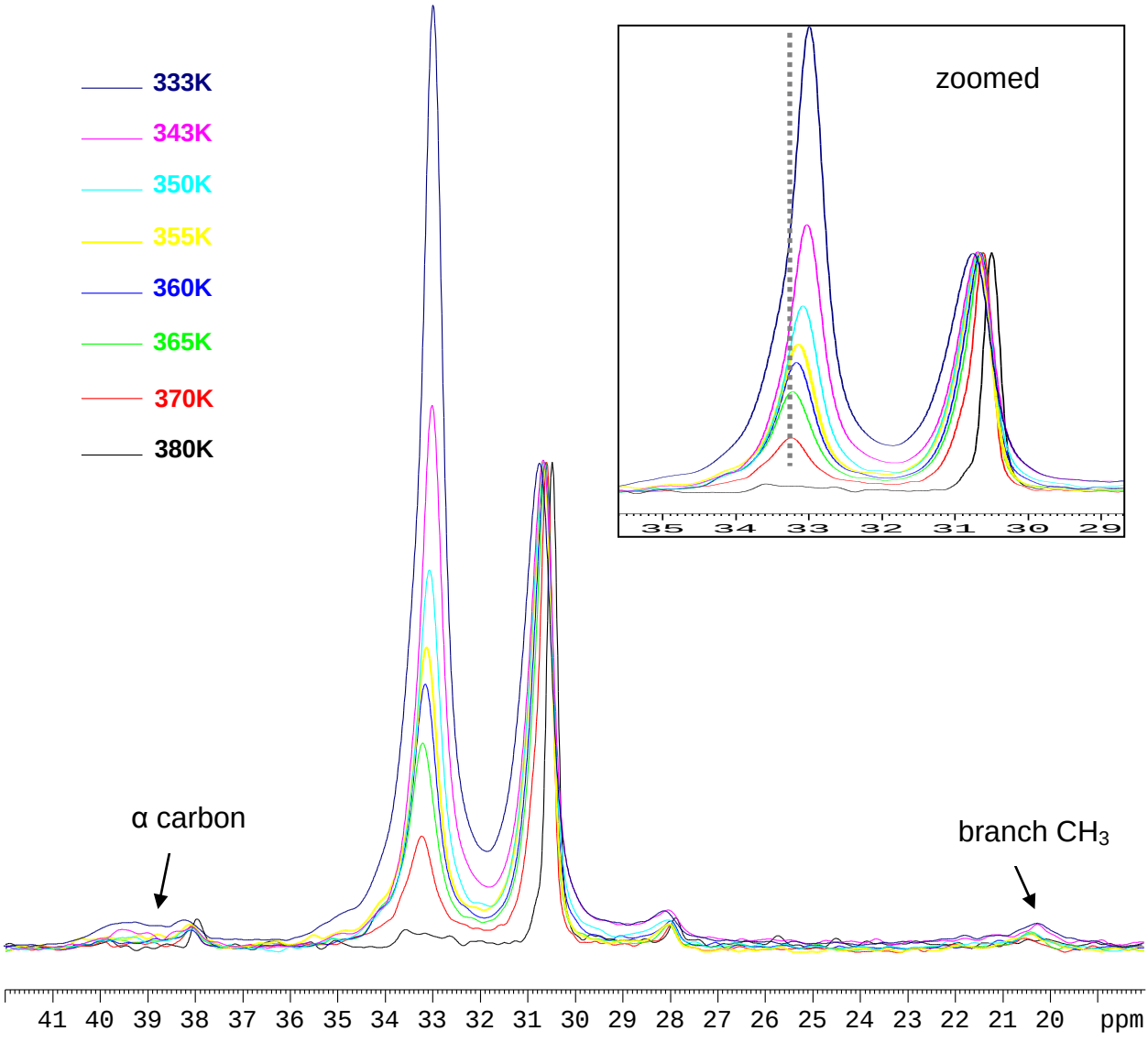

Figure 7-6. Temperature dependent ^{13}C spectra of PE39-CH_3-hmw using SPE with dipolar decoupling: cooling from the melt at a rate of 0.2 ºC/min. The spectra are normalized with reference to the amorphous CH_2 peak.

The duplication of line broadening in PE39-CH_3-hmw abolishes the previous hypothesis of low molecular weight effect. Then, what are the origins of these broadening? Since it's known that the methyl branches exist in both the crystalline regions and the non-crystalline regions, the answer to such a question will reveal the chain packing behaviors and the orientations of the methyl branches relative to the backbone.

Figure 7-6 shows the ^{13}C spectra of PE39-CH_3-hmw at various temperatures when cooling slowly from the melt. Beside the unusual line broadening for the branch and α carbon, there is another interesting observation: the temperature dependent chemical shifts of the *all-trans* conformation in crystalline regions and the *gauche* conformation in amorphous regions. It can be seen clearly from the expanded spectrum that the *all-trans* crystalline and the *gauche* amorphous peak move to each other when cooling, i.e., the chemical shift of crystalline CH_2 decreases at lower temperature while the trend for non-crystalline CH_2 is the opposite. The quantitative data of these deviations are shown in Table 7-2. The correlation of chemical shift difference between crystalline and non-crystalline regions versus the system temperature is illustrated in Figure 7-7. It is clear that the chemical shift difference shortens as temperature goes down and this trend of decreasing becomes more significant at lower temperatures.

Since the chemical shift is very sensitive to the chemical environment for the nucleus at site, such deviations remind us that the complex crystalline structures are possible to be represented in SS-NMR by such a simple parameter as chemical shift.

Table 7-2. Quantitative data of chemical shifts and peak information for PE39-CH_3-hmw in Figure 7-6.

T, °K	α carbon, ppm	$FWHM_\alpha$ Hz	CH_2 (CR), ppm	CH_2 (NCR), ppm	Δδ, ppm	Ratio of CR/NCR (intensity)	CH_3 branch, ppm	$FWHM_{CH3}$ Hz
RT_1	39.05	382	32.73	31.01	1.72	12.82	21.37	595
380	37.96	69	--	30.49	--	0	--	--
370	38.07	71	33.23	30.60	2.63	0.23	20.55	105
365	38.07	374	33.22	30.63	2.59	0.42	20.42	117
360	38.09	322	33.16	30.64	2.52	0.54	20.43	195
355	38.11	372	33.14	30.67	2.47	0.62	20.43	198
350	38.06	425	33.07	30.66	2.41	0.78	20.39	352
343	38.08	420	33.02	30.68	2.34	1.12	20.27	360
333	38.20	405	32.95	30.71	2.24	1.96	20.23	522
RT_2	39.17	458	32.71	30.89	1.06	8.85	20.10	632

FWHM: full width at half maximum
CR: crystalline region
NCR: non-crystalline region
Δδ= chemical shift of CR-chemical shift of NCR
Ratio of CR/NCR: the intensity ratio of CR over NCR
RT_1: room temperature (sample as received from synthesis)
RT_2: room temperature (sample recrystallized from the melt)

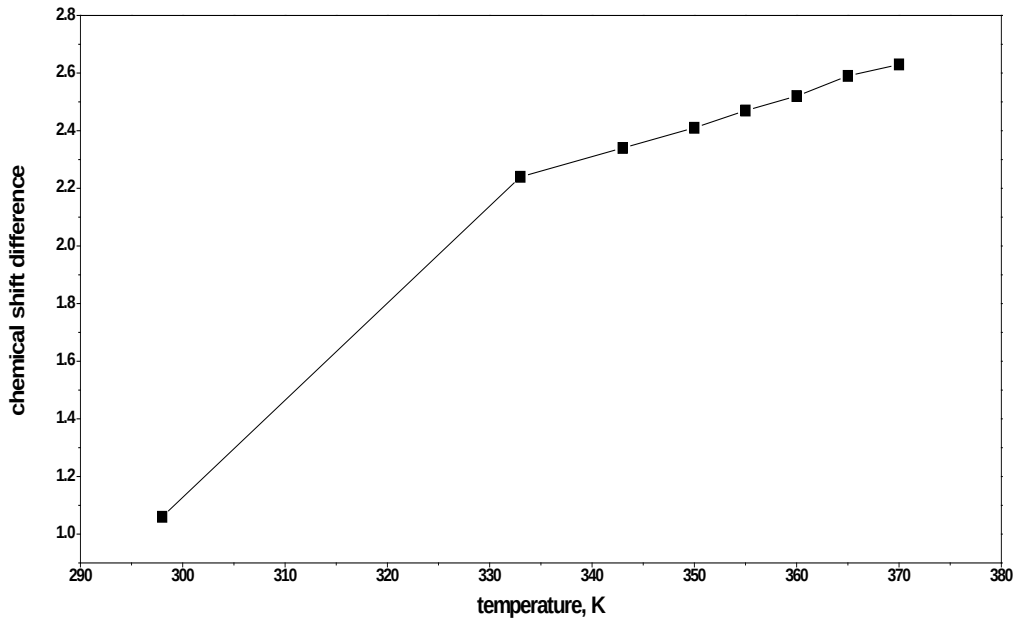

Figure 7-7. Plot of chemical shift difference between crystalline and non-crystalline CH_2 as a function of temperature. Data from Table 7-2

It is well-known that the solution-crystallized and melt-crystallized polyethylenes behave differently.[81, 113, 114] A more restricted local chain dynamics in non-crystalline regions of the solution-crystallized UHMWPE and the largely isotropic motion of melt-crystallized sample have been observed. Figure 7-8 shows the ^{13}C spectra of PE39-CH_3-hmw at various crystallization conditions. As expected, the non-crystalline CH_2 recrystallized from the melt displays more isotropic motion than that from the synthesis (polymer was achieved via precipitation). Moreover, the broad peaks at around 21 ppm assigned from methyl branches are nearly identical, indicating the crystallization condition is among the parameters that play important roles in determining the orientation distribution of CH_3 branches.

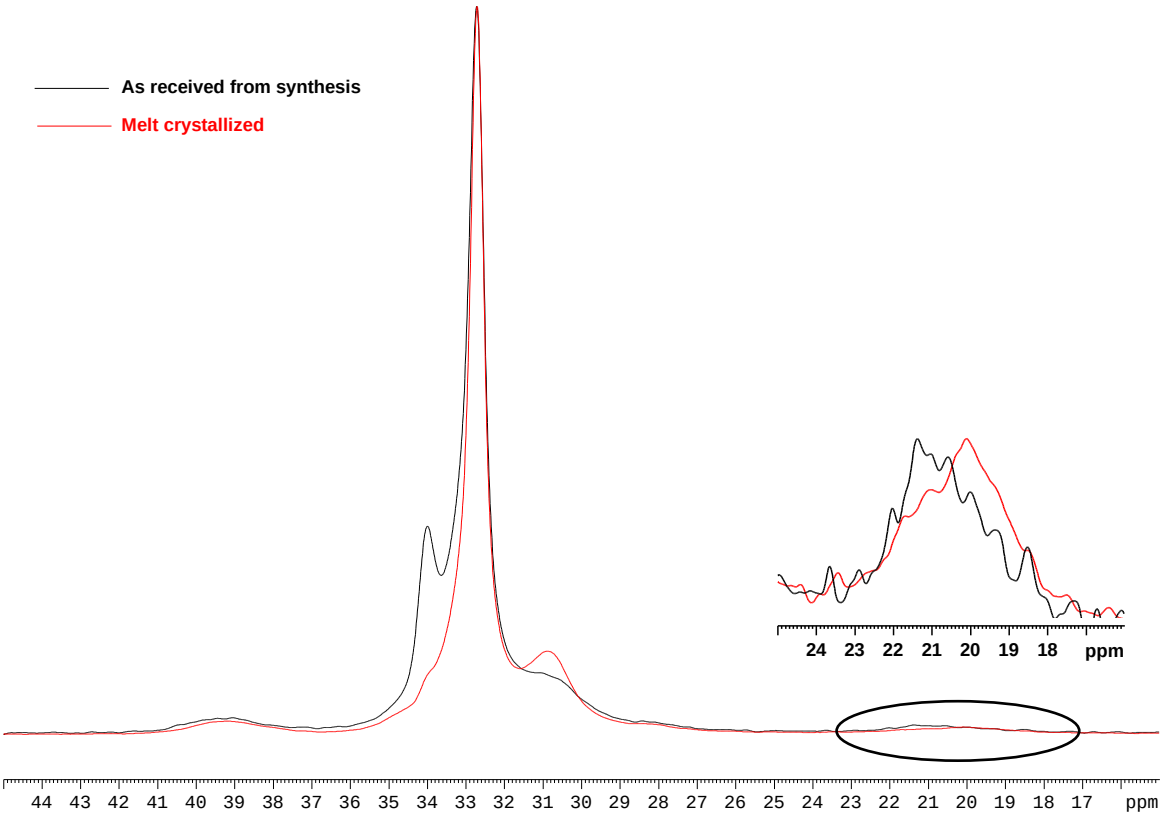

Figure 7-8. ^{13}C spectra of PE39-CH_3-hmw from various crystallization conditions. Measurements were done at room temperature. The broad methyl branch peaks are amplified for clarity.

7.4 Conclusion

The ADMET precision polyethylenes with low branch frequency show unique thermal, morphological, and micro-structural properties distinguished from those with high branch frequency. The rather low content of branching offers high melting temperature closer to the T_m of HDPE, implying the possibility of modeling HDPE by PE39-R polymers. The SS-NMR measurements show interesting line broadening of the peaks for the methyl branch and α carbon. This line broadening is independent of the molecular weight and its distribution. Temperature variable experiments indicate that the broad methyl peak is born quickly when cooling from the melt and seems not affected by the crystallization conditions.

Considering that the lamellar thickness of UHMWPE is around 12 nm, and that of PE21-CH_3 is around 10 nm, PE39-CH_3-hmw should fold into lamellar structure with thickness at similar magnitude. The distance between two adjacent methyl branches for an all-trans conformation is nearly 4.7 nm, which means for a specific chain stem, there are maximum two methyl branches can be incorporated in the crystalline regions prior to the occurrence of chain folding.

A morphological model can be proposed. Since the methyl branches in the amorphous regions undergo typically isotropic motions, the resulting chemical shift should be solution-like, i.e., these branches do not contribute to the unusual line broadening for the case of PE39-CH_3. So there leaves us the methyl branches in the crystalline regions and interphase. The methyl branches in the crystalline regions actually may be in anisotropic local environments. The remote spacing between branches allows us to treat the branches more like the intra-chain defects, just as the case in HDPE or UHMWPE. In contrast to PE21-CH_3, in which the branches

communicate with each other and behave more like normal parts composed of the unit cells, the branches in PE39-CH_3, are too far away to work together in disturbing the ordinary orthorhombic PE structures. Therefore, these intra-chain defects suffer static irregularity and display a wide distribution of space orientation relative to the main chain. Complimentary X-ray and TEM measurements will be very helpful in confirming the hypothesis.

CHAPTER 8
SUMMARY AND OUTLOOK

Summary

This dissertation aimed to gain an understanding of the relationship of structure-property-performance for commercial polyethylene utilizing acyclic diene metathesis polymers as structural models. It has been demonstrated that the macroscopic properties of ADMET precision and random polymers are strongly related to the branch identity, branch spacing, and branch distribution. Solid state NMR and X-ray scattering used herein are proved to be powerful and well-suited as two major analytical tools in investigating this subject.

Structural Modeling

Commercial PE resins are classified based on their densities, which are determined by branching. HDPE consists primarily of non-branched ethylene sequences; LDPE is characterized by its incorporation of both short-chain and long-chain branches; LLDPE contains a substantial number of short-chain branches; VLDPE is known for its much high level of short-chain branches. ADMET precision polymers maintain controlled primary structures, i.e., predetermined branch identity regularly spaced on the ethylene backbone. ADMET random polymers possess more variables: either predetermined branch identity with irregular branch distribution, or precise branch distribution with heterogeneous branch identities. From the ADMET precision polymers to ADMET random polymer and then to the commercial PE-based polymers, the progression of structure modeling can be envisioned from a point to a surface to a cuboid, corresponding to increasing freedom of branching from zero to two and then to three. Therefore, the investigation of commercial polyethylene-based structures by

fixing some of the branching variables while varying one parameter is highly feasible. By varying the content or type of branches, the ADMET precision and random polyolefins can be effectively used to model commercial LLDPE, VLDPE, HDPE, or even LDPE.

Polymer Synthesis

The deuterium labeling was chosen as a means of investigation because the ^{2}H SS-NMR lineshape is extremely sensitive to segmental motions. This characteristic observation offers a powerful method to study polymer microstructure as well as chain dynamics.

Synthesis of perdeuterated polymer samples was accomplished via acyclic diene metathesis polycondensation. The starting symmetric diene monomers were made via either malonate-based or cyanide chemistry. Unsaturated ADMET precision polymers were then hydrogenated to provide saturated versions. The ADMET random polymers were prepared by copolymerization of two α,ω diene monomers followed by exhaustive hydrogenation. One particular challenge was the residue of transition metal catalysts, which by all attempts could not be completely removed from the final products. Purification of ADMET polymers to eliminate trace catalyst residue has been a hot subject in metathesis chemistry. However, several questions are not yet clear and need further investigation: Does the presence of transition metal catalyst will affect some physical properties of ADMET polymers? What is the relationship of catalyst residue concentration and the affected properties?

Branch Spacing Effect

When the branch spacing varies, morphology, crystallinity, and the thermal behavior of ADMET precision polymers change correspondingly. For polymers with identical branch identity, there is generally a qualitative relation between branch spacing

and melting temperature. The smaller the branch spacing, the lower the melting temperature. However, when the spacing is too small to allow segments of chains to pack into ordered structures, totally amorphous polymer will be formed.

Sampled with three methyl-branched precision polymers, PE21-CD_3, PE15-CD_3, and PE9-CD_3, ^{2}H SS-NMR and ^{13}C SS-NMR measurements were analyzed jointly. By studying these regularly branched model polyolefins prepared though metathesis chemistry by advanced solid state NMR, twist defects around the branches in the crystalline regions are observed. For PE with low branch content (in the case of PE15-CD_3), the twist motions are decoupled (pinned defects), for higher branch contents collective motion (rotator phase) is observed. For branched polyethylenes, this is the first time that clear evidence of a rotator phase has been found, consistent with the results of X-ray scattering and electron microscopy.

The longest branch spacing to date, 39, is different from other precision polymers. The WAXS determination indicates more than one crystal structures is present. ^{13}C SS-NMR displays the rather broader peaks for methyl branches, methine carbons, and α-carbons; these breadths arise from the dispersed heterogeneous orientation of these carbon atoms with respect to the ethylene backbone. In the case of these ADMET precision polyethylenes with the lowest branch frequency, the branches can be considered more reasonably as defects in the ethylene packing array. Such a consideration leads us to conclude polymers with low branch frequency are rather similar to the polyethylene structures in reality, especially high density polyethylene.

Branch Identity Effect

The type and size of branches are crucial as well. This dissertation employed a series of ADMET precision polymers with various alkyl branches spaced along the

polyethylene main chain. WAXD measurements indicates that the smaller branches, such as methyl and ethyl groups, can be incorporated into the unit cells, while the larger branches, propyl groups or bigger, are excluded from the unit cells. This conclusion from XRD is in agreement with the evidence from thermal analysis and SS-NMR. The latter method was used to study the dynamics of different parts in the precision polymers of interest, and it was observed that the methyl branches in PE21-Methyl display two dynamics, slow and fast, representing the methyl branches in ordered crystalline regains and disordered non-crystalline regions, respectively. In contrast, the CH_3 part of the butyl branches in PE21-Butyl exhibit only one fast recoupling constant, indicating that the butyl branches are present only in disordered non-crystalline regions, as expected based on XRD measurements and thermal analysis.

Indeed, the ADMET polyolefins provide perfect structural models for commercial polyethylene-related materials by fixing one or two of the branching variables. The branch spacing, branch identity, and branch distribution are all significant parameters in determining microstructure and consequently the macromolecular properties and eventually the performance of the ADMET polyolefins.

Outlook

The fundamental understanding of the structure-property-performance relationship for ADMET polyolefins offers not only reasonable structural models for industrial PE-based materials, but also a potential application of ADMET PEs as additives during processing. Much like the use of additives in the industrial production of thermoplastics, addition of a trace amount of ADMET precision monomer/polymer may tune the structure and properties of the commercial material. Considering the substantial effects

of precision versus randomness on microstructures and physical properties, one would expect that ADMET polyolefins may function well as industrial additives.

The branch frequency plays an important role in the organization of crystal structures and consequently the melting temperature. The linear fit of melting temperature as a function of the branch content allows us to predict the thermal behavior of the ADMET polyolefins which have yet been synthesized. This prediction will both guide future synthesis and reduce unnecessary attempts.

Since all attempts to remove the residue of transition metal catalysts present in the final polymer products failed, it is then worth investigating the effect of catalyst on the physical properties, including nuclear relaxation. The applicable methodology of purification, the acceptable content of the catalyst, and the influence of the catalyst residue on physical properties are all of special interest. These issues can be more interesting in SS-NMR due to the fact that paramagnetic metal nuclei can affect the relaxation time significantly.

At present, only the primary structure is controlled precisely via ADMET chemistry. How to manipulate the precision in the secondary or even the tertiary structures in polyolefins will be of particular interest. Since a polymer is in fact a mixture of polymer chains with heterogeneous sizes, microstructures and orientations, a structure with higher level of regularity will minimize the complexity and will function as a perfect structural model in several disciplines, including the chemical industry, physics, and material science.

APPENDIX A
LAMELLAR THICKNESS DETERMINATION

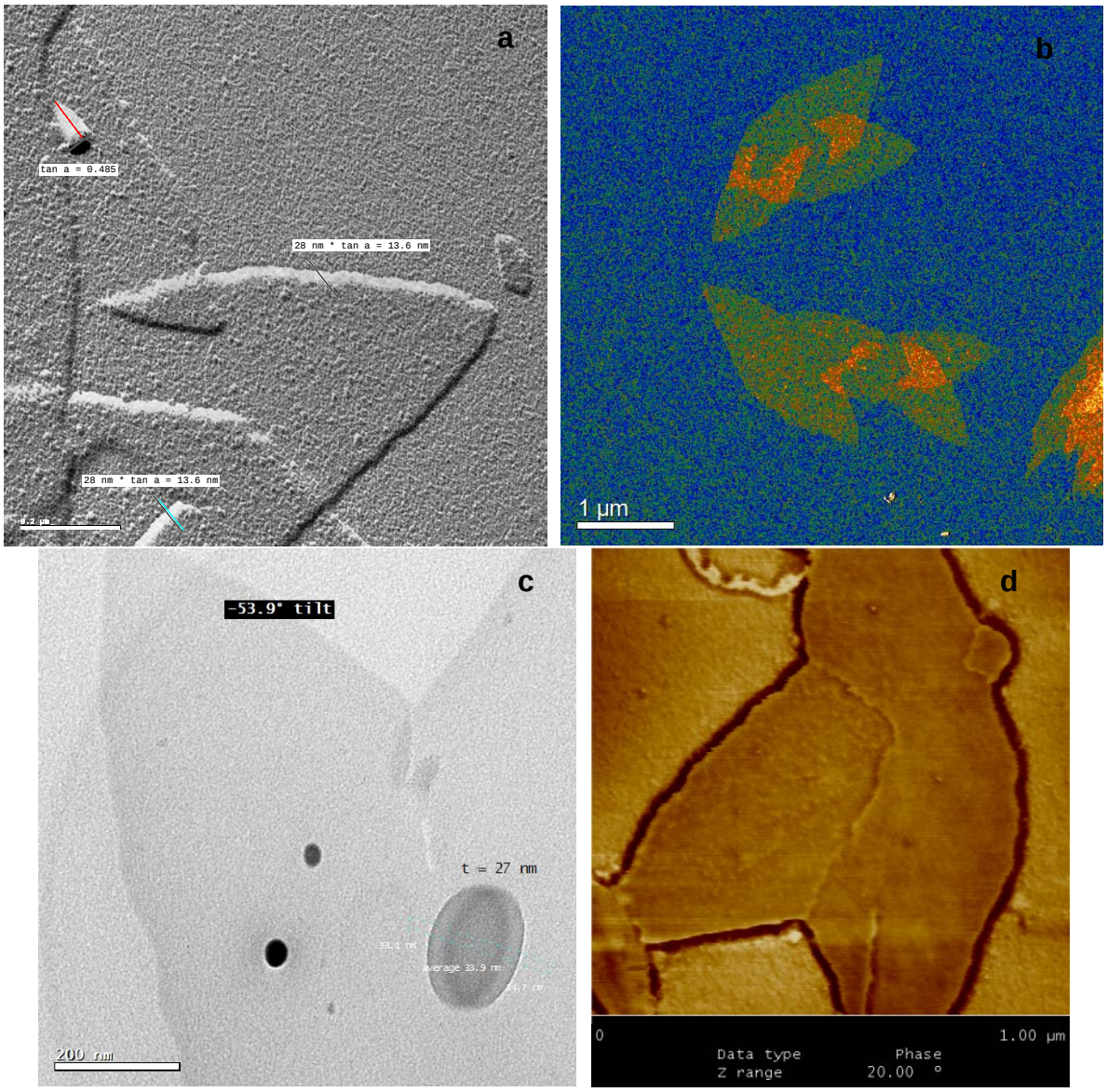

Lamellar thickness measurements for PE21-CD_3 (measured at Max Planck Institute for Polymer Research by Dr. Ingo Lieberwirth): (a) by TEM using Pt-shadowing; (b) by TEM using ectron Energy Loss Spectroscopy; (c) by TEM using stereoscopic method; (d) by AFM

APPENDIX B
DEUTERIUM 2D EXCHANGE NMR SPECTRA

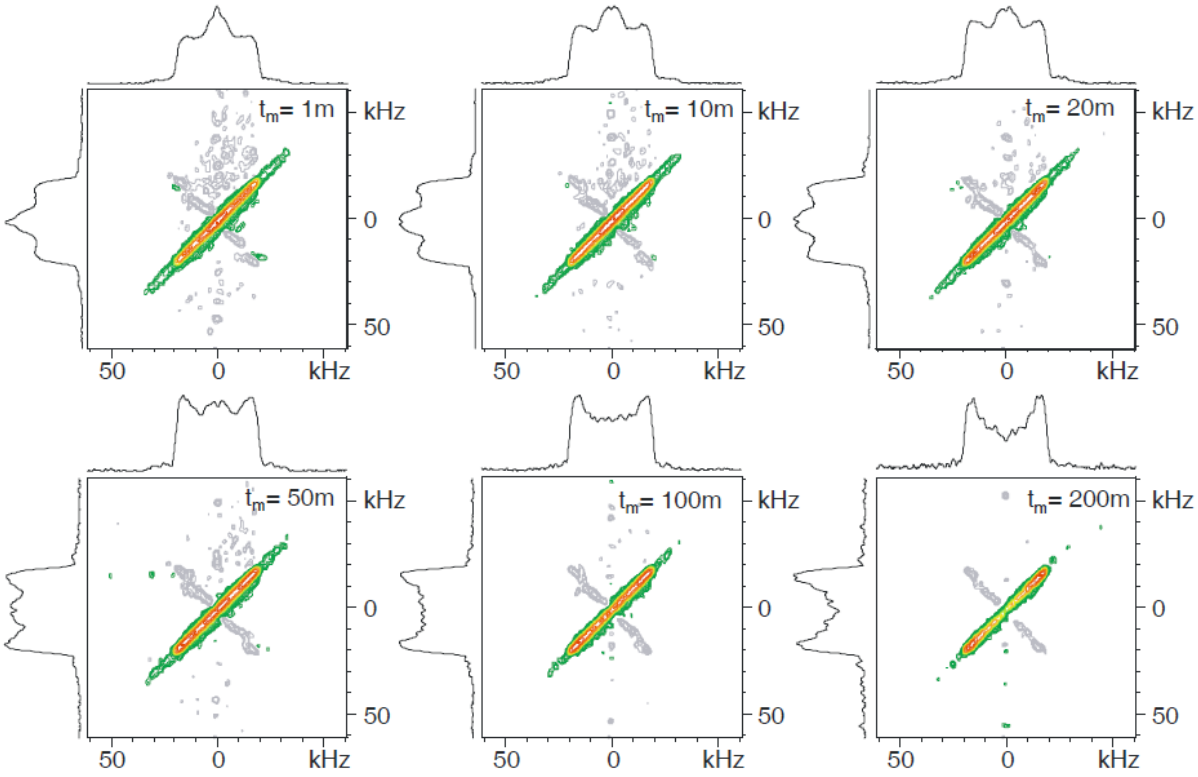

2-dimensional ^2H exchange NMR spectra for PE21-CD_3 at 296 K. The absence of off-diagonal intensity indicates no slow reorientations on the exchange time scale.

LIST OF REFERENCES

(1) Von Pechmann, H. *Ber. Dtsch. Chem. Ges.* **1898**, *31*.

(2) Peacock, A. J. *Handbook of polyethylene: structures, properties, and applications*; New York Marcel Dekker, Inc., 2000.

(3) Brydson, J. A. *Plastics Materials*; Elsevier Butterworth-Heinemann, 1999.

(4) Vasile, C.; Pascu, M. *Practical guide to polyethylene*; Smithers Rapra, 2005.

(5) Fawcett, E. W.; Gibson, R. O.; Perrin, M. W.; Patton, J. G.; Williams, E. G.: B Patent, 1937.

(6) Fox, J. J.; Martin, A. E. *Trans. Faraday Soc.,* **1940**, *36*, 897-911.

(7) Field, E.; Feller, M. *Industrial & Engineering Chemistry* **1957**, *49*, 1883-1884.

(8) Schultz, J. M. *Polymer crystallization : the development of crystalline order in thermoplastic polymers*; Oxford: American Chemical Society, 2001.

(9) Alamo, R. G.; VanderHart, D. L.; Nyden, M. R.; Mandelkern, L. *Macromolecules* **2000**, *33*, 6094-6105.

(10) Alamo, R. G.; Jeon, K.; Smith, R. L.; Boz, E.; Wagener, K. B.; Bockstaller, M. R. *Macromolecules* **2008**, *41*, 7141-7151.

(11) Bunn, C. W. *Transactions of the Faraday Society* **1939**, *35*, 482-491.

(12) Vand, V. *Acta Crystallographica* **1951**, *4*, 104-105.

(13) Swan, P. R. *Journal of Polymer Science* **1962**, *56*, 403-407.

(14) Swan, P. R. *Journal of Polymer Science* **1962**, *56*, 409-416.

(15) Zhan, C.-M. *Journal of Macromolecular Science, Part B* **1991**, *30*, 63 - 73.

(16) Abou-Kandil, A. I.; Windle, A. H. *Polymer* **2007**, *48*, 5069-5079.

(17) Werner, P. E. *Journal of Applied Crystallography* **1976**, *9*, 216-219.

(18) Tashiro, K.; Sasaki, S.; Kobayashi, M. *Macromolecules* **1996**, *29*, 7460-7469.

(19) Bassett, D. C.; Block, S.; Piermari.Gj *Journal of Applied Physics* **1974**, *45*, 4146-4150.

(20) Tonelli, A. E. *NMR Spectroscopy and Polymer Microstructure*; Wiley-VCH: Weinheim, 1989.

(21) Strobl, G. *The Physics of Polymers*, 2nd ed.; Springer-Verlag: Berlin, 1997.

(22) Bruce, H. P. *Advances in Polymer Technology* **1983**, *3*, 271-275.

(23) Gedde, U. W.; Mattozzi, A. *Long-Term Properties of Polyolefins* **2004**, *169*, 29-73.

(24) Lohse, D. J.; Milner, S. T.; Fetters, L. J.; Xenidou, M.; Hadjichristidis, N.; Mendelson, R. A.; Garcia-Franco, C. A.; Lyon, M. K. *Macromolecules* **2002**, *35*, 3066-3075.

(25) Baughman, T. W.; Sworen, J. C.; Wagener, K. B. *Macromolecules* **2006**, *39*, 5028-5036.

(26) Smith, J. A.; Brzezinska, K. R.; Valenti, D. J.; Wagener, K. B. *Macromolecules* **2000**, *33*, 3781-3794.

(27) Rojas, G.; Baughman, T. W.; Wagener, K. B. *Synthetic Communications* **2007**, *37*, 3923-3931.

(28) Rojas, G.; Berda, E. B.; Wagener, K. B. *Polymer* **2008**, *49*, 2985-2995.

(29) Rojas, G.; Inci, B.; Wei, Y.; Wagener, K. B. *Journal of the American Chemical Society* **2009**, *131*, 17376-17386.

(30) Rojas, G.; Wagener, K. B. *Journal of Organic Chemistry* **2008**, *73*, 4962-4970.

(31) Sworen, J. C.; Smith, J. A.; Berg, J. M.; Wagener, K. B. *Journal of the American Chemical Society* **2004**, *126*, 11238-11246.

(32) Sworen, J. C.; Smith, J. A.; Wagener, K. B.; Baugh, L. S.; Rucker, S. P. *Journal of the American Chemical Society* **2003**, *125*, 2228-2240.

(33) Sworen, J. C.; Pawlow, J. H.; Case, W.; Lever, J.; Wagener, K. B. *Journal of Molecular Catalysis a-Chemical* **2003**, *194*, 69-78.

(34) Sworen, J. C.; Wagener, K. B. *Macromolecules* **2007**, *40*, 4414-4423.

(35) John, E. S.; Kenneth, B. W. *Macromolecular Chemistry and Physics* **2005**, *206*, 1461-1471.

(36) Zuluaga, F.; Inci, B.; Nozue, Y.; Hosoda, S.; Wagener, K. B. *Macromolecules* **2009**, *42*, 4953-4955.

(37) Rojas, G.; Wagener, K. B. *Macromolecules* **2009**, *42*, 1934-1947.

(38) Matloka, P. P.; Sworen, J. C.; Zuluaga, F.; Wagener, K. B. *Macromolecular Chemistry and Physics* **2005**, *206*, 218-226.

(39) Matloka, P. P.; Wagener, K. B. *Journal of Molecular Catalysis a-Chemical* **2006**, *257*, 89-98.

(40) Matloka, P. P.; Kean, Z.; Greenfield, M.; Wagener, K. B. *Journal of Polymer Science Part a-Polymer Chemistry* **2008**, *46*, 3992-4011.

(41) Matloka, P. P.; Kean, Z.; Wagener, K. B. *Journal of Polymer Science Part a-Polymer Chemistry* **2010**, *48*, 1866-1877.

(42) Wagener, K. B.; Zuluaga, F.; Wanigatunga, S. *Trends in Polymer Science* **1996**, *4*, 157-163.

(43) Boz, E.; Ghiviriga, I.; Nemeth, A. J.; Jeon, K.; Alamo, R. G.; Wagener, K. B. *Macromolecules* **2008**, *41*, 25-30.

(44) Boz, E.; Nemeth, A. J.; Alamo, R. G.; Wagener, K. B. *Advanced Synthesis & Catalysis* **2007**, *349*, 137-141.

(45) Boz, E.; Nemeth, A. J.; Ghiviriga, I.; Jeon, K.; Alamo, R. G.; Wagener, K. B. *Macromolecules* **2007**, *40*, 6545-6551.

(46) Boz, E.; Nemeth, A. J.; Wagener, K. B.; Jeon, K.; Smith, R.; Nazirov, F.; Bockstaller, M. R.; Alamo, R. G. *Macromolecules* **2008**, *41*, 1647-1653.

(47) Boz, E.; Wagener, K. B. *Polymer Reviews* **2007**, *47*, 511-541.

(48) Boz, E.; Wagener, K. B.; Ghosal, A.; Fu, R. Q.; Alamo, R. G. *Macromolecules* **2006**, *39*, 4437-4447.

(49) Leonard, J. K.; Hopkins, T. E.; Chaffin, K.; Wagener, K. B. *Macromolecular Chemistry and Physics* **2008**, *209*, 1485-1494.

(50) Hopkins, T. E.; Pawlow, J. H.; Koren, D. L.; Deters, K. S.; Solivan, S. M.; Davis, J. A.; Gomez, F. J.; Wagener, K. B. *Macromolecules* **2001**, *34*, 7920-7922.

(51) Hopkins, T. E.; Wagener, K. B. *Macromolecules* **2003**, *36*, 2206-2214.

(52) Hopkins, T. E.; Wagener, K. B. *Journal of Molecular Catalysis a-Chemical* **2004**, *213*, 93-99.

(53) Hopkins, T. E.; Wagener, K. B. *Macromolecules* **2004**, *37*, 1180-1189.

(54) Leonard, J. K.; Turek, D.; Sloan, K. B.; Wagener, K. B. *Macromolecular Chemistry and Physics* **2010**, *211*, 154-165.

(55) Zuluaga, F.; Valderruten, N. E.; Wagener, K. B. *Polymer Bulletin* **1999**, *42*, 41-46.

(56) Opper, K. L.; Fassbender, B.; Brunklaus, G.; Spiess, H. W.; Wagener, K. B. *Macromolecules* **2009**, *42*, 4407-4409.

(57) Opper, K. L.; Markova, D.; Klapper, M.; Mullen, K.; Wagener, K. B. *Macromolecules* **2010**, *43*, 3690-3698.

(58) Opper, K. L.; Wagener, K. B. *Macromolecular Rapid Communications* **2009**, *30*, 915-919.

(59) Schwendeman, J. E.; Wagener, K. B. *Macromolecules* **2004**, *37*, 4031-4037.

(60) Schwendeman, J. E.; Wagener, K. B. *Macromolecular Chemistry and Physics* **2009**, *210*, 1818-1833.

(61) Aitken, B. S.; Lee, M.; Hunley, M. T.; Gibson, H. W.; Wagener, K. B. *Macromolecules* **2010**, *43*, 1699-1701.

(62) Petkovska, V. I.; Hopkins, T. E.; Powell, D. H.; Wagener, K. B. *Macromolecules* **2005**, *38*, 5878-5885.

(63) Petkovska, V. I.; Hopkins, T. E.; Powell, D. H.; Wagener, K. B. *Analytical Chemistry* **2006**, *78*, 3624-3631.

(64) Baker, C. H.; Mandelkern, L. *Polymer* **1966**, *7*, 71-83.

(65) Davis, G. T.; Eby, R. K.; Martin, G. M. *Journal of Applied Physics* **1968**, *39*, 4973-4981.

(66) Swan, P. R. *Journal of Polymer Science* **1960**, *42*, 525-534.

(67) Koenig, J. L. *Spectroscopy of Polymers*; Amsterdam: Elsevier, 1999.

(68) Stuart, B. *Polymer analysis. Analytical techniques in the sciences*; Wiley-VCH, 2002.

(69) Groenewoud, W. M. *Characterisation of polymers by thermal analysis*; Amsterdam: Elsevier, 2001.

(70) Cheremisinoff, N. P. *Polymer Characterization - Laboratory Techniques and Analysis*; William Andrew Publishing/Noyes, 1996.

(71) Elias, H.-G. *An introduction to polymer science*; Weinheim: VCH, 1997.

(72) Painter, P. C.; Coleman, M. M. *Fundamentals of Polymer Science: An Introductory Text*, 2nd. ed.; CRC Press, 2000.

(73) Elias, H.-G. *Macromolecules: Volume 2: Industrial Polymers and Syntheses*; WILEY-VCH, 2007.

(74) Elias, H.-G. *Macromolecules: Volume 1: Chemical Structures and Syntheses*; WILEY-VCH, 2007.

(75) Richardson, T. L. *Industrial plastics: Theory and application*, 5th. ed.; Albany, N.Y.: Delmar, 1989.

(76) David, W. I. F. *Structure determination from powder diffraction data*; Oxford: Oxford University Press, 2002.

(77) Duer, M. J. *Solid-state NMR spectroscopy : principles and applications* Malden, MA: Blackwell Science, 2002.

(78) Kasai, N.; Kakudo, M. *X-ray diffraction by macromolecules*; Tokyo: Kodansha, 2005.

(79) Schmidt-Rohr, K.; Spiess, H. W. *Multidimensional Solid-State NMR and Polymers*; Academic Press: London, 1994.

(80) Ernst, R. R. *Angewandte Chemie-International Edition in English* **1992**, *31*, 805-823.

(81) Yao, Y.; Chen, Q.; Graham, A. W. In *Annual Reports on NMR Spectroscopy*; Academic Press, 2010; Vol. Volume 69, pp 199-224.

(82) Martin, G. E.; Zekter, A. S. *Two-Dimensional NMR Methods for Establishing Molecular Connectivity*; VCH Publishers: New York, 1988.

(83) Purcell, E. M.; Torrey, H. C.; Pound, R. V. *Physical Review* **1946**, *69*, 37.

(84) Bloch, F. *Physical Review* **1946**, *70*, 460.

(85) Ernst, R. R. *Review of Scientific Instruments* **1965**, *36*, 1689-&.

(86) Ernst, R. R.; Anderson, W. A. *Review of Scientific Instruments* **1965**, *36*, 1696-&.

(87) Overhauser, A. W. *Physical Review* **1953**, *92*, 411.

(88) Levitt, M. H. *Spin Dynamics: Basics of Nuclear Magnetic Resonance*; John Wiley & Sons, LTD, 2001.

(89) Keeler, J. *Understanding of NMR Spectroscopy*; Wiley: Chichester, 2006.

(90) Duer, M. J. *Introduction to solid-state NMR spectroscopy* Oxford, UK ; Malden, MA : Blackwell, 2004.

(91) Spiess, H. W. *Colloid and Polymer Science* **1983**, *261*, 193-209.

(92) Saalwachter, K.; Schnell, I. *Solid State Nuclear Magnetic Resonance* **2002**, *22*, 154-187.

(93) Rose, M. E. *Elementary theory of angular momentum*; Wiley: New York, 1957.

(94) Spiess, H. W. *Journal of Polymer Science Part a-Polymer Chemistry* **2004**, *42*, 5031-5044.

(95) Khuong, T. A. V.; Dang, H.; Jarowski, P. D.; Maverick, E. F.; Garcia-Garibay, M. A. *Journal of the American Chemical Society* **2007**, *129*, 839-845.

(96) Liu, S. F.; Mao, J. D.; Schmidt-Rohr, K. *Journal of Magnetic Resonance* **2002**, *155*, 15-28.

(97) Tycko, R.; Dabbagh, G.; Mirau, P. A. *Journal of Magnetic Resonance* **1989**, *85*, 265-274.

(98) Eden, M. *Concepts in Magnetic Resonance Part A* **2003**, *18A*, 24-55.

(99) Lieser, G.; Wegner, G.; Smith, J. A.; Wagener, K. B. *Colloid and Polymer Science* **2004**, *282*, 773-781.

(100) Qiu, W. L.; Sworen, J.; Pyda, M.; Nowak-Pyda, E.; Habenschuss, A.; Wagener, K. B.; Wunderlich, B. *Macromolecules* **2006**, *39*, 204-217.

(101) Sumpter, B. G.; Noid, D. W.; Liang, G. L.; Wunderlich, B. *Atomistic Modeling of Physical Properties* **1994**, *116*, 27-72.

(102) Piel, C.; Starck, P.; Seppala, J. V.; Kaminsky, W. *Journal of Polymer Science Part a-Polymer Chemistry* **2006**, *44*, 1600-1612.

(103) Islam, A.; Hussein, I. A. *Journal of Applied Polymer Science* **2006**, *100*, 5019-5033.

(104) Alamo, R. G.; Blanco, J. A.; Agarwal, P. K.; Randall, J. C. *Macromolecules* **2003**, *36*, 1559-1571.

(105) Hussein, I. A.; Hameed, T.; Williams, M. C. *Journal of Applied Polymer Science* **2006**, *102*, 1717-1728.

(106) Born, R.; Spiess, H. W. *Macromolecules* **1995**, *28*, 7785-7795.

(107) Greenfield, M. S.; Ronemus, A. D.; Vold, R. L.; Vold, R. R.; Ellis, P. D.; Raidy, T. E. *Journal of Magnetic Resonance* **1987**, *72*, 89-107.

(108) Hentschel, D.; Sillescu, H.; Spiess, H. W. *Macromolecules* **1981**, *14*, 1605-1607.

(109) Macho, V.; Brombacher, L.; Spiess, H. W. *Applied Magnetic Resonance* **2001**, *20*, 405-432.

(110) Vanderhart, D. L. *Journal of Magnetic Resonance* **1981**, *44*, 117-125.

(111) Mansfield, M.; Boyd, R. H. *Journal of Polymer Science Part B-Polymer Physics* **1978**, *16*, 1227-1252.

(112) Schmidtrohr, K.; Spiess, H. W. *Macromolecules* **1991**, *24*, 5288-5293.

(113) Yao, Y. F.; Graf, R.; Spiess, H. W.; Lippits, D. R.; Rastogi, S. *Physical Review E* **2007**, *76*, 060801(R).

(114) Yao, Y. F.; Graf, R.; Spiess, H. W.; Rastogi, S. *Macromolecules* **2008**, *41*, 2514-2519.

(115) Yao, Y. F.; Graf, R.; Spiess, H.; Rastogi, S. *Macromolecular Rapid Communications* **2009**, *30*, 1123-1127.

(116) Sirota, E. B.; Herhold, A. B. *Polymer* **2000**, *41*, 8781-8789.

(117) Kaji, H.; Horii, F. *Macromolecules* **2007**, *40*, 5420-5423.

(118) Helfand, E.; Wasserman, Z. R.; Weber, T. A.; Skolnick, J.; Runnels, J. H. *Journal of Chemical Physics* **1981**, *75*, 4441-4445.

(119) He, Y. Y.; Lutz, T. R.; Ediger, M. D.; Ayyagari, C.; Bedrov, D.; Smith, G. D. *Macromolecules* **2004**, *37*, 5032-5039.

(120) Cory, D. G.; Ritchey, W. M. *Macromolecules* **1989**, *22*, 1611-1615.

(121) Okuom, M. O.; Metin, B.; Blum, F. D. *Langmuir* **2008**, *24*, 2539-2544.

(122) Metin, B.; Blum, F. D. *Journal of Chemical Physics* **2006**, *124*, -.

(123) O'Connor, R. D.; Ginsburg, E. J.; Blum, F. D. *Journal of Chemical Physics* **2000**, *112*, 7247-7259.

(124) Blum, F. D.; Xu, G.; Liang, M. H.; Wade, C. G. *Macromolecules* **1996**, *29*, 8740-8745.

(125) Borsa, F.; Torgeson, D. R.; Martin, S. W.; Patel, H. K. *Physical Review B* **1992**, *46*, 795.

(126) Hentschel, D.; Sillescu, H.; Spiess, H. W. *Makromolekulare Chemie-Macromolecular Chemistry and Physics* **1979**, *180*, 241-249.

(127) Hentschel, R.; Spiess, H. W. *Journal of Magnetic Resonance* **1979**, *35*, 157-162.

(128) Olf, H. G.; Peterlin, A. *Journal of Polymer Science Part a-2-Polymer Physics* **1970**, *8*, 791-&.

(129) Olf, H. G.; Peterlin, A. *Journal of Polymer Science Part a-2-Polymer Physics* **1970**, *8*, 771-&.

(130) Olf, H. G.; Peterlin, A. *Journal of Polymer Science Part a-2-Polymer Physics* **1970**, *8*, 753-&.

(131) Hu, W. G.; Boeffel, C.; Schmidt-Rohr, K. *Macromolecules* **1999**, *32*, 1611-1619.

(132) Vanderhart, D. L. *Journal of Magnetic Resonance* **1976**, *24*, 467-470.

(133) Eastman, M. A.; Nanny, M. A. *Journal of Magnetic Resonance* **2007**, *184*, 302-314.

(134) Schwendeman, J. E.; Wagener, K. B. *Macromolecular Chemistry and Physics* **2005**, *206*, 1461-1471.

(135) Wunderlich, B. In *Macromolecular Physics*; Academic Press inc.: New York, 1973; Vol. 1, pp 401-407.

(136) Hu, W.; Srinivas, S.; Sirota, E. B. *Macromolecules* **2002**, *35*, 5013-5024.

(137) Hu, W.; Sirota, E. B. *Macromolecules* **2003**, *36*, 5144-5149.

(138) Androsch, R.; Blackwell, J.; Chvalun, S. N.; Wunderlich, B. *Macromolecules* **1999**, *32*, 3735.

(139) Suhm, J.; Schneider, M. J.; Mulhaupt, R. *Journal of Polymer Science Part a-Polymer Chemistry* **1997**, *35*, 735-740.

(140) Schneider, M. J.; Suhm, J.; Mulhaupt, R.; Prosenc, M. H.; Brintzinger, H. H. *Macromolecules* **1997**, *30*, 3164-3168.

(141) Suhm, J.; Schneider, M. J.; Mulhaupt, R. *Journal of Molecular Catalysis a-Chemical* **1998**, *128*, 215-227.

(142) McKnight, A. L.; Waymouth, R. M. *Chemical Reviews* **1998**, *98*, 2587-2598.

(143) Schwerdtfeger, E. D.; Irwin, L. J.; Miller, S. A. *Macromolecules* **2008**, *41*, 1080-1085.

(144) Salata, M. R.; Marks, T. J. *Macromolecules* **2009**, *42*, 1920-1933.

(145) Hadjichristidis, N.; Xenidou, M.; Iatrou, H.; Pitsikalis, M.; Poulos, Y.; Avgeropoulos, A.; Sioula, S.; Paraskeva, S.; Velis, G.; Lohse, D. J.; Schulz, D. N.; Fetters, L. J.; Wright, P. J.; Mendelson, R. A.; Garcia-Franco, C. A.; Sun, T.; Ruff, C. J. *Macromolecules* **2000**, *33*, 2424-2436.

(146) Baughman, T. W.; Sworen, J. C.; Wagener, K. B. *Tetrahedron* **2004**, *60*, 10943-10948.

(147) Organ, S. J.; Keller, A. *Journal of Materials Science* **1985**, *20*, 1571-1585.

BIOGRAPHICAL SKETCH

Yuying Wei was born in the city of Xi'an, Shaanxi province, China, in 1973. She is daughter of Zhanxian Wei and Huamei Li, sister of Yuning Wei, wife of Liwen Jin, and mother of Abbie Jin.

Yuying received the Bachelor of Science in Chemical Engineering from *Northwest University*, Xi'an, China. After that she worked as a lecturer in *Xi'an aerotechnique College* for two years. In 1996, she joined the graduate school in *University of Petroleum*, Beijing, China, where she received the Master of Science in Chemical Engineering and met Liwen Jin. They got married in 1999.

In 1999-2001, Yuying worked as a chemical engineer at *Beijing Research Institute of Chemical Industry*, China Petroleum & Chemical Corporation, designing and producing industrial catalyst. Later on, she and her husband moved to the United States for better understanding of the world and life. In 2002, their first child was born at Greenville Memorial Hospital, located at Greenville, South Carolina. Yuying studied polymer physics at the Chemistry Department, University of Clemson for two years.

In 2006, Yuying moved to Gainesville, Florida and entered the Ph.D. program in the Chemistry Department at the University of Florida, majoring in analytical division. She joined Prof. Ken Wagener's research group in the same year, working on synthesis and characterization of deuterated precision polyolefins.

In 2008 & 2010, Yuying visited Max Planck Institute for Polymer Research, Mainz, Germany, and worked with Prof. Dr. Hans Spiess for 6 months in total. She learned modern solid state NMR techniques, and opened her insights of doing research.

In August 2010, Yuying will have completed her PhD study at the University of Florida.